# AO/1-9934/19/D/SR
# Tumbling motion assessment for space debris objects

## Final Presentation

A. Vananti

Astronomical Institute, University of Bern (AIUB), Switzerland

9th of September 2022

Teleconference with ESOC

# Outlook

- Introduction
- Attitude models
- IOTA software
- Observation campaign
- Radar observations
- Amplitude method
- Epoch method
- Attitude evolution
- Conclusions

# Introduction

- Space debris population growth
- Possible solution: Active Debris Removal
- Knowledge of attitude is necessary
- Current project: development of methods for attitude determination and prediction:
  - Attitude models
  - Attitude determination (amplitude and epoch method)
  - Software for attitude prediction and observation simulations
  - Observations (CCD, photon counter, SLR, radar)
  - Process and product formats and standards

# Outlook

- Introduction
- Attitude models
- IOTA software
- Observation campaign
- Radar observations
- Amplitude method
- Epoch method
- Attitude evolution
- Conclusions

# Attitude models

| Orbit | Object | Grav. grad. | Eddy curr. | SRP | Dissip. | Long term behav. |
|---|---|---|---|---|---|---|
| LEO | R/B | ✓ | ✓ | | ✓ | Stable |
| | Satell. | ✓ | ✓ | ✓ | ✓ | Almost stable |
| GEO | R/B | | | | ✓ | Rotating |
| | Satell. | | | ✓ | ✓ | Rotating |

- Idealized categories
- LEO: stronger influence of gravity gradient and eddy currents
- Eddy currents is stabilizing perturbation
- Satellites have solar panels and SRP is not stabilizing
- MEO/GEO: stronger influence of SRP

# Eddy currents

- Eddy currents torque $\mathbf{M}_{EC} = \left[\mathbb{S}\left(\boldsymbol{\omega} \times \mathbf{B} - (\mathbf{v}, \nabla)\mathbf{B} - \dot{\mathbf{B}}\right)\right] \times \mathbf{B}.$
- Dissipative term (Eddy current): $\boldsymbol{\omega} \times \mathbf{B}$
- Related to orbital motion: $(\mathbf{v}, \nabla)\mathbf{B}$ and $\dot{\mathbf{B}}$
- Dissipative terms dominates at first (proportional angular velocity)
- Orbital terms dominate after spin velocity has diminished (in the phase of gravitational capture)
- Orbital terms tend to align momentum vector to orbit normal and stabilize to a momentum depending on the orbit

- Magnetic tensor M: $\vec{T} = (M\vec{\Omega}) \times \vec{B}.$
- E.g. spherical shell $M = \frac{2\pi}{3}\sigma R^4 e \begin{bmatrix} 1 & 0 & 0 \\ 0 & 1 & 0 \\ 0 & 0 & 1 \end{bmatrix}$
- For flat surfaces computation similar to moment of inertia
- Distribution of conductive material σ

# Eddy currents

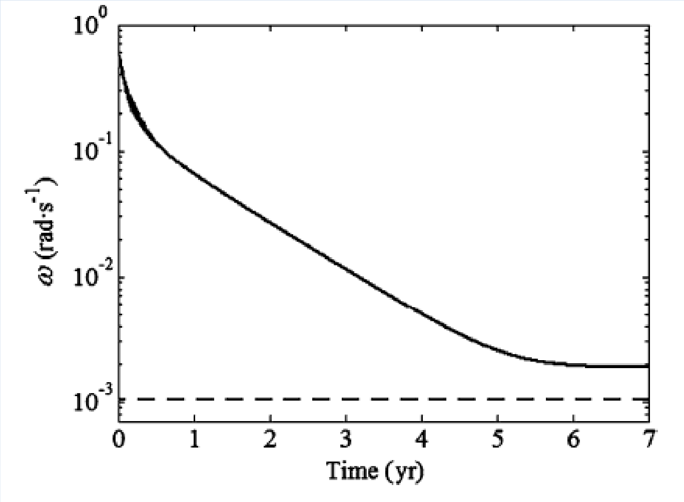


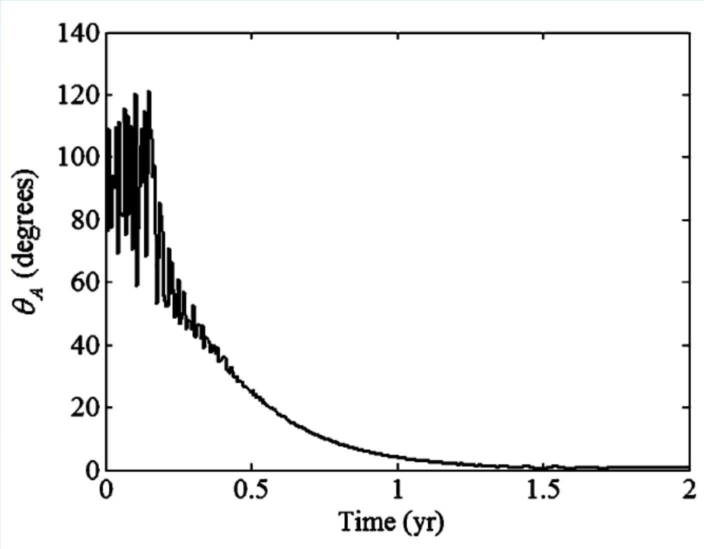


3 phases:

- Dissipation -> flat spin
- Exponential decay
- Stabilization

$\theta_A$ angle between angular velocity and major axis of inertia (dissipation phase)

# Gravity gradient

- No contribution to energy loss (conservative)
- Big contribution to change of momentum direction
- Ideally, precession of momentum around orbit normal (decay phase)
- E.g. rocket body:

$$P_g = \frac{2\pi^2 I_0 r^3}{GM_e \Delta I P_{rot} \cos\theta}$$

- Not ideal precession due to orbit precession:

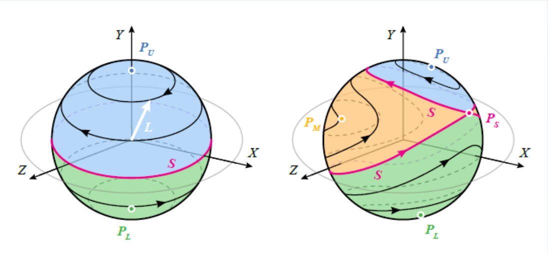

- With low spin rate (gravitational capture phase):
  => alignment to orbit normal
- Oscillations during capture, motion like a pendulum

# Eddy current + grav. grad.

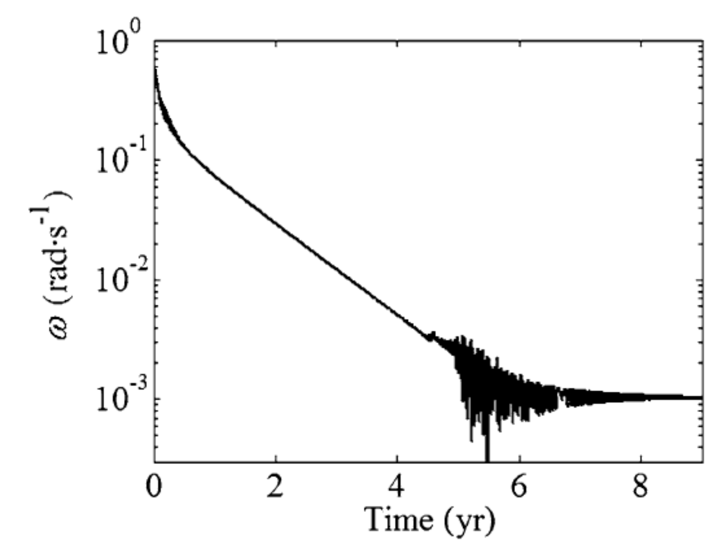


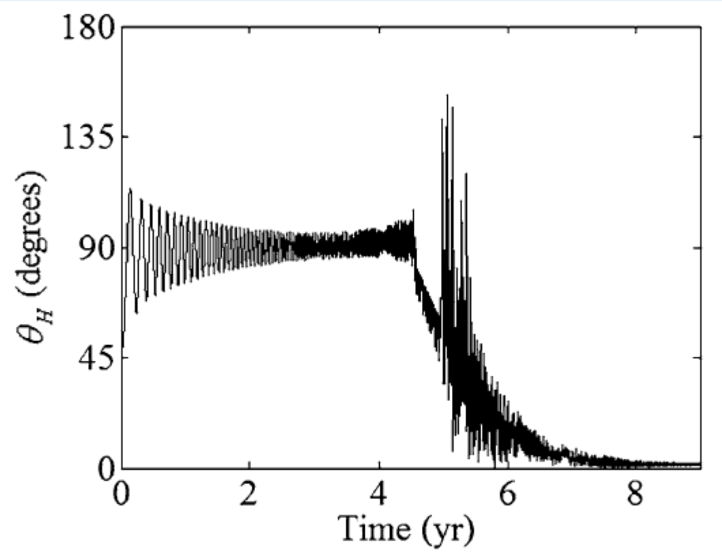


$\theta_H$ angle between angular momentum and normal to orbital plane

Gravitational capture:

- Angular rotation low
- Gravity gradient bigger than eddy currents

=> gravity gradient aligns momentum vector to orbit normal

=> Spin-orbit resonance (mostly 1:1, but depends on orbit)

# Solar Radiation Pressure

- No magnetic dissipation effect
- Spin rate constant or changes due to SRP
- Mostly S/C with large illuminated surfaces
- Increase/decrease spin rate:
  - Asymmetric solar panels
  - Offset of center of mass w.r.t. figure
- Cyclic and secular trends

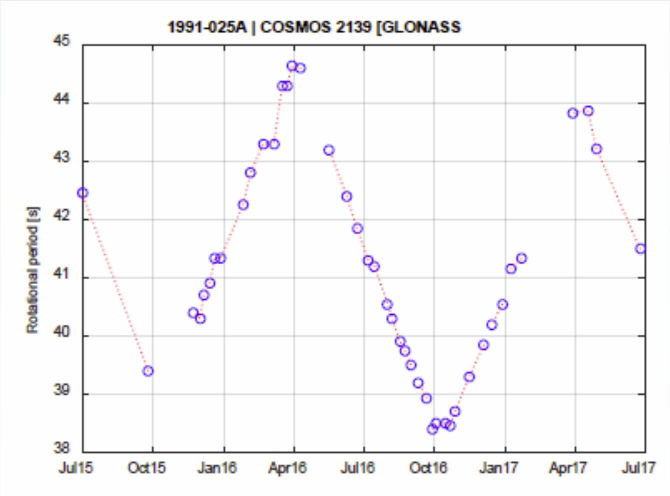

# Simulation: wind wheel

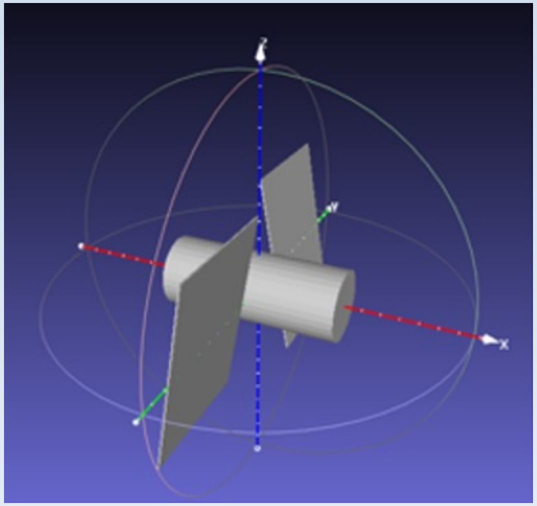


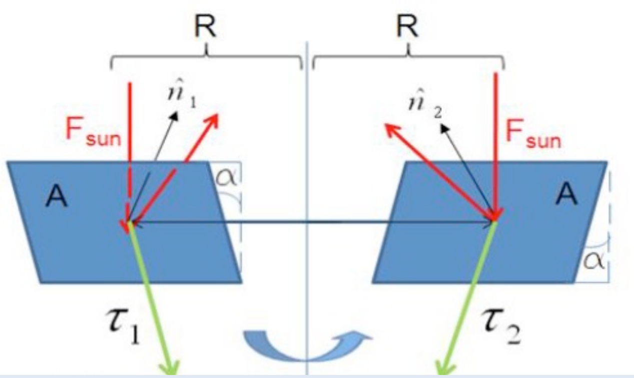


- Wind wheel, rotation around x axis
- Sun illumination parallel to x => torque along x
- Sun illumination in x-y plane => partial torque along x, no torque with Sun parallel to y
- Simulations:
  - Polar orbit, 36'000 km altitude
  - Moments of inertia are $3 \times 10^3$, $3 \times 10^3$, $1 \times 10^3$ kg $m^2$
  - Box (2 x 2 x 2 m), wings (1 x 2 m)
  - 10° canting angle

# Periodic pattern

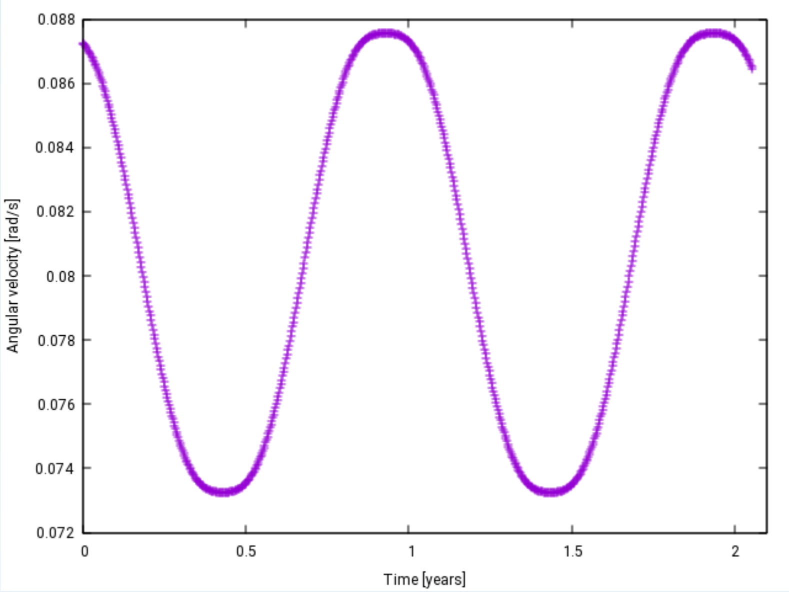


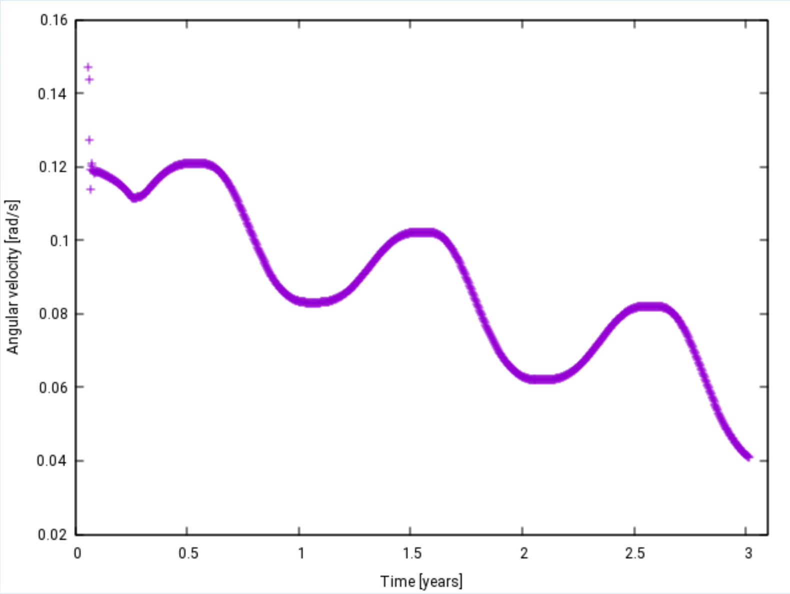


- Initial rotation
  => stabilize the direction of angular velocity
  => throughout the year Sun illuminates front/back of wheel
  => increase/decrease: yearly period
- Different front/back reflection coefficient
  => increase/decrease stronger in the first half of year
  => secular slope

# Pseudo periodicity

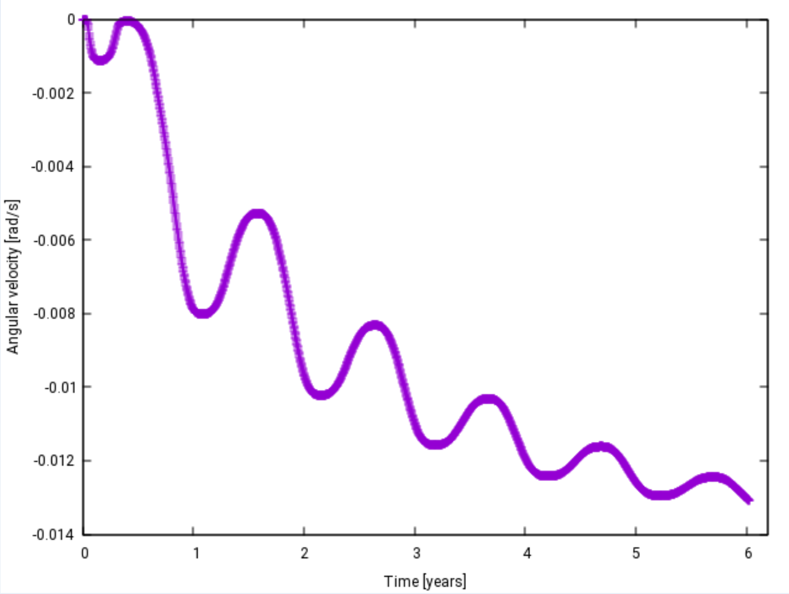


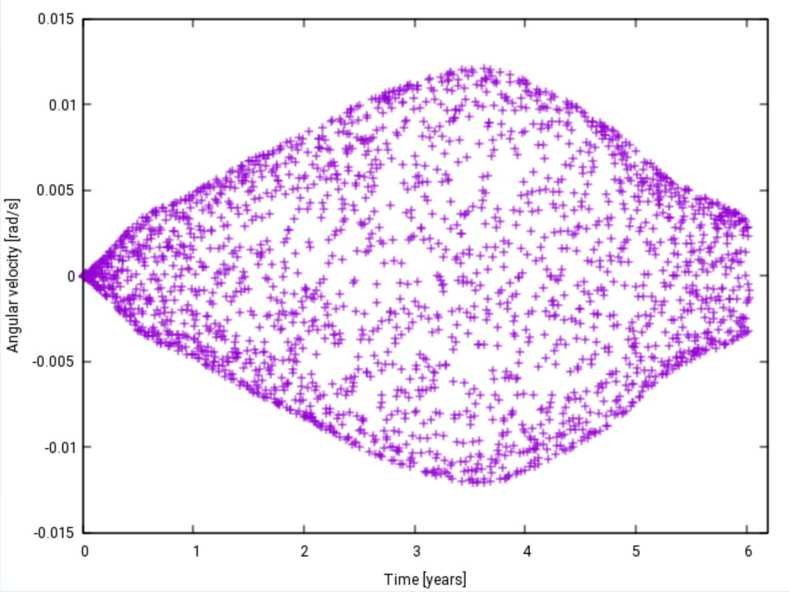


- No initial velocity + different front/back coeff.

  => secular + periodic trend

  => pseudo periodic (chaotic)
- Same results with only 1 wing

# Monotonic trend

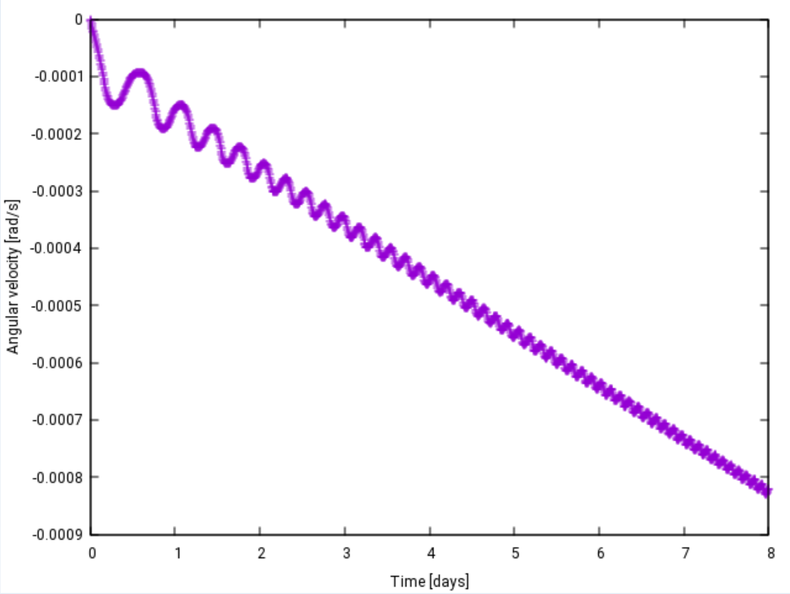


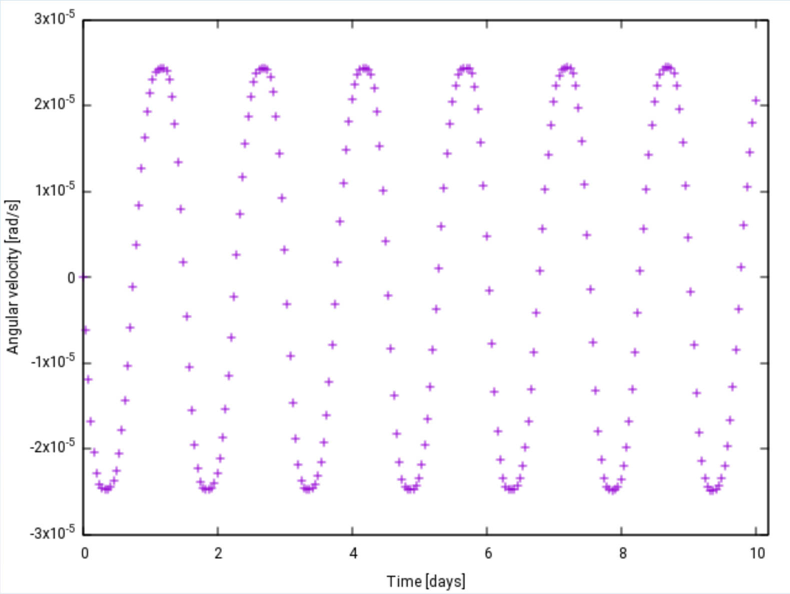


- 1 wing with no canting
  => monotonic trend (radiometer)
  => or almost static attitude (wind vane)

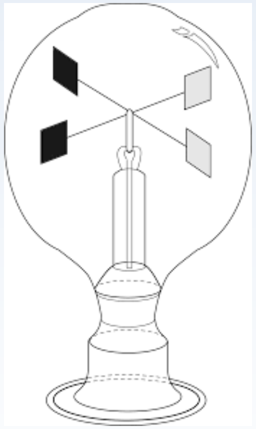

# Different behaviours

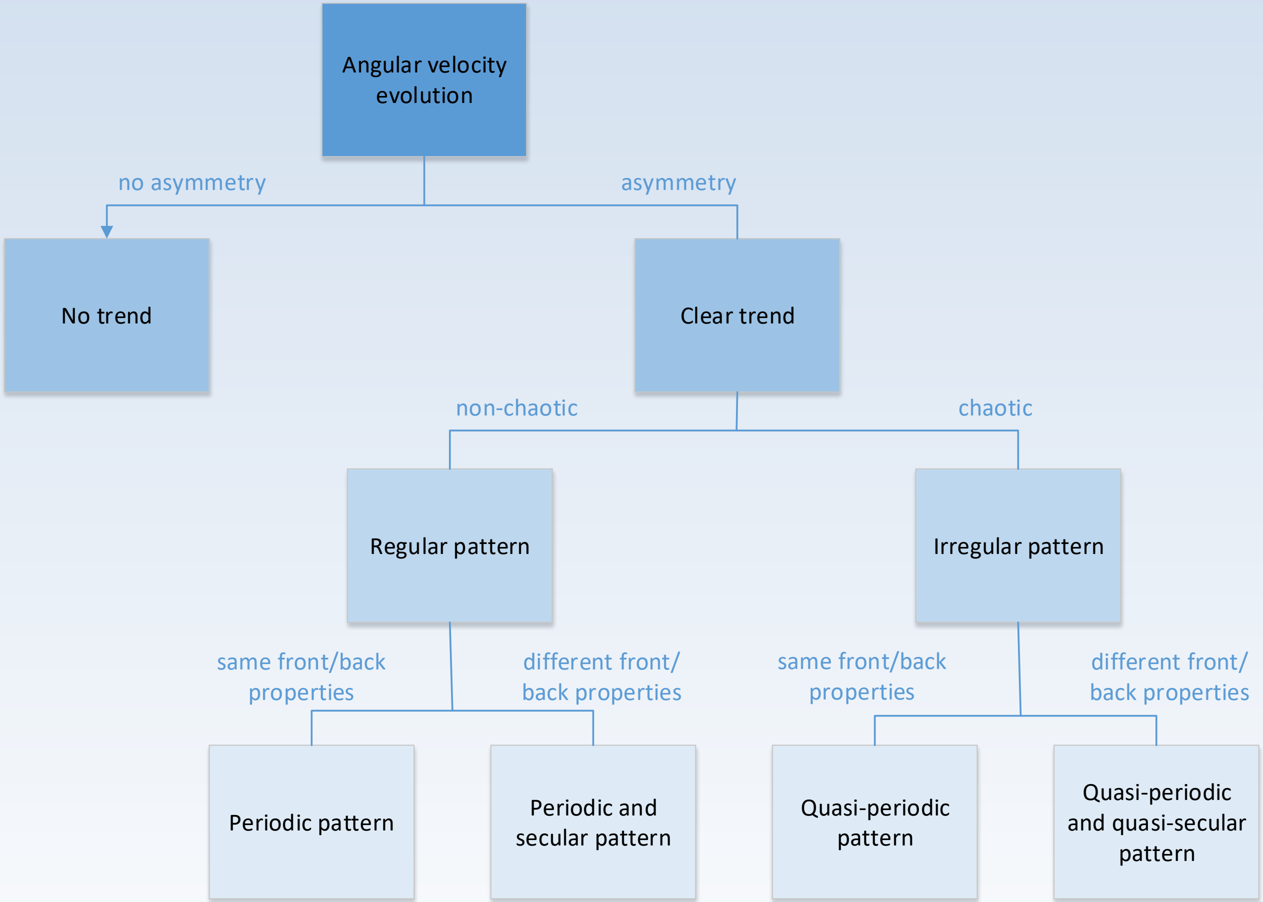

# Outlook

- Introduction
- Attitude models
- IOTA software
- Observation campaign
- Radar observations
- Amplitude method
- Epoch method
- Attitude evolution
- Conclusions

# Amplitude method

- Method proposed by V. Williams (1979)
- Determination of the spin axis orientation
- Cylindrical elongated objects: R/B
- Stable attitude state (flat spin)
- Diffuse reflection of Sun light
- No reflection on top/bottom of cylinder
- Constant spin axis during one observation passage
- Constant spin axis over time period of several observations

# Amplitude method

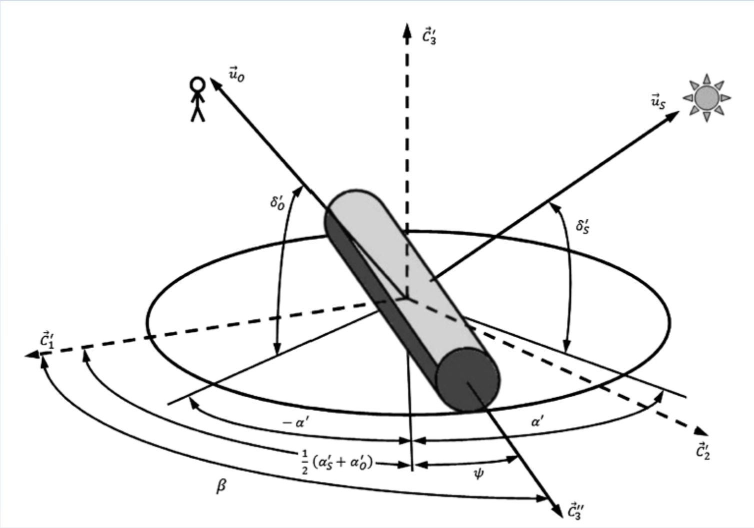


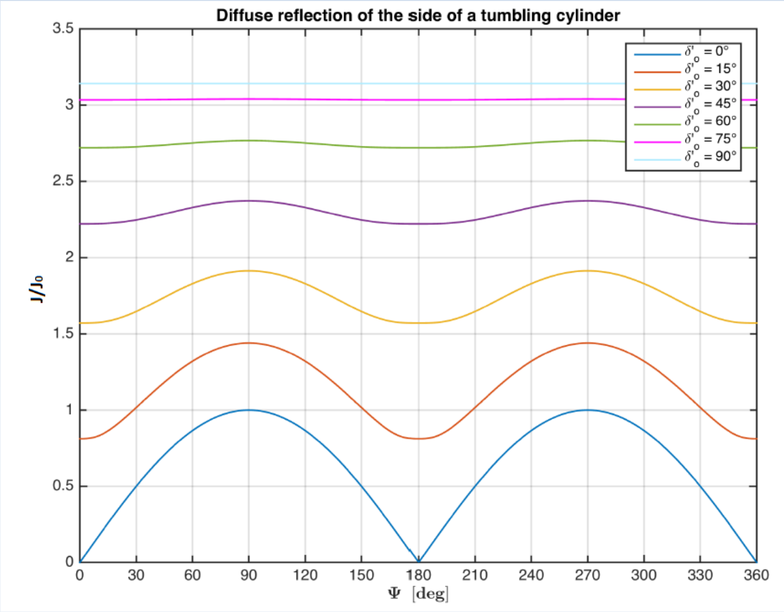


$\alpha' = 0°, \delta_S' = 90°$

- Brightness ratio (BR): $M_{max} - M_{min} = -2.5 \log_{10} \frac{J_{max}}{J_{min}}$
- Ratio depends on direction of spin axis
- For given Sun/observer direction and brightness ratio => there is a set of solutions
- More ratios are necessary for a unique solution

# Amplitude method

- Measurement of brightness ratio from light curve.
- Determination of the celestial coordinates of satellite, Sun, observer.
- Calculation of the phase angle.
- Construction of the satellite coordinate system
- Numerical search of tumble axis directions comparing measured and simulated brightness ratios.
- Conversion of tumble axis directions in celestial coordinates.
- Iteration of the previous steps for at least three different observation geometries of the same object.

# Amplitude method: CZ-3B R/B

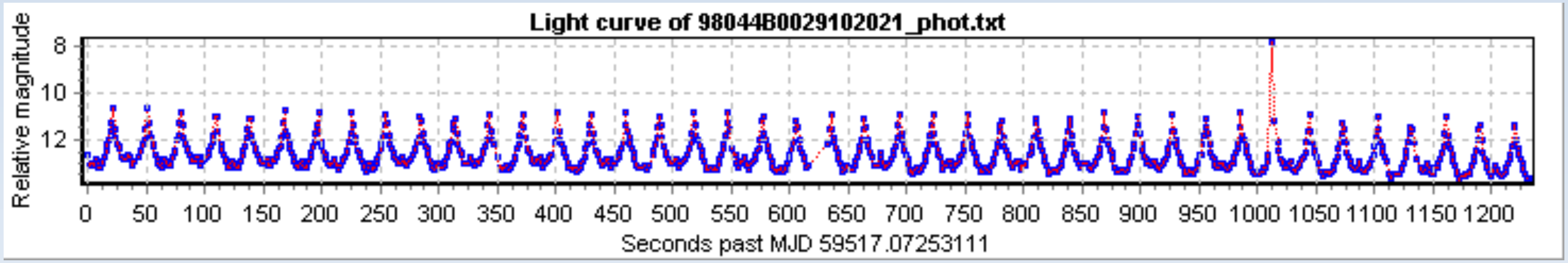


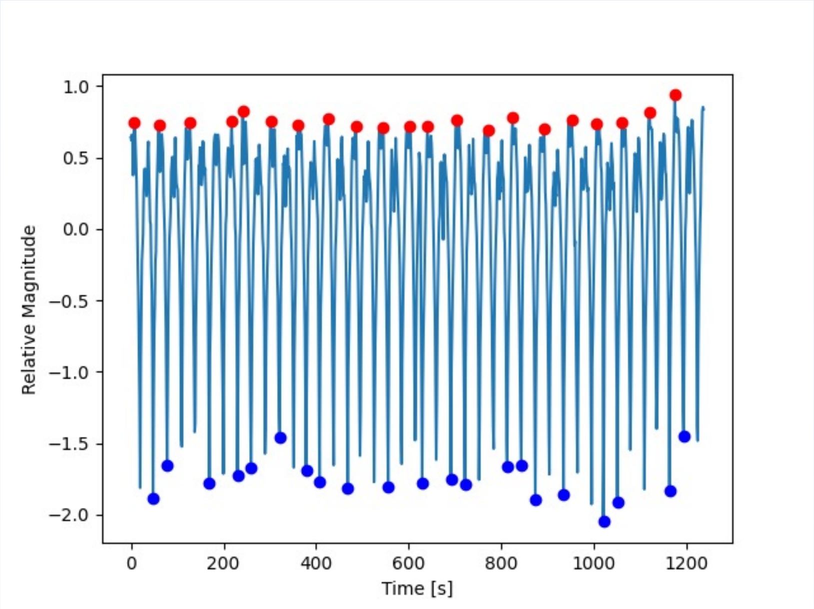


| Epoch | Phase angle [deg] | Brightness ratio | Std. deviation | Threshold |
|---|---|---|---|---|
| 21-Aug-2021 01:13:00 | 82 | -3.14 | 0.30 | ±1σ |
| 13-Sep-2021 23:10:00 | 49 | -2.81 | 0.38 | ±1σ |
| 30-Oct-2021 01:54:00 | 32 | -2.38 | 0.14 | ±1σ |

# Amplitude method: CZ-3B R/B

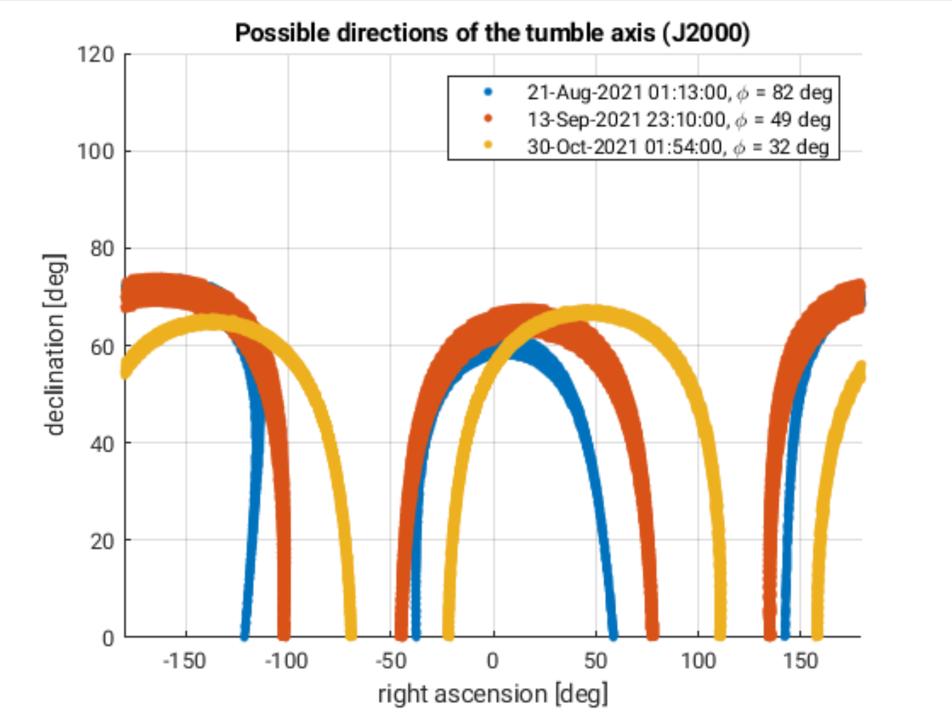


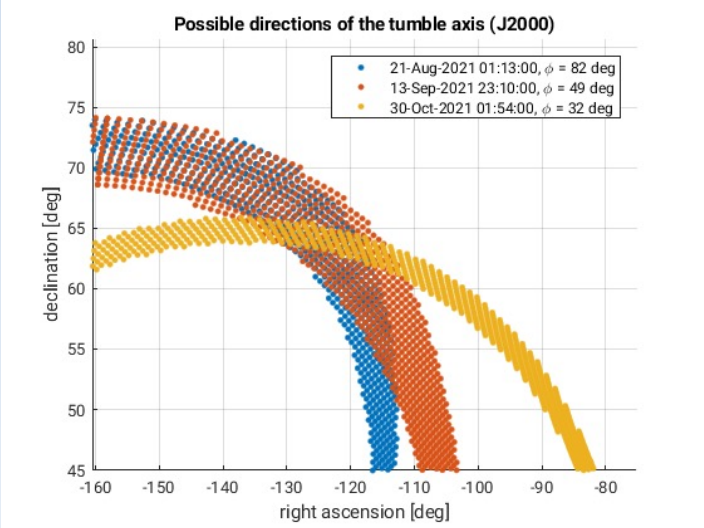


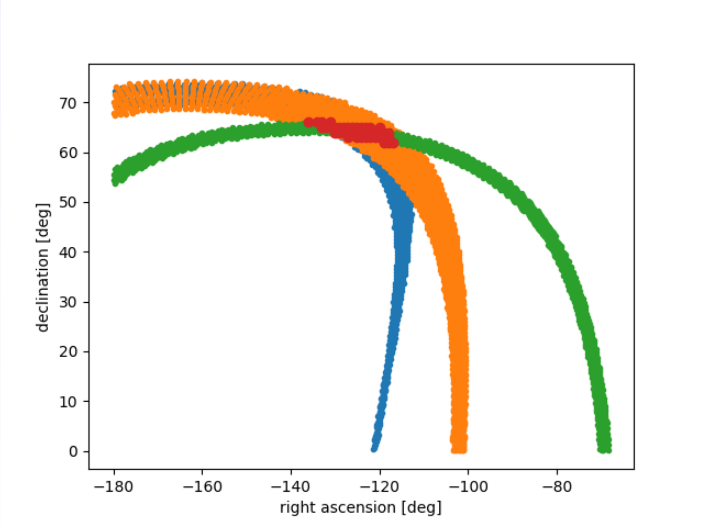


- Solution regions for 3 light curves
- Intersection shows spin axis direction
- Script identifies region of overlapping

# Simulated light curves:  CZ-3B R/B

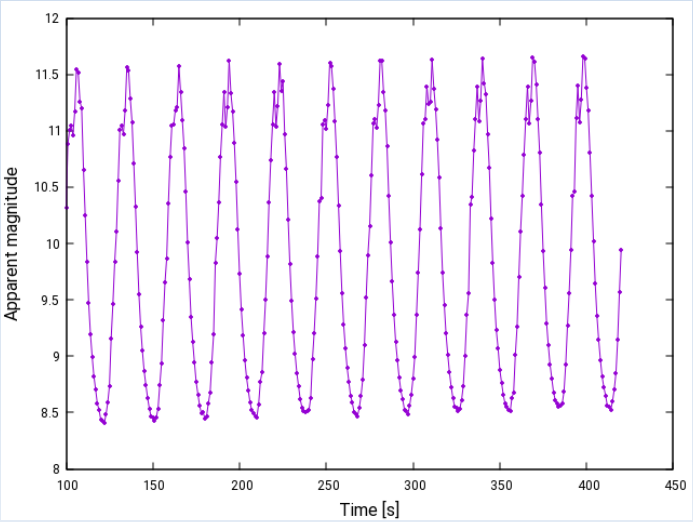


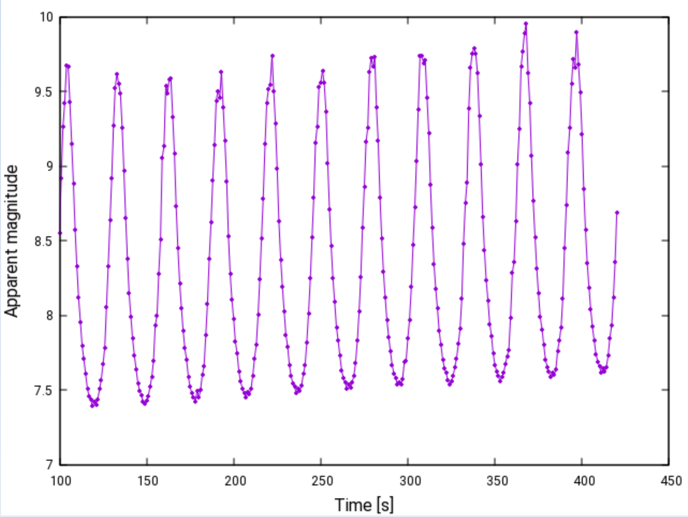


- IOTA simulations at 3 obs. epochs
- Top/bottom absorption coeff. = 1
- Rotation axis (RA 235.2°, DEC 64.1°)
- Brightness ratios from obs.:
  -3.1, -2.8, -2.4
- Simulated brightness ratios:
  -3.1, -2.3, -2.0
- Possible divergence due to shape/reflection model

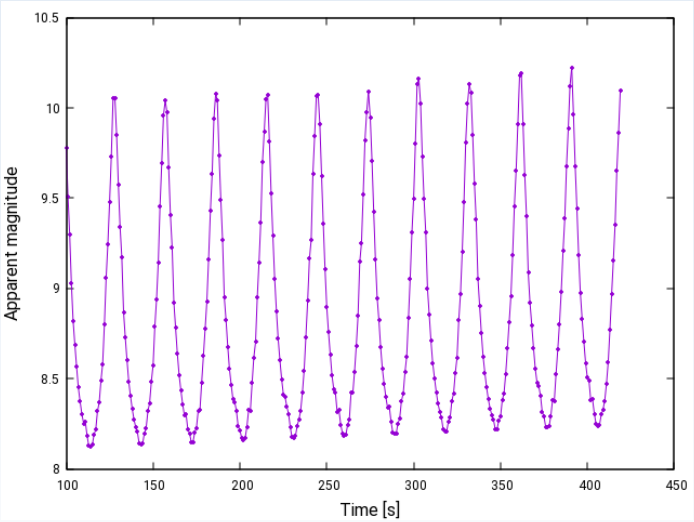

# Solution evaluation

- Graphical intersection shows that in principle there is a solution
- Although unlikely, it can be that intersection shows not the real spin axis
- If assumption not fulfilled, error exceeds the formal value given by measurement noise
- If spin axis not constant, solution is kind of an average orientation

- Simulations for the above case CZ-3B R/B on GTO orbit:
  - Time interval of 3 observations is about 2 months
  - Gravity gradient torque causes precession of spin axis
  - Spin axis might change orientation of 30° within 2 months
- Ideally for low orbits: observation series within few days

# Simulated light curves: Envisat

- Validation of IOTA simulated light curves
- Availability of quite accurate Envisat attitude state in the past
- Joint CMOS-SLR-Radar campaign 21.09.2016 (previous ESA Attitude project)

| **Solution ID** | **Passage** | **Source** | **roll, pitch, yaw [deg]** | **angular velocity vector: Wx, Wy, Wz [deg/s]** |
|---|---|---|---|---|
| **1.1** | **ENVISAT 2016-09-21 18:53 UTC** | ISAR, refined | 147, -76, -102 | 0.04, 0.025, -1.659 |
| **3.1** | **ENVISAT 2016-09-21 20:31:18.6 UTC** | SLR, time corrected | 117.0, -46.3, -69.8 | 0.0, 0.0, -1.6774 |

# Simulated light curves: Envisat

| | a286 (stainless steel) | aa7075 (aluminum alloy) | cfrp (polymer composite) | cfrp-new (polymer composite) | envi-comp1 | s1-sarmat (radar antenna) | sol-ar-swarm (solar panel) |
|---|---|---|---|---|---|---|---|
| nominal | 0.5 / 0.47 | 0.5 / 0.16 | 1 / 0 | 1 / 0 | 0.5 / 0.16 | 0.5 / 0.5 | 1 / 0.9 |
| modified | 0.1 / 0.9 | 0.1 / 0.1 | 0.9 / 0.1 | 0.9 / 0.1 | 0.9 / 0.1 | 0.1 / 0.1 | 0.2 / 0.98 |

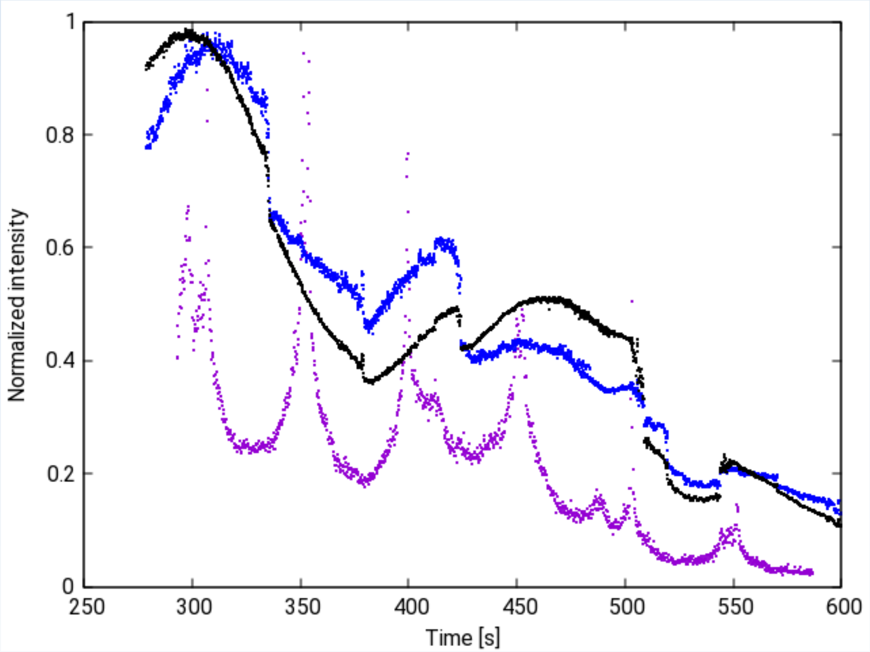


- Violet: observed light curve
- Black: one material
- Blue: nominal material reflection coeff.

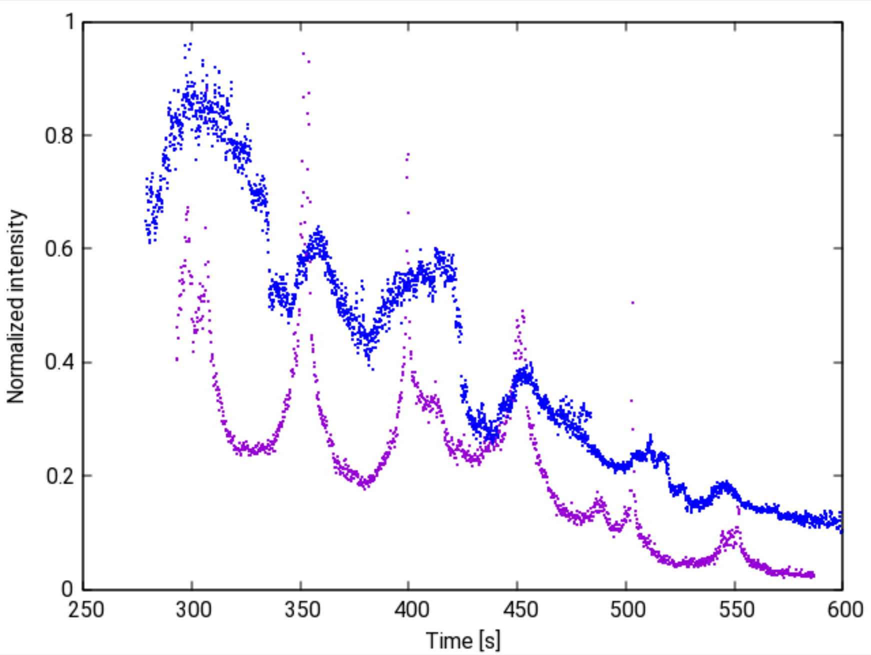


- Violet: observed light curve
- Blue: modified material reflection coeff.

# Simulated light curves: Envisat

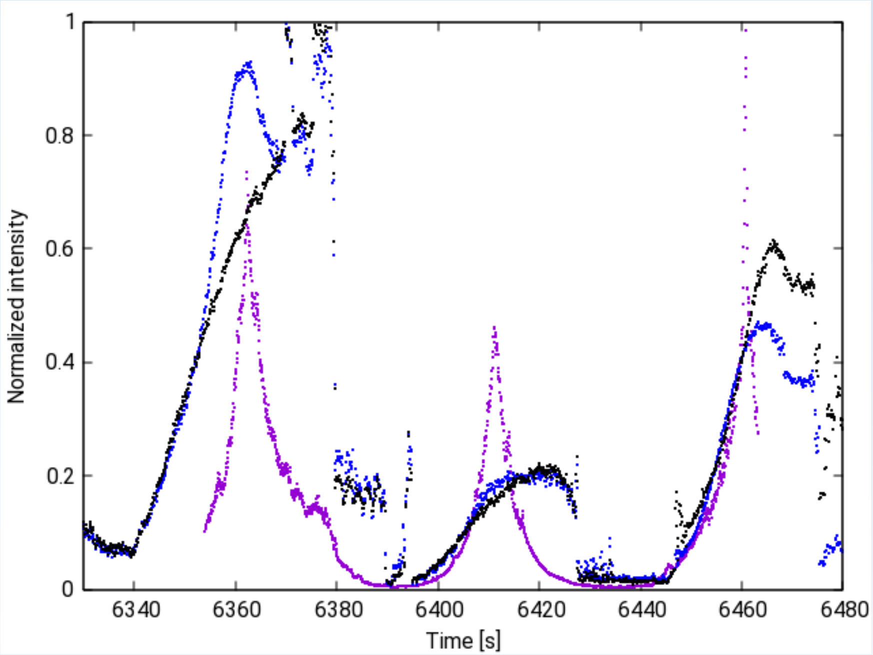


- Violet: observed light curve
- Black: one material
- Blue: nominal material reflection coeff.

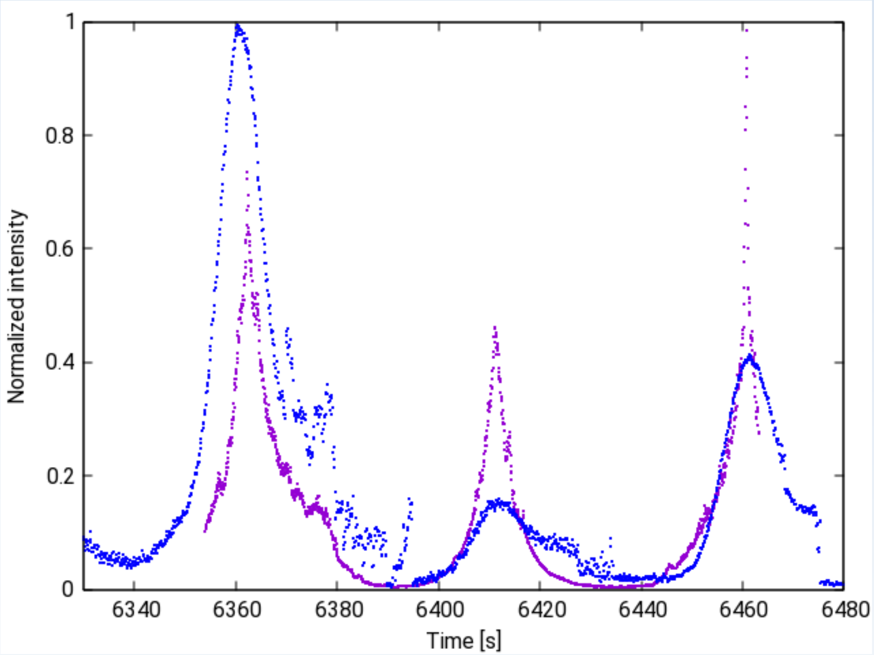


- Violet: observed light curve
- Blue: modified material reflection coeff.

# Method of Yanagisawa et al.

- Simple formulation for ellipsoid, function of $\theta$
- $\alpha$ phase angle, $M$ optic coeff.

$$A = (1 + M\alpha)A_0 \qquad A_0 = \frac{a\sqrt{b^2\cos^2\theta + c^2\sin^2\theta}}{b\sqrt{a^2\cos^2\theta + c^2\sin^2\theta}}$$

- For cylinder:

$$A_0 = 1/\left(\cos\theta + \frac{\pi}{4}Rd\sin\theta\right)$$

- $d$ diameter divided by length
- $R$ albedo of bottom/top divided by side albedo
- Solution as least squares problem
- At least as many observations as parameters
- Precession parameters can be estimated

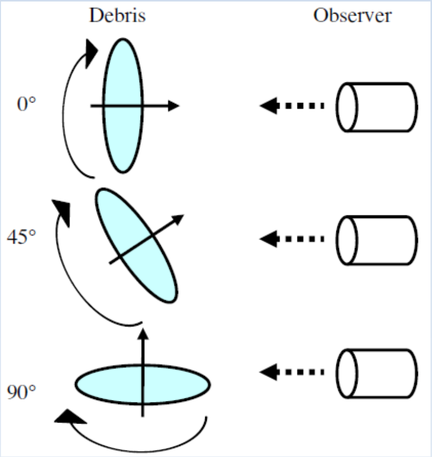


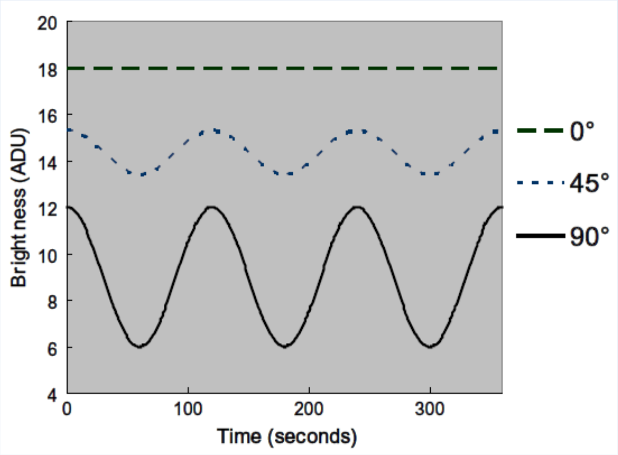

# Precession

$$A_0 = 1/\left(\cos\theta + \frac{\pi}{4} Rd \sin\theta\right)$$

$$R.A. = RA_0 + D\sin(2\pi t/T + \beta)/\cos(Dec.)$$
$$Dec. = Dec_0 + D\cos(2\pi t/T + \beta)$$
$$l = \cos(R.A.)\cos(Dec.)$$
$$m = \sin(R.A.)\cos(Dec.)$$
$$n = \sin(Dec.)$$

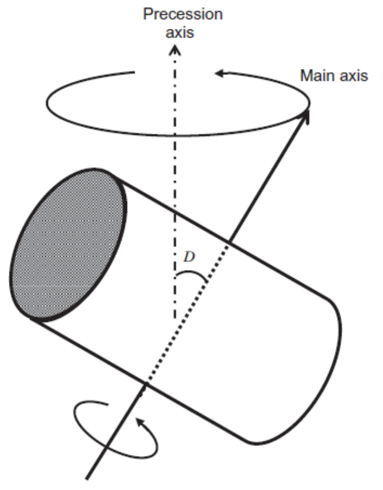


- $RA_0$ $Dec_0$ (precession axis)
- RA, Dec (rot. axis)
- Approximation for small D
- For larger D it is more complicated (e.g. Rodrigues rotation formula)
- Additional estimated parameters:
  - $RA_0$ $DEC_0$
  - D (precession angle), T (precession period), β (phase)

# LSQ convergence

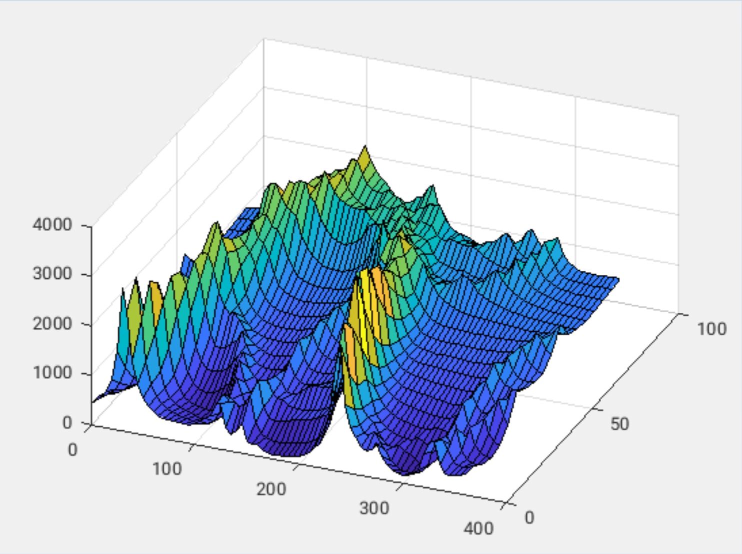


- Loss function vs RA/DEC of spin axis
- Tests with all precession parameters show low reliability
- Use several starting points (multiple local minima)
- Tests w/o precession parameters show reproducible results (different LSQ start points with same result).
- However, high residuals
- Problem of Yanagisawa model?

# Comparison with Williams

- Yanagisawa depends on phase angle through an empirical formula: $(1 + M\alpha)$
- But it does not depend on the absolute direction of Sun and of the spin axis
- Compare with Williams, no top/bottom reflection (R=0) => $\frac{F_{min}}{F_{max}} = \frac{|\cos\theta|}{1+M\alpha}$

=> Yanagisawa model: approximation for $\theta$ close to 90°

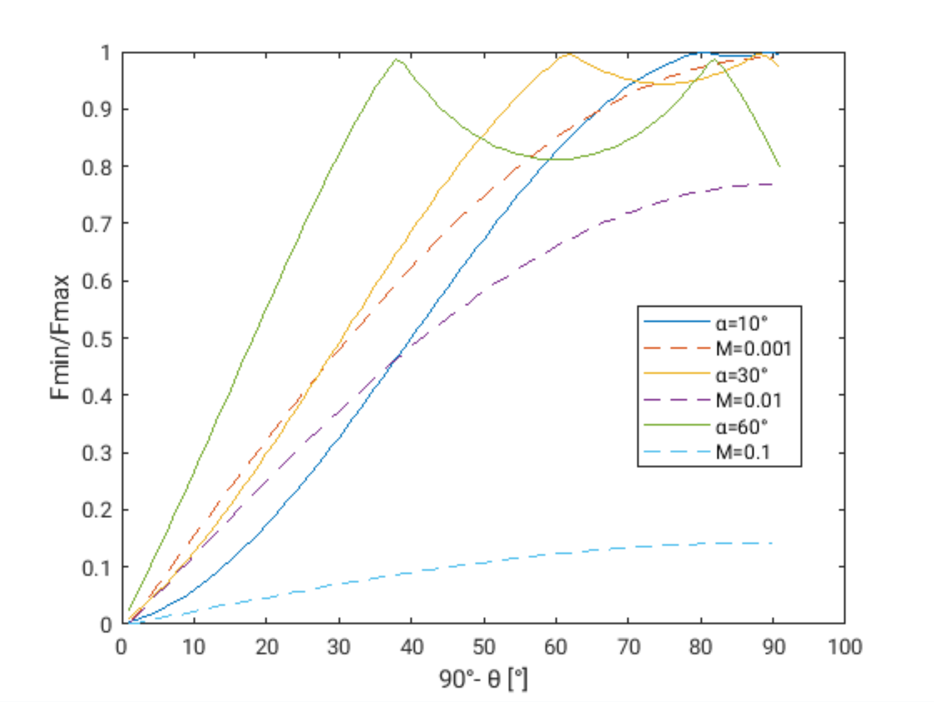

# Outlook

- Introduction
- Attitude models
- IOTA software
- Observation campaign
- Radar observations
- Amplitude method
- Epoch method
- Attitude evolution
- Conclusions

# Attitude evolution

- Compare IOTA simulations with literature results
- Orbit: 800 km, inclination 70°, angular velocity 1 rad/s
- Only effect of Eddy currents
- Exponential damping and stabilization
- Angle $\theta_A$ betw. angular velocity and axis of maximum inertia => flat spin
- Eddy currents: transition phase (typical bend) after 1 year
- $I$ = 5 x $10^3$ kg $m^2$, $M$ = 2 x $10^5$ S $m^4$, B = 40’000 nT

=> Decay rate $\tau \approx \frac{I}{M\,B_\perp^2} \approx 2.2\ \text{yr}^{-1}$

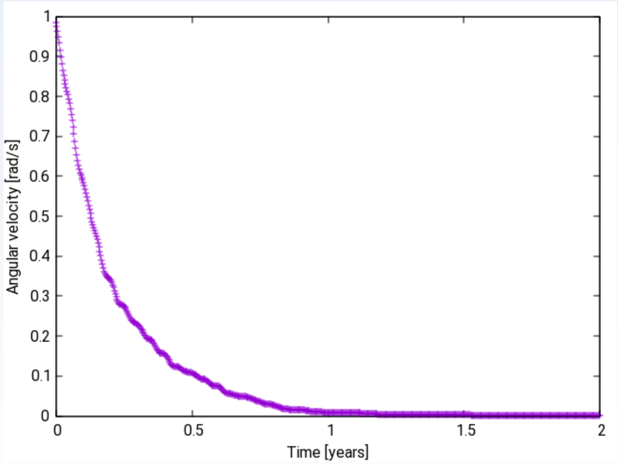


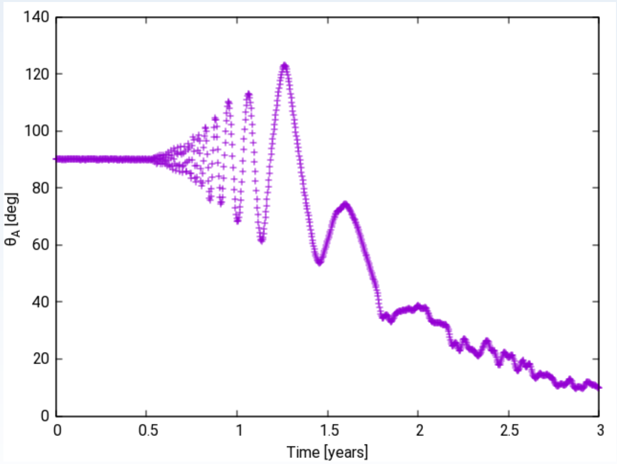


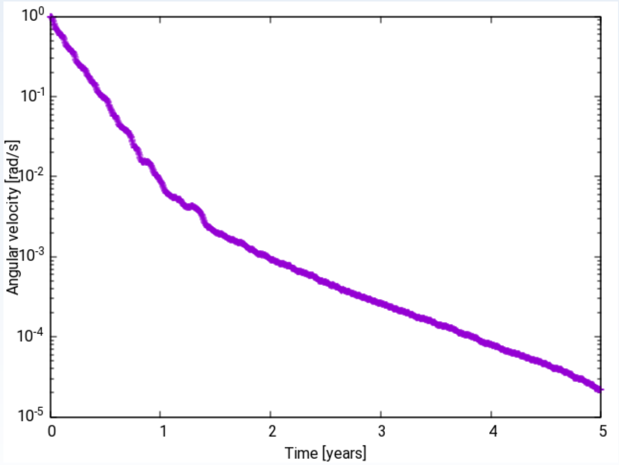

# Attitude evolution

- Combined effect of eddy currents and gravity gradient
- Initial angular velocity 0.5°/s
- Precession of angular moment, phase $\varphi_L$ relates to projection angular momentum onto the orbital plane
- $P_{rot}$ = 60 s, orbit at 600 km altitude, ratio $\frac{I_0}{I_0 - I_3} \approx 1.28$, and $\theta$ = 70°
- $P_g = \frac{2\pi^2 I_0 r^3}{\mu(I_0 - I_3) P_{rot} cos\theta} \approx$ 2 weeks
- Stabilization with gravity gradient torque
- Orbital resonance 1:1, angular velocity 0.06°/s
- Oscillation of angular velocity (capture phase) $\omega_g = \sqrt{\frac{2\mu(I_0 - I_3)}{I_0 r^3}} \approx$ 1.3 h

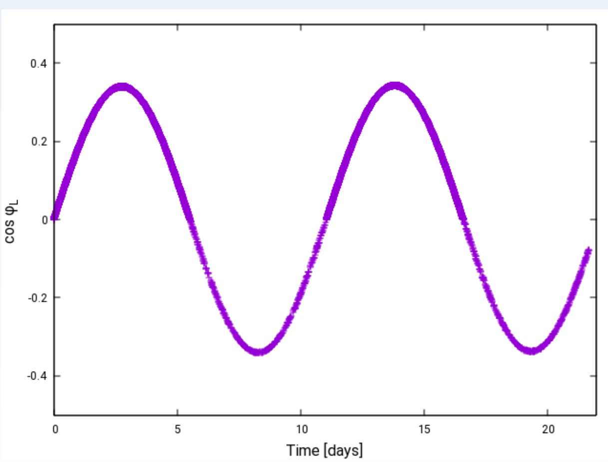


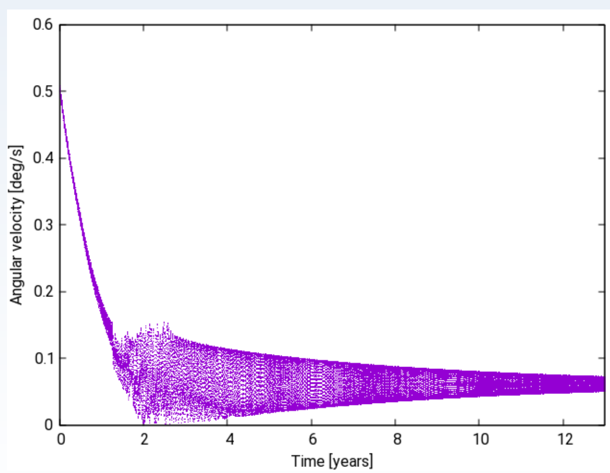


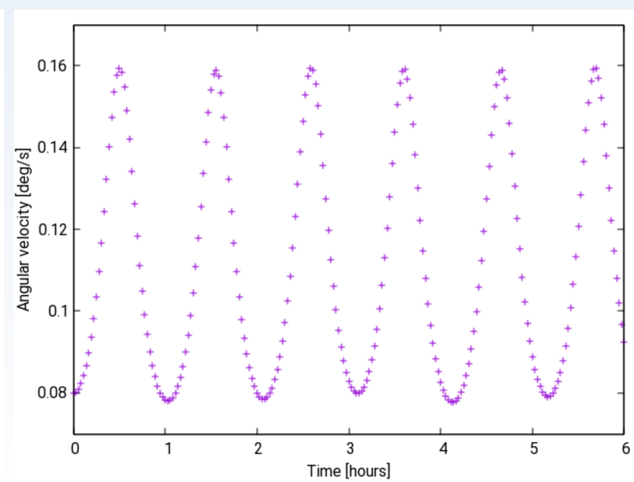

# Attitude evolution

- IOTA with only Solar Radiation Pressure considered
- Box (2 x 2 x 2 m), wings (1 x 2 m), 10° canting angle, polar orbit
- Simulation with different front/back panel properties
- Annual variation with secular slope of 0.02 rad/s
- Earth radiation force and penumbra with LEO at 800 km
- Surface of 8 $m^2$ => $10^{-5}$ N expected
- Penumbra time in LEO about 10s

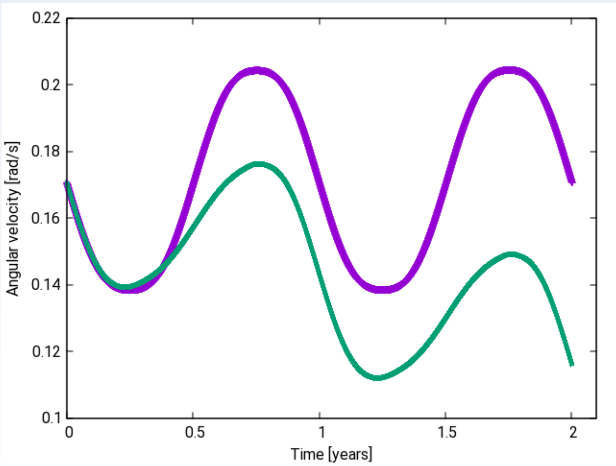


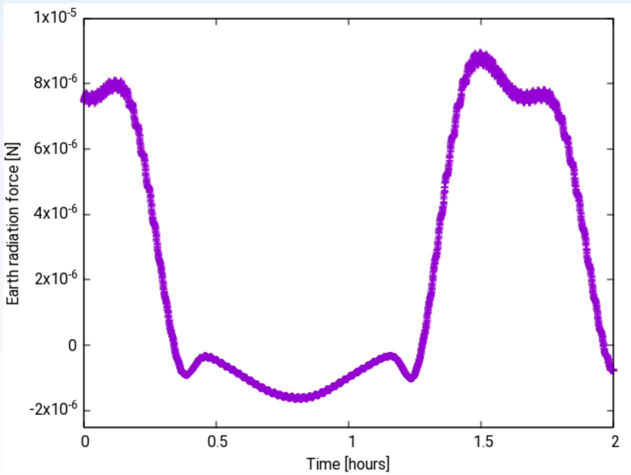


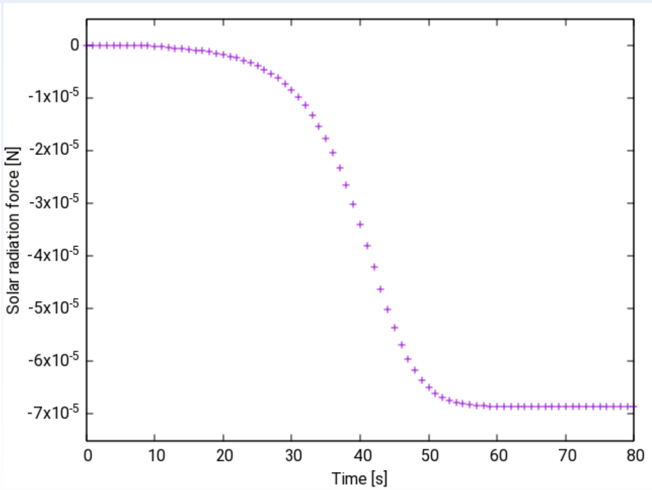

# Spin rate evolution: CZ-3B R/B

- Combination of observations from Graz, Zimmerwald, TIRA
- Evolution of spin rate determined for several objects
- Check the consistency of the extracted periods
- Example: CZ-3B rocket body (2019-090D) => $\tau \approx \frac{I}{M\,B_{\perp}^{2}}$
- IOTA simulation: consider real distribution of Earth magnetic field

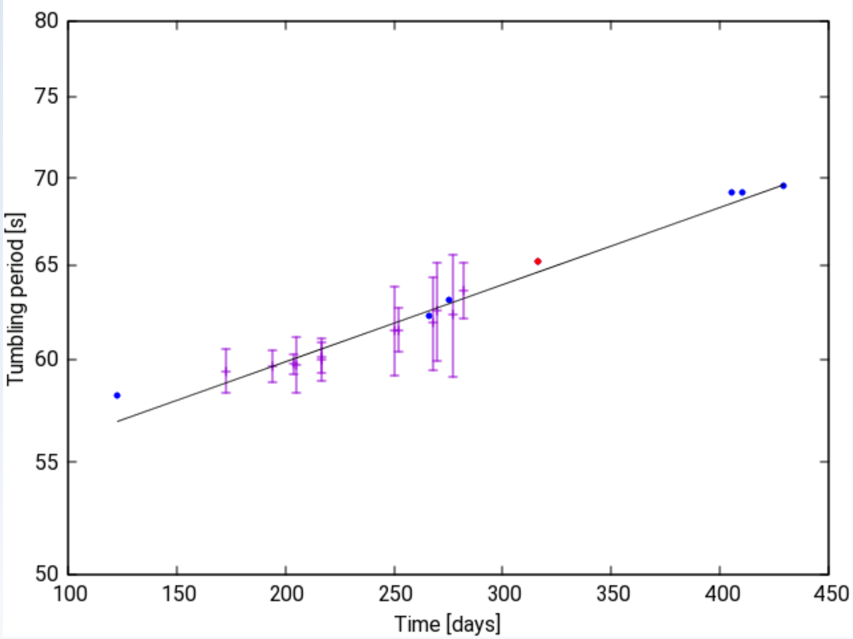


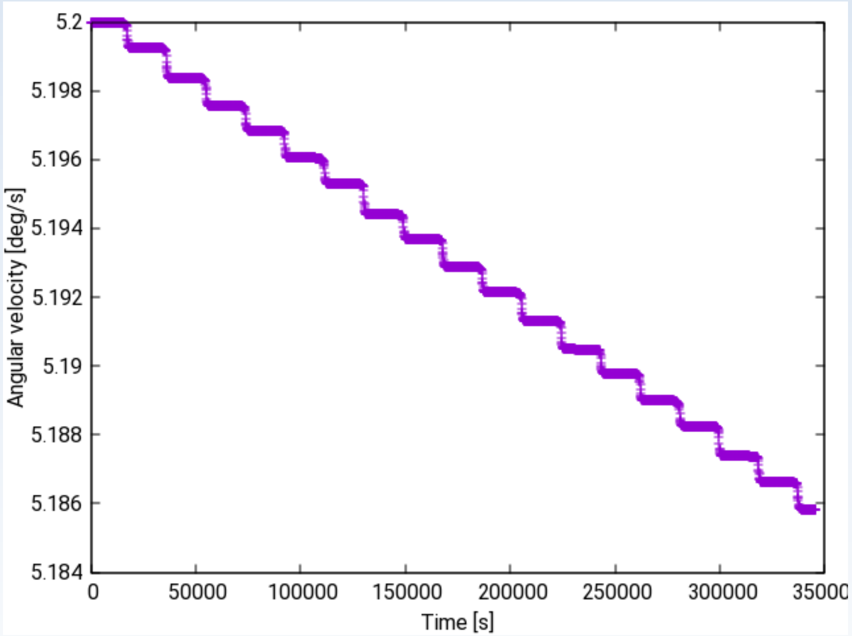


- Violet: Graz photon counter
- Red: TIRA, Blue: Zimmerwald
- Spin rate from fit: 0.24 $yr^{-1}$

- Consider: CZ-3B ~ Ariane 4 H10
- Refined values: 35’000 km $m^2$ , 4 x $10^6$ S $m^4$
- Simulation gives: ~ 0.2 $yr^{-1}$

# Spin rate evolution: Jason-2

- Low effect of damping eddy currents, 1300 km altitude
- Solar panels => effect of SRP
- From SLR, radar: spin axis approx. perpendicular to orbit plane
- From radar: solar panels almost orthogonal
- Different reflection coeff. for front/back side of panels

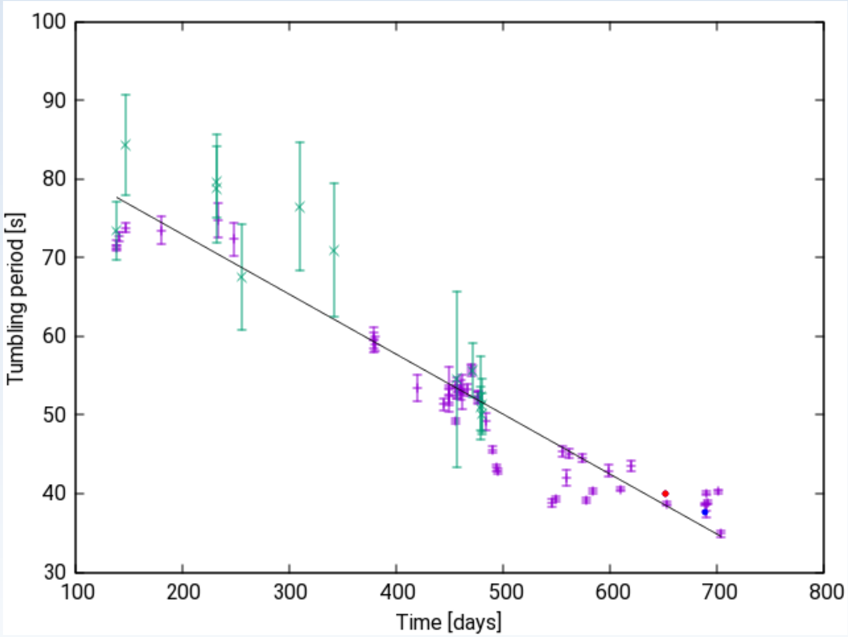


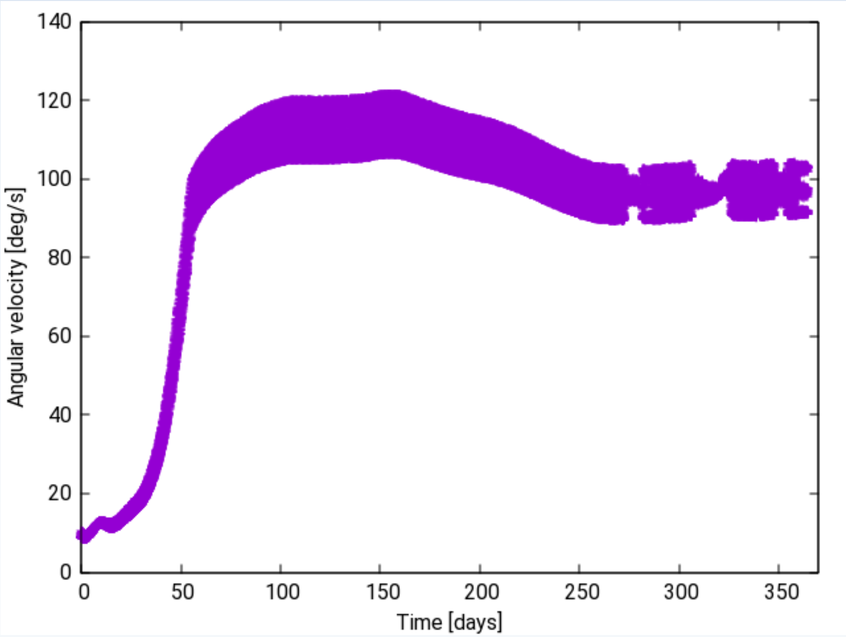


- Violet: Graz photon counter
- Green: Graz SLR
- Red: TIRA, Blue: Zimmerwald

- Spin rate increase, not regular pattern
- Low angular velocity does not keep attitude stable
- Wind wheel model not applicable

# Outlook

- Introduction
- Attitude models
- IOTA software
- Observation campaign
- Radar observations
- Amplitude method
- Epoch method
- Attitude evolution
- Conclusions

# Conclusions

- Development of attitude models, attitude determination methods, simulation s/w
- Attitude determination: amplitude method
  - Method of Williams: spin axis orientation of R/B can be determined with 3 or more observations
  - Accuracy from few to tens of degrees
  - Some assumption, e.g. constant spin axis during observations interval, strongly influence the accuracy
  - Method of Yanagisawa uses approximate model and can be used only in a limited range of observation geometries
- Attitude determination: epoch method
  - Characterization of the limits and required spin period accuracy

  => Improvement of preprocessing for period extraction. Savitzky-Golay on local data samples for successful detrended time derivative series
  - Apparent motion is a limiting factor: in GEO too small
  - In LEO enough apparent motion, but accuracy limits a significant prediction of spin orientation
- Attitude simulation software and evolution models
  - Simulation of light curves for objects with different materials (Envisat, R/B)
  - Simulation of attitude evolution under the effect of eddy currents, gravity gradient, solar radiation
  - Prediction of spin rate for R/B
  - Large amount of observations, more than 20 objects, over 2 and more years, spin periods and trends
- Definition of new process and product formats and standards

# Tumbling motion assessment for space debris objects

**Final presentation**

September 9, 2022

# IOTA improvements in WP4000

- Major tasks
  - Pre-computed coefficients
  - Magnetic tensor model
  - Earth radiation model
  - IOTA GUI simulation manager and simulation setup
- Minor tasks
  - S/C geometry surface reflectivity
  - Dynamic solar activity for the aerodynamics model
  - Geometry handling optimization
  - TLE import via CSTATE
  - Earth shadow penumbra region
  - Generic  attitude damping function
  - Space-based observer
  - Thermosphere wind model (HWM14)
  - Output extension: Sun direction, along-track, and radial vectors [and torque vectors as debug output]

# Pre-computed Aerodynamic and Radiation pressure coefficients

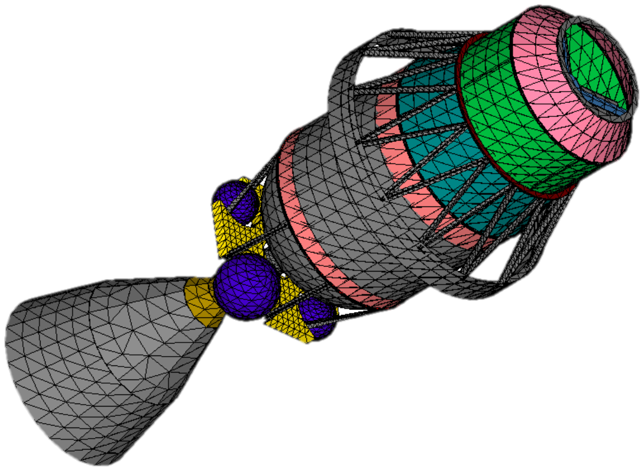

# Pre-computed Aerodynamic and Radiation pressure coefficients

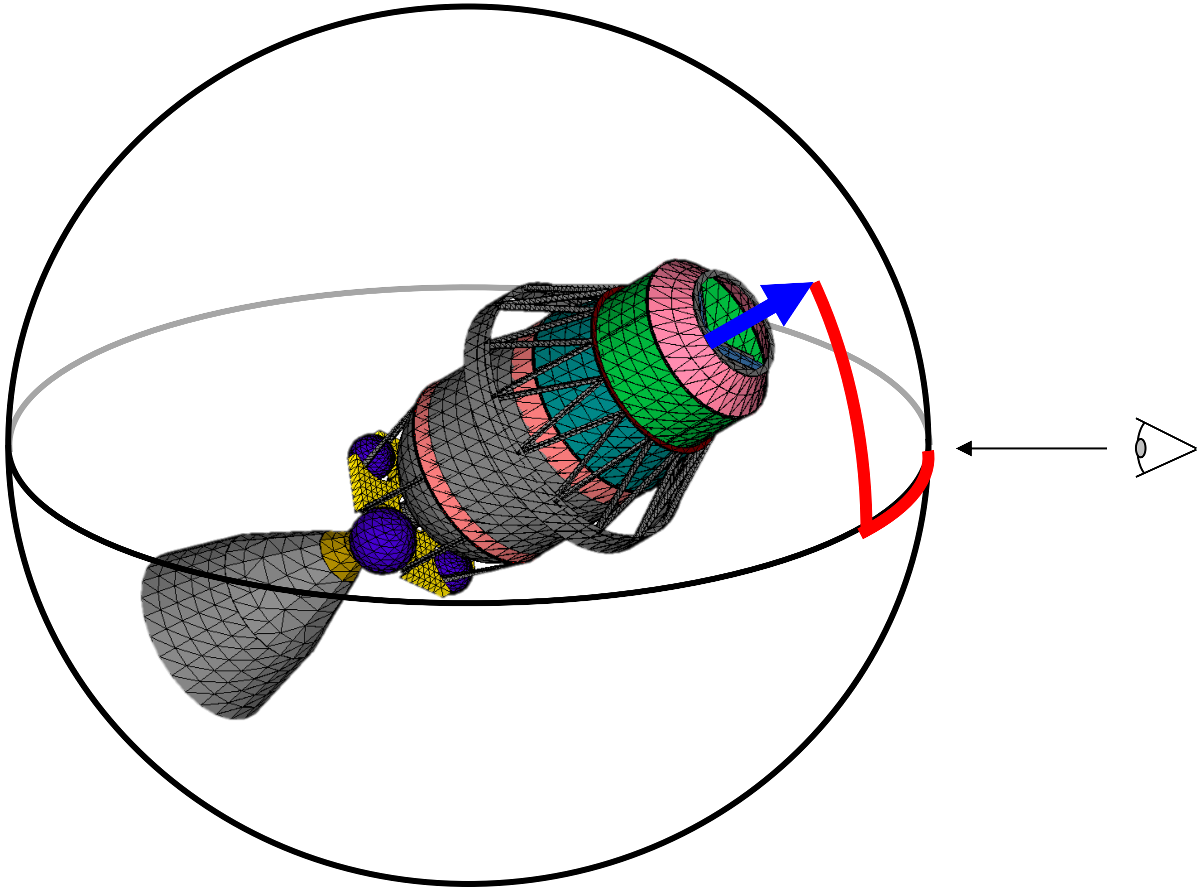

# Pre-computed Aerodynamic and Radiation pressure coefficients

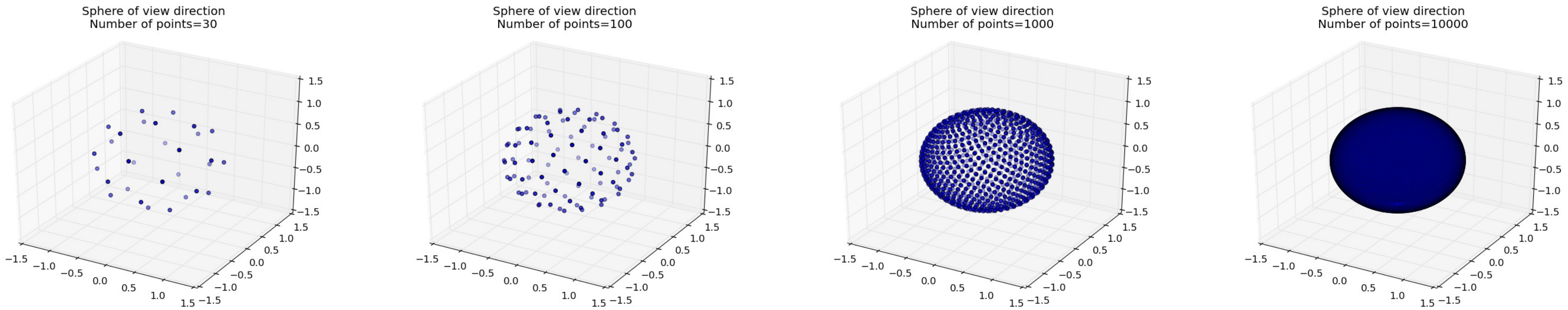

# Pre-computed Aerodynamic and Radiation pressure coefficients

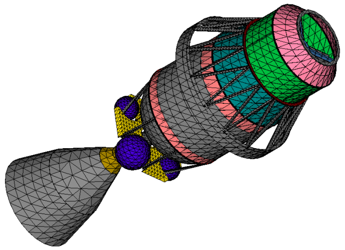

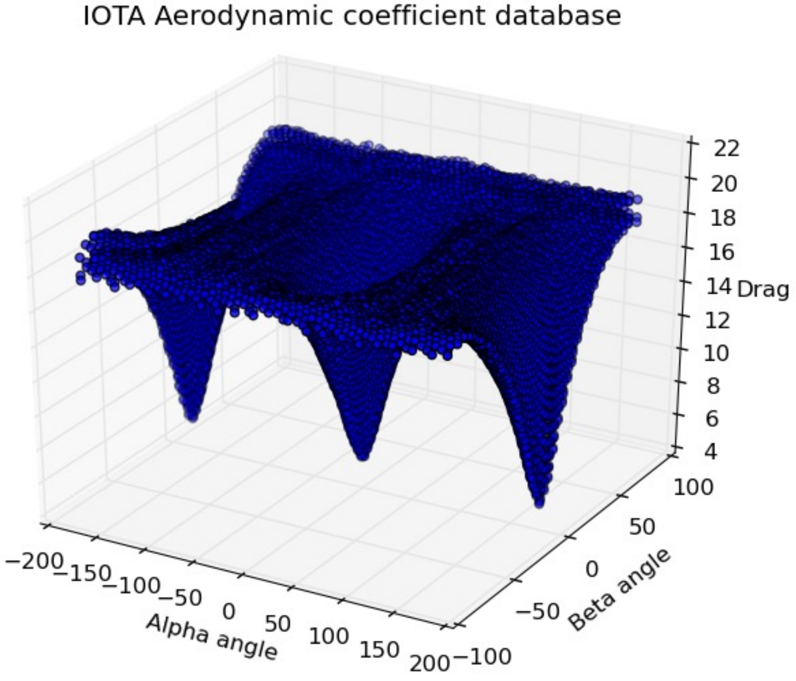


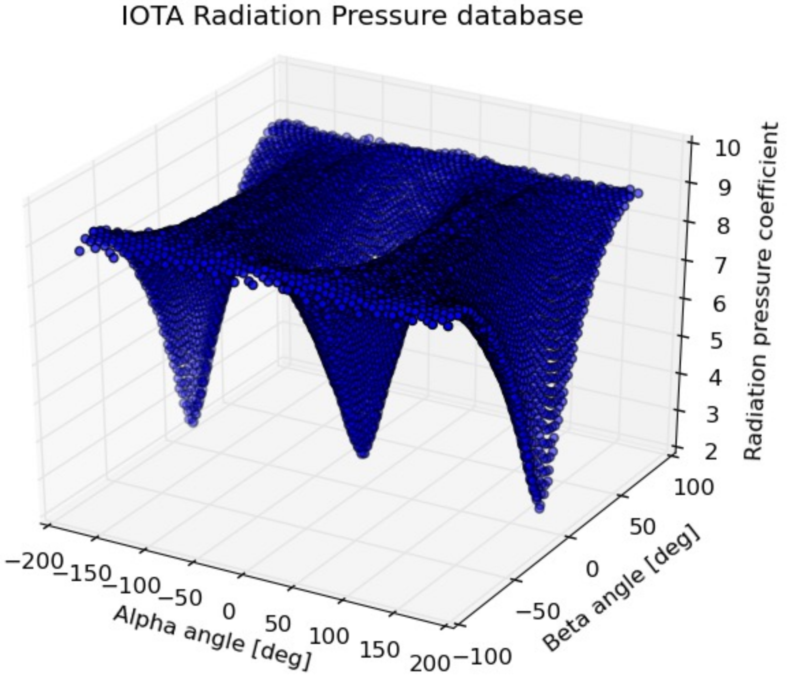

# Magnetic tensor model

The S/C is seen as a rotating conductive body in the presence of magnetic field. This induce **eddy current torques** on the body, which decrease its rotational speed and cause a change in the direction of the the rotation axis.

$$T_{eddy} = \mathrm{M}(\bar{\omega} \times \bar{B}) \times \bar{B}$$

M~ Magnetic tensor
$\bar{B}$~ Magnetic field
$\bar{\omega}$~ Angular velocity

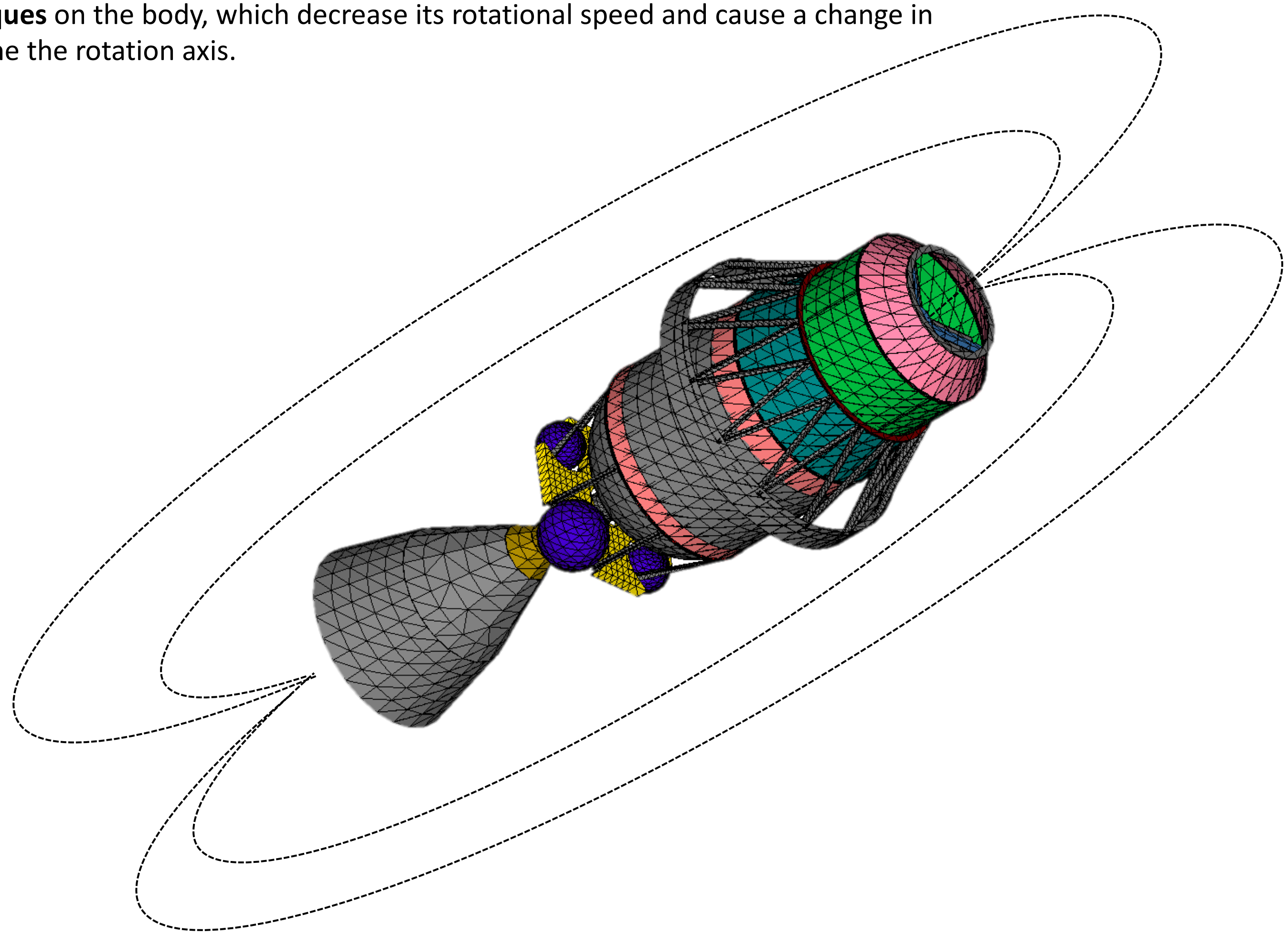

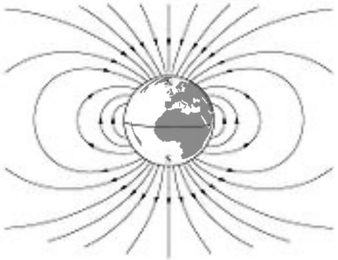

# Illumination of Earth surface with acceleration due to ERP and SRP

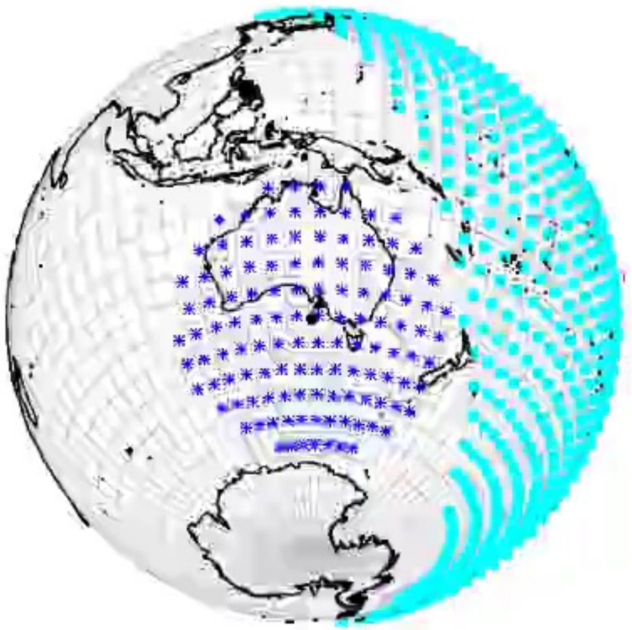

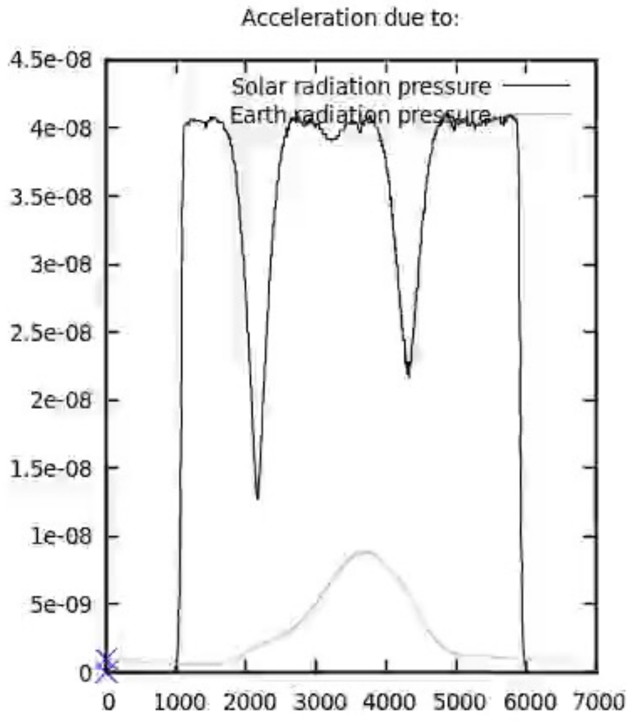

# IOTA GUI simulation manager and simulation setup

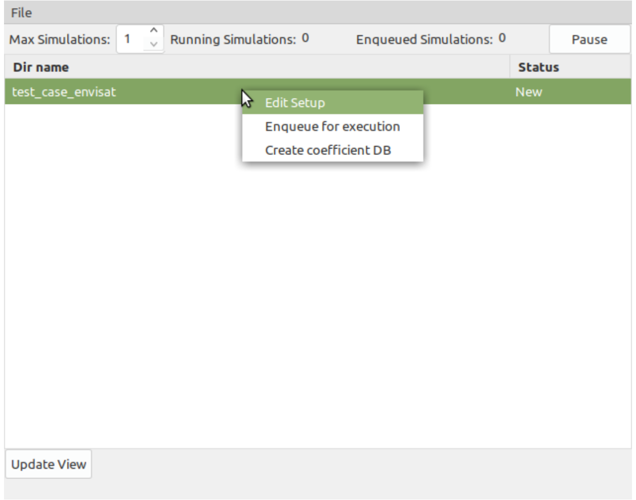


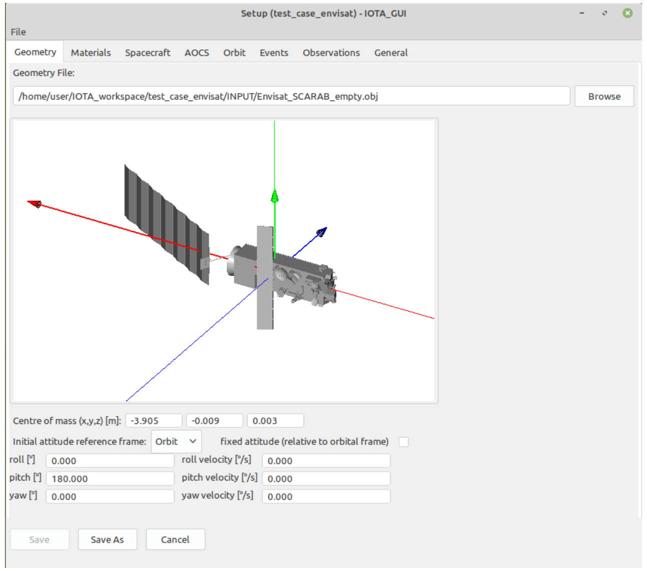


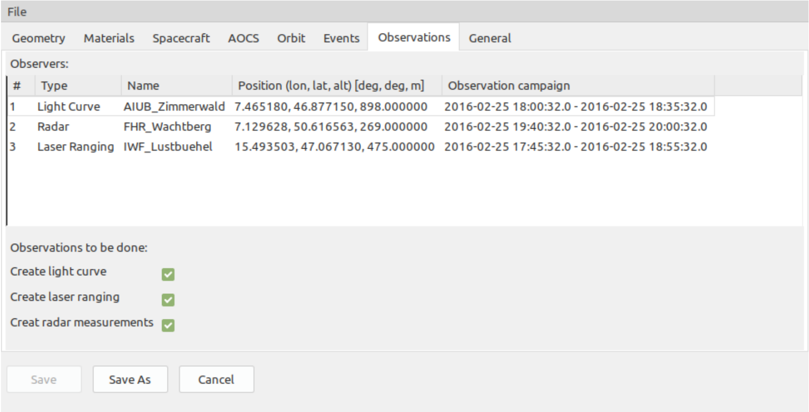


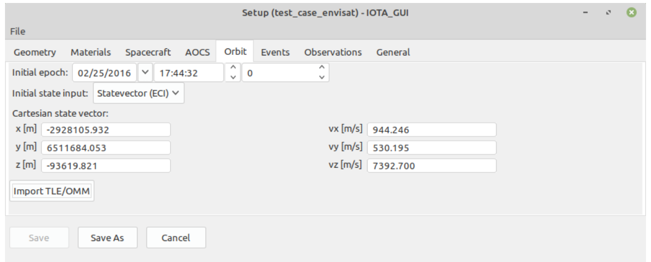


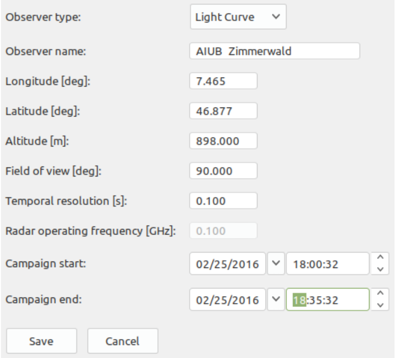

# IOTA GUI result view

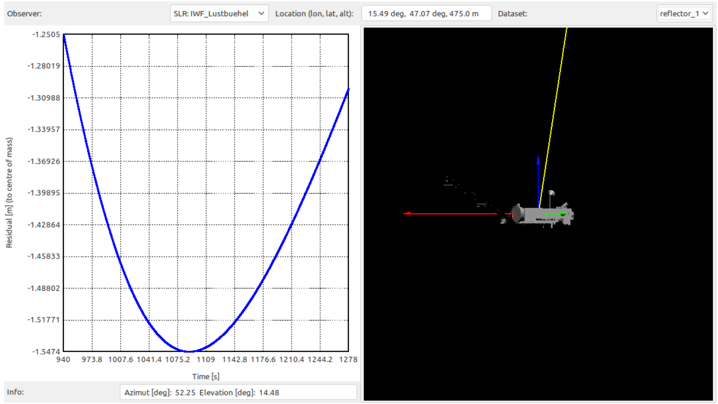


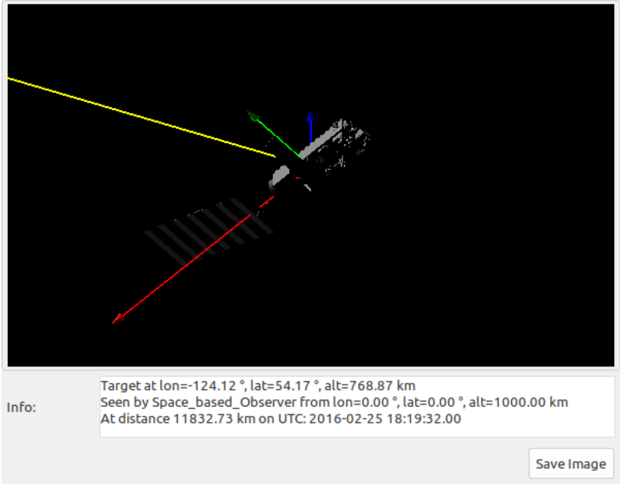


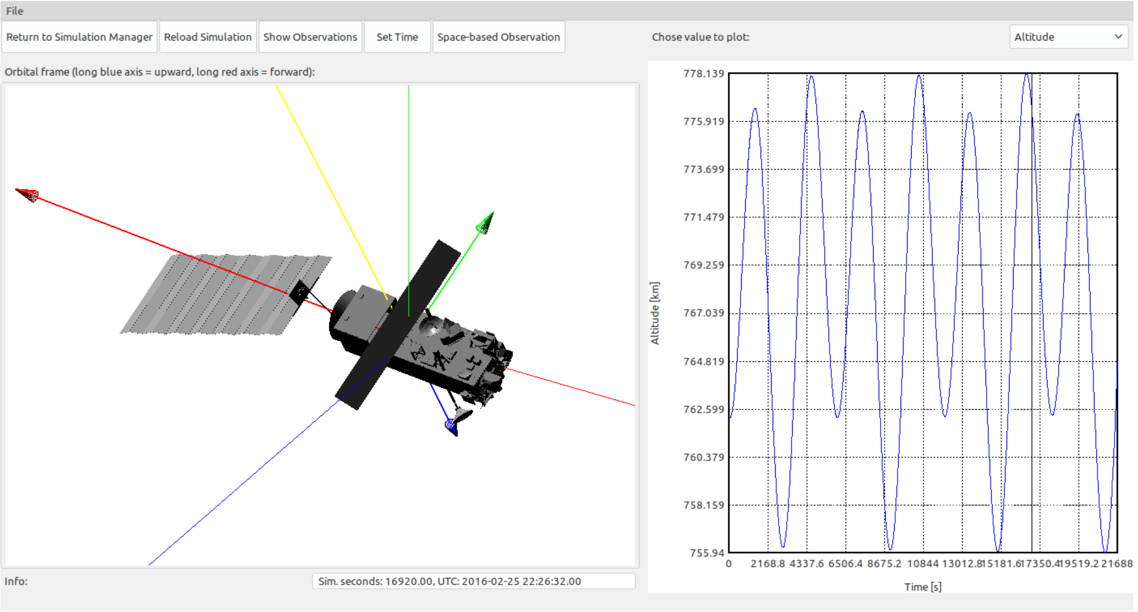

## Possible future improvments

- General
  - Uncertainty Quantification via MC for simulation input (similar to SCARAB4)
  - pyIOTA – Python wrapper (similar to pyDRAMA/pyMASTER)
  - Write full precision snapshots to allow continuation of a simulation
    - Recover from a crash or continue with modified settings

```python
import pyIOTA
import os

# creates a configuration
setup = pyIOTA.get_basic_job_setup()

# change path to geometry in basic setup
setup["geometry"] = os.path.abspath( "/home/user/path/to/geom.obj" )

# run job with setup
job = pyIOTA.run(setup)

# extract results from job
time = pyIOTA.data_processing.get_simulation_time(job)
anglar_momentum = pyIOTA.data_processing.get_angular_momentum(job)

# plot
pyIOTA.plot.ground_track( job )
```

- Models and methods
  - Extend eddy current damping for slow tumbling objects (DD-0002 Eq. 6)
  - Parallelisation of the coefficient DB calculation
  - Rotating S/C parts, e.g. solar arrays (similar to DMF-03)
  - Use pre-computed coefficients for light curve generation (similar to DMF-05)
  - Improve RCS model (similar to DMF-05, model TBD)
  - Implement MIRAD micro-particle impact model
  - Consider YORP effect

Thank you for listening

Any questions?

# TUMBLING MOTION ASSESSMENT FOR SPACE DEBRIS OBJECTS

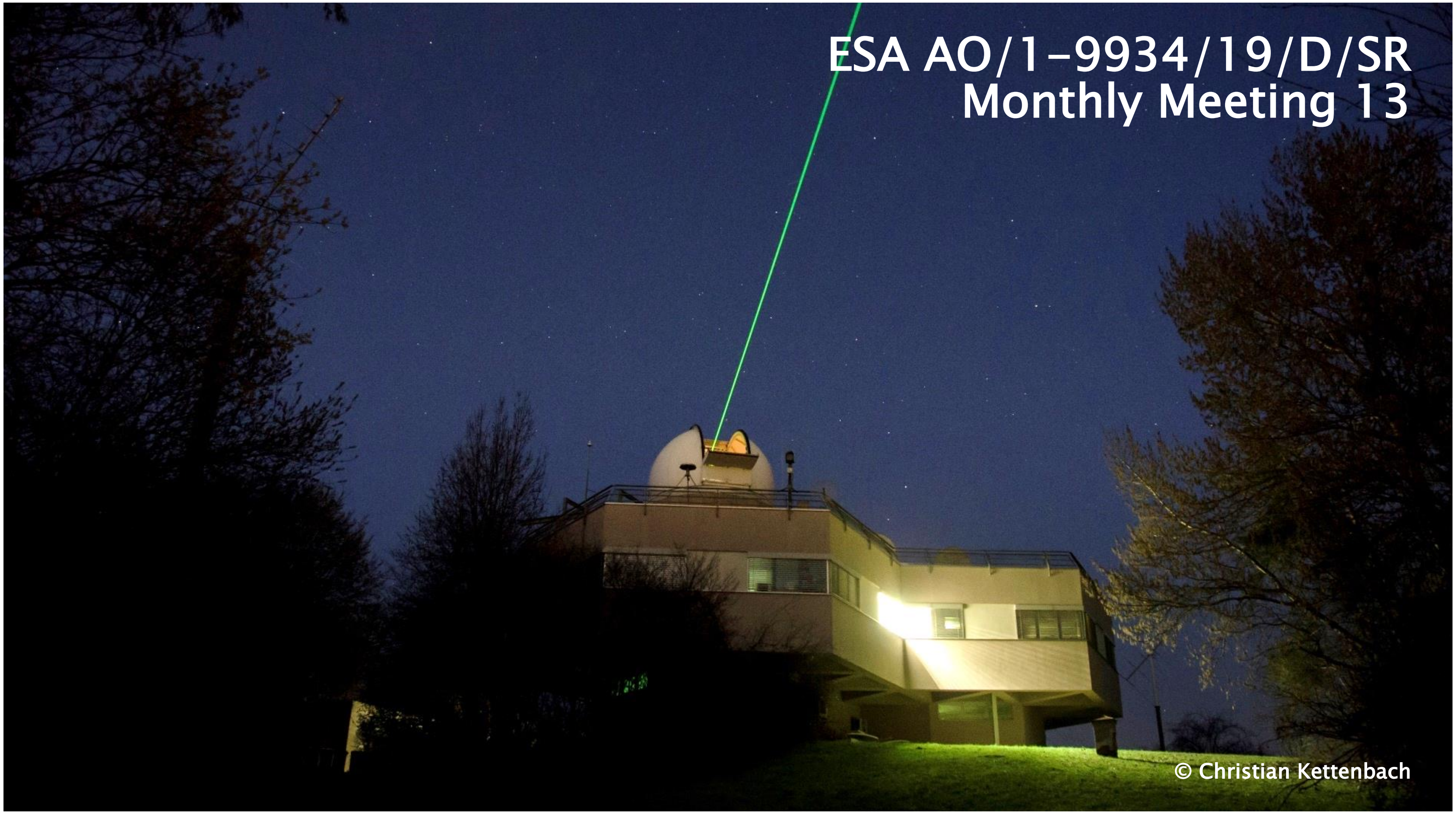


Michael Steindorfer, Daniel Kucharski, Franz Koidl, Georg Kirchner, Peiyuan Wang
Institut für Weltraumforschung, Österreichische Akademie der Wissenschaften

# OBSERVATION CAMPAIGN OVERVIEW

1) Historic data: 2018-2020, especially from former ILRS targets

2) Pre selection campain 2020: analysing current rotation behavior and „quality“ of light curves

3) Based on 2): reduction of target catalog to „object of interest“ catalog: 26 targets

4) Graz extensive observation campaign of 26 targets mainly performed in 2021

5) Few targets selected for joint tracking campain with different sensors

| Target | NORAD ID | Graz ID |
|---|---|---|
| Jason 2 | 33105 | JA2 |
| Envisat | 27386 | ENV |
| SL-16 rocket body | 25407 | 335 |

ÖAW IWF

# OBJECTS OF INTEREST LARGE LIST

| Orbit type | Number |
|---|---|
| <1500 km LEO objects | 6 |
| 1500 – 3000 km LEO | 2 |
| MEO | 5 |
| MEO elliptical | 1 |
| GTO | 3 |
| GEO | 3 |
| Special Interest / LEO | 3 |

| Eccentricity | Number |
|---|---|
| < 0.02 | 18 |
| > 0.5 | 5 |
| | |
| | |
| | |
| | |
| | |

| Inclination | Number |
|---|---|
| 80-100 ° | 6 |
| 60-80° | 5 |
| 40-60° | 6 |
| 20-40° | 0 |
| 0-20° | 6 |
| | |
| | |

| | Category | NORAD | CosparID | Name | Photometric pattern periodicity [s] | Observation techniques | | | Attitude determination methods | | | Launch date | RCS [m2] | Apogee altitude [km] | Perigee altitude [km] | Eccentricity | Inclination [deg] | Orbital period [h] |
|---|---|---|---|---|---|---|---|---|---|---|---|---|---|---|---|---|---|---|
| | | | | | | Optical imaging | Hypertemporal photon counting | Laser ranging | Amplitude methods | Epoch methods | Laser range analysis | | | | | | | |
| 1 | LEO < 1500 km, circular, DEB | 38345 | 2012-025F | h-2a_deb | 40.0 | Y | Y | Y | N | Y | Y | 17-May-2012 | 2.7 | 628 | 621 | 0.0005 | 98.2 | 1.6 |
| 2 | LEO < 1500 km, circular, DEB | 38346 | 2012-025G | h-2a_deb | 110.0 | Y | Y | Y | N | Y | Y | 17-May-2012 | 2.2 | 616 | 609 | 0.0005 | 98.2 | 1.6 |
| 3 | LEO < 1500 km, circular, R/B | 25407 | 1998-045B | sl-16_r_b | 30.0 | Y | Y | Y | Y | Y | Y | 28-Jul-1998 | 11.3 | 836 | 823 | 0.0008 | 71.0 | 1.7 |
| 4 | LEO < 1500 km, circular, P/L | 18187 | 1987-060A | cosmos_1867 | 90.0 | Y | Y | Y | N | Y | Y | 10-Jul-1987 | 3.3 | 803 | 778 | 0.0017 | 65.0 | 1.7 |
| 5 | LEO < 1500 km, circular, P/L | 33105 | 2008-032A | jason_2 | 19.8 | Y | Y | Y | N | Y | Y | 20-Jun-2008 | 3.2 | 1310 | 1298 | 0.0008 | 66.0 | 1.9 |
| 6 | LEO < 1500 km, circular, P/L | 18123 | 1987-053A | dmsp_5d-2_f8_usa_26 | 9.2 | Y | Y | Y | N | Y | Y | 9-Jun-1905 | 3.0 | 827 | 809 | 0.0013 | 98.7 | 1.7 |
| 7 | LEO 1500-3000 km, P/L | 25770 | 1999-031A | globalstar_m025 | 2.5 | Y | Y | N | N | Y | N | 10-Jun-1999 | 2.3 | 2045 | 2043 | 0.0002 | 52.0 | 2.1 |
| 8 | LEO 1500-3000 km, P/L | 26083 | 2000-008C | globalstar_m060 | 28.4 | Y | Y | N | N | Y | N | 8-Feb-2000 | 2.0 | 1612 | 1604 | 0.0005 | 52.0 | 2.0 |
| 9 | MEO, R/B | 39167 | 2013-023B | atlas_5_centaur_r_b | 6.7 | Y | Y | N | Y | Y | N | 15-May-2013 | 0.5 | 21421 | 20554 | 0.0158 | 56.2 | 12.5 |
| 10 | MEO, R/B | 40535 | 2015-013B | delta_4_r_b | 209.0 | Y | Y | N | Y | Y | N | 7-Jul-1905 | 26.2 | 20960 | 20785 | 0.0032 | 52.2 | 12.4 |
| 11 | MEO, R/B, highly elliptical | 44867 | 2019-090D | cz-3b_r_b | 27.5 | Y | Y | N | Y | Y | N | 16-Dec-2019 | ? | 17767 | 230 | 0.5703 | 55.2 | 5.3 |
| 12 | MEO, P/L | 23205 | 1994-050C | cosmos_2288_glonass | 9.2 | Y | Y | Y | N | Y | Y | 11-Aug-1994 | 3.9 | 19133 | 19124 | 0.0002 | 65.0 | 11.3 |
| 13 | MEO, P/L | 23833 | 1996-019A | navstar_37_usa_117 | 8.9 | Y | Y | N | N | Y | N | 28-Mar-1996 | 4.0 | 20747 | 20697 | 0.0009 | 53.5 | 12.3 |
| 14 | MEO, P/L | 28112 | 2003-056A | cosmos_2404_glonass | 125.0 | Y | Y | Y | N | Y | Y | 10-Dec-2003 | 3.4 | 19235 | 19027 | 0.0041 | 63.7 | 11.3 |
| 15 | GTO, R/B | 20947 | 1990-100C | ariane_42p_r_b | 11.9 | Y | Y | N | Y | Y | N | 20-Nov-1990 | 28.4 | 21739 | 278 | 0.6172 | 5.1 | 6.3 |
| 16 | GTO, R/B | 25405 | 1998-044B | cz-3b_r_b | 26.6 | Y | Y | N | Y | Y | N | 18-Jul-1998 | 21.9 | 35729 | 607 | 0.7154 | 17.5 | 10.6 |
| 17 | GTO, R/B | 38094 | 2012-009B | atlas_5_centaur_r_b | 20.8 | Y | Y | N | Y | Y | N | 24-Feb-2012 | 17.7 | 35203 | 3265 | 0.6235 | 19.1 | 11.3 |
| 18 | GEO, P/L | 15484 | 1985-007A | gorizont_11 | 24.3 | Y | Y | N | N | Y | N | 18-Jan-1985 | 5.0 | 35796 | 35772 | 0.0003 | 9.8 | 23.9 |
| 19 | GEO, P/L | 22653 | 1993-031A | astra_1c | 190.0 | Y | Y | N | N | Y | N | 15-Jun-1905 | 14.1 | 36230 | 36156 | 0.0009 | 12.5 | 24.3 |
| 20 | GEO, P/L, highly elliptical | 23230 | 1994-056A | ets_6 | 11.1 | Y | Y | N | N | Y | N | 28-Aug-1994 | 38.6 | 38794 | 8447 | 0.5058 | 16.7 | 14.4 |
| 21 | Special Interest Object | 23560 | 1995-021A | ers_2 | ? | Y | Y | Y | N | Y | Y | 21-Apr-1995 | 9.5 | 487 | 480 | 0.0005 | 98.6 | 1.6 |
| 22 | Special Interest Object | 24277 | 1996-046A | adeos | ? | Y | Y | Y | N | Y | Y | 17-Aug-1996 | 22.2 | 799 | 796 | 0.0002 | 98.9 | 1.7 |
| 23 | Special Interest Object | 27386 | 2002-009A | envisat | ? | Y | Y | Y | N | Y | Y | 1-Mar-2002 | 18.6 | 767 | 766 | 0.0001 | 98.1 | 1.7 |

ÖAW IWF

# GRAZ LARGE CAMPAIGN STATISTICS

Graz campaign data summary including historic data

- 2018 - 2022
- Data uploaded on servers
- Light curves from all of the large catalog targets
- Best tracking coverage: Jason 2 -> ~ 200 LC + 600 SLR passes

| Year | LC | SLR | SDLR | Comment |
|---|---|---|---|---|
| 2018 | 40 | 391 | 11 | Historic data, mainly JA2, ENV, ER2, G67, G92 |
| 2019 | 47 | 278 | 14 | Historic data, mainly JA2, ENV, ER2, G67, G92 |
| 2020 | 75 | 41 | 22 | Mainly historic data |
| 2021 | 421 | 102 | 24 | Campaign data |
| 2022 | 82 | 79 | 4 | Some targets of interest continued, JA2, ENV |

ÖAW IWF

# STATISTICS 2018

Historic data: mainly

- Envisat, Jason-2, ERS-2, 2 Glonass satellites

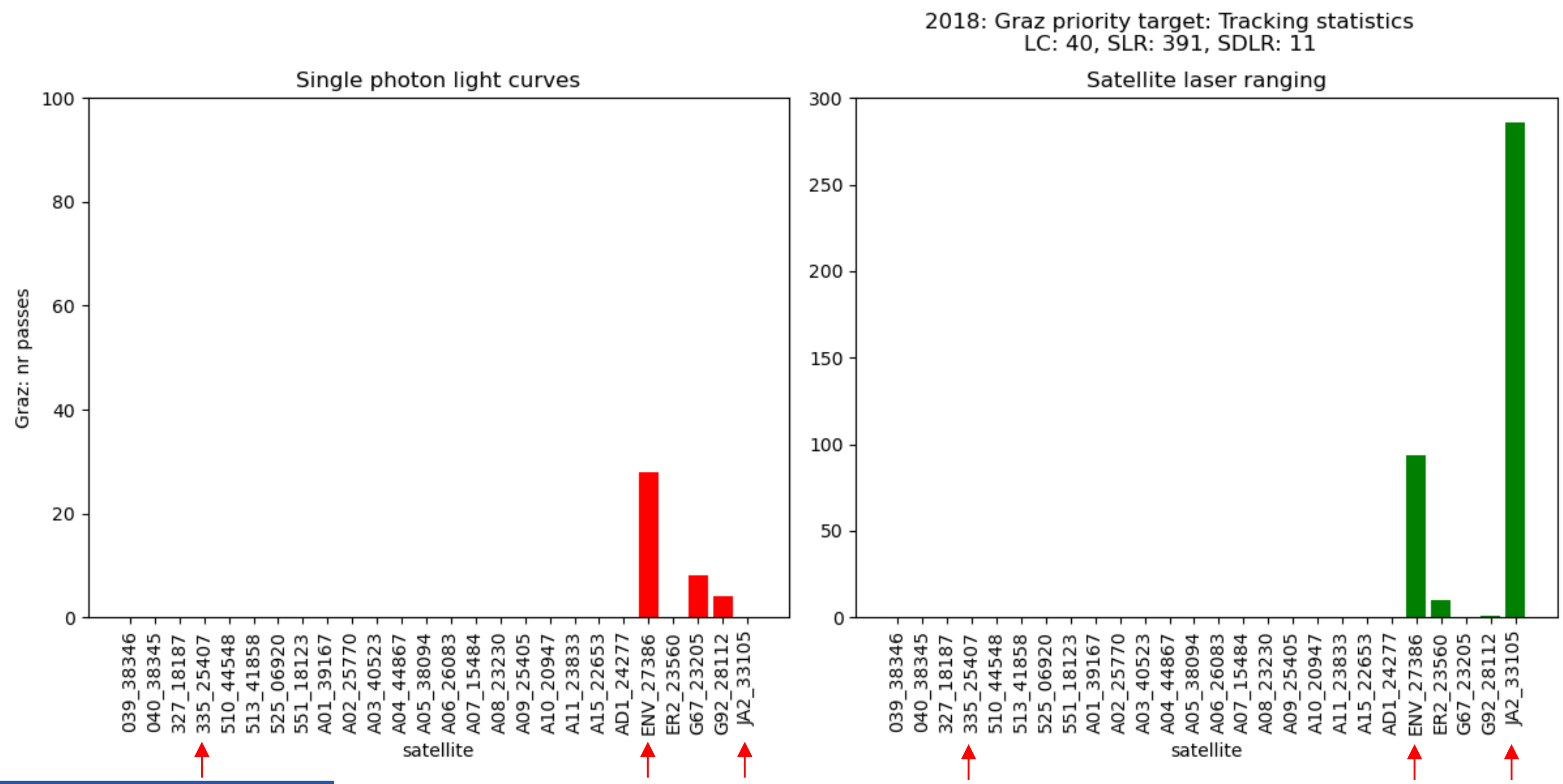

# STATISTICS 2019

Historic data: mainly

- Envisat, Jason-2, ERS-2, 2 Glonass satellites

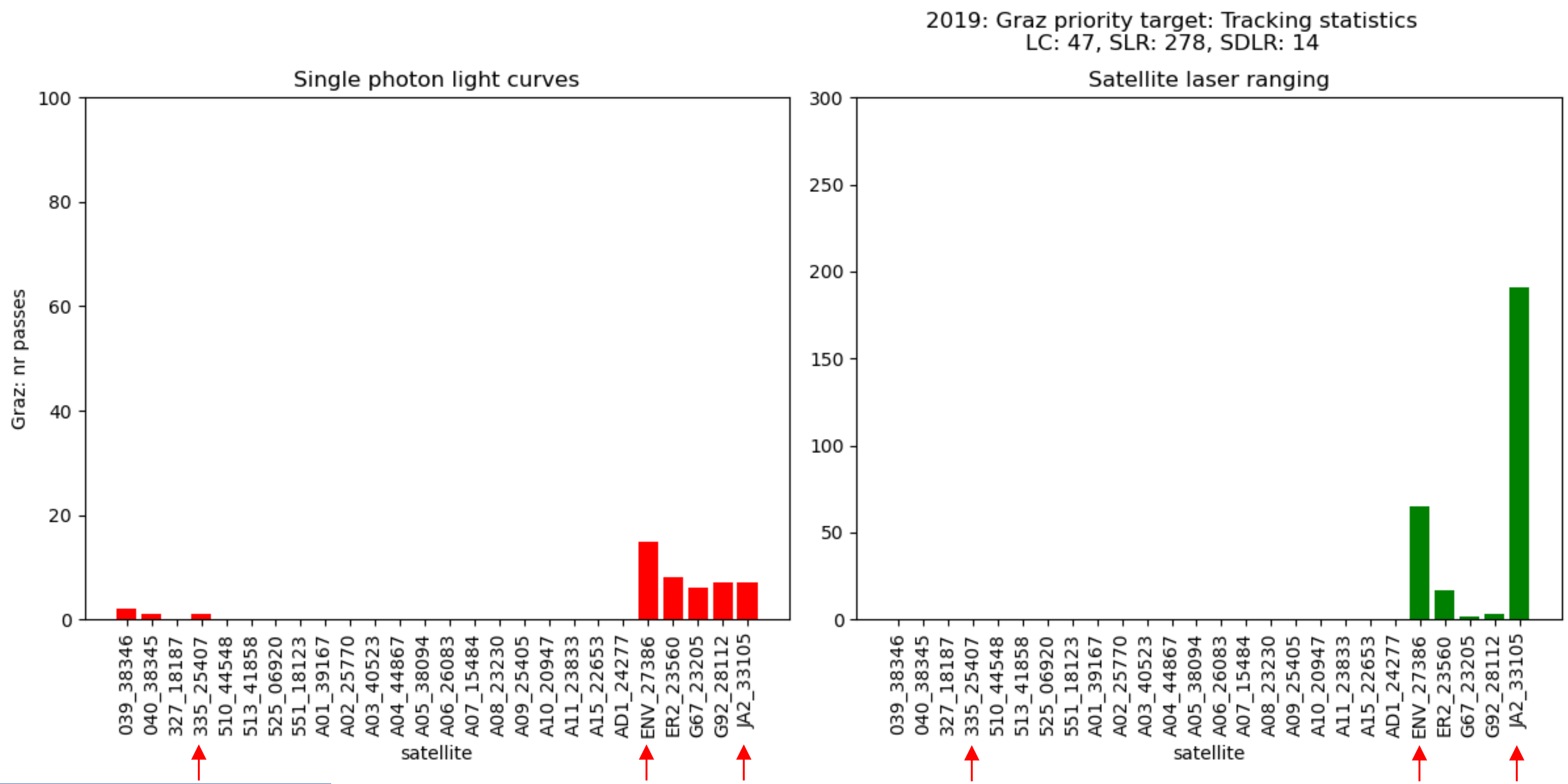

ÖAW IWF

# STATISTICS 2020

Historic data: mainly

- Envisat, Jason-2, ERS-2, 2 Glonass satellites

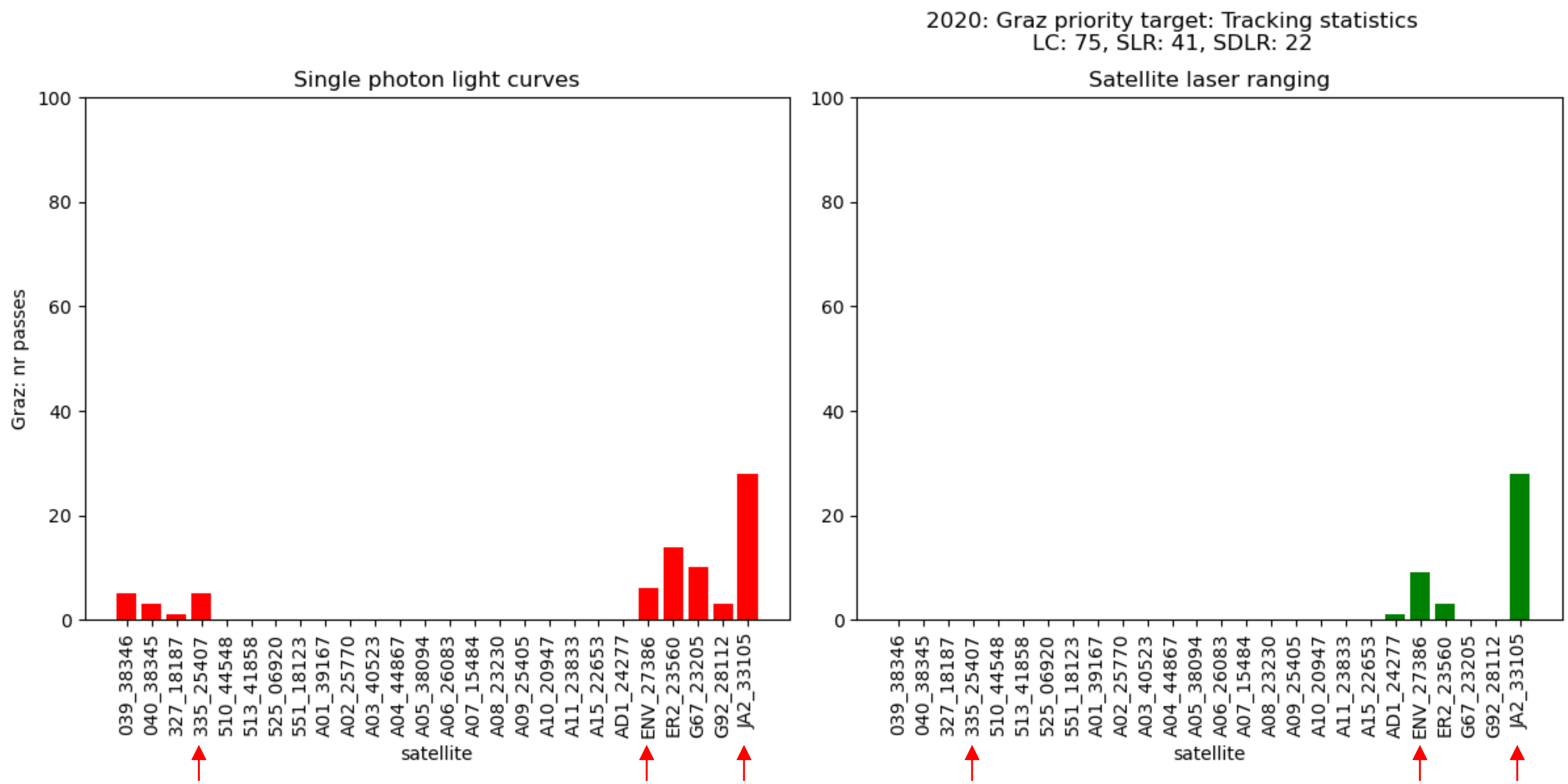

# STATISTICS 2021

## Observation campaign

- Mainly SLR + LC
- 421 light curves, 102 SLR, 24 SDLR

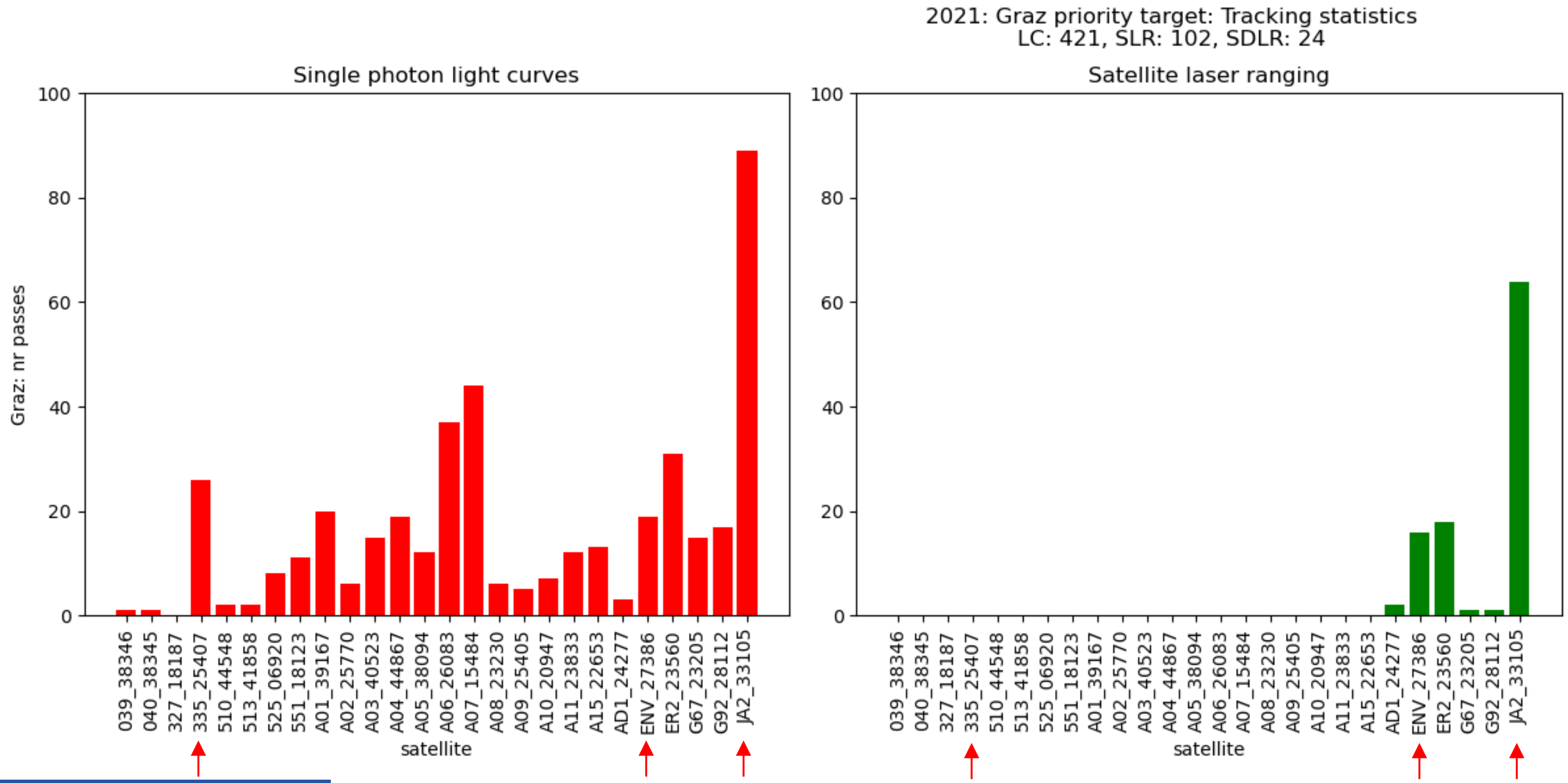

ÖAW IWF

# STATISTICS 2022

Some targets still monitored by IWF

- Jason-2, Envisat

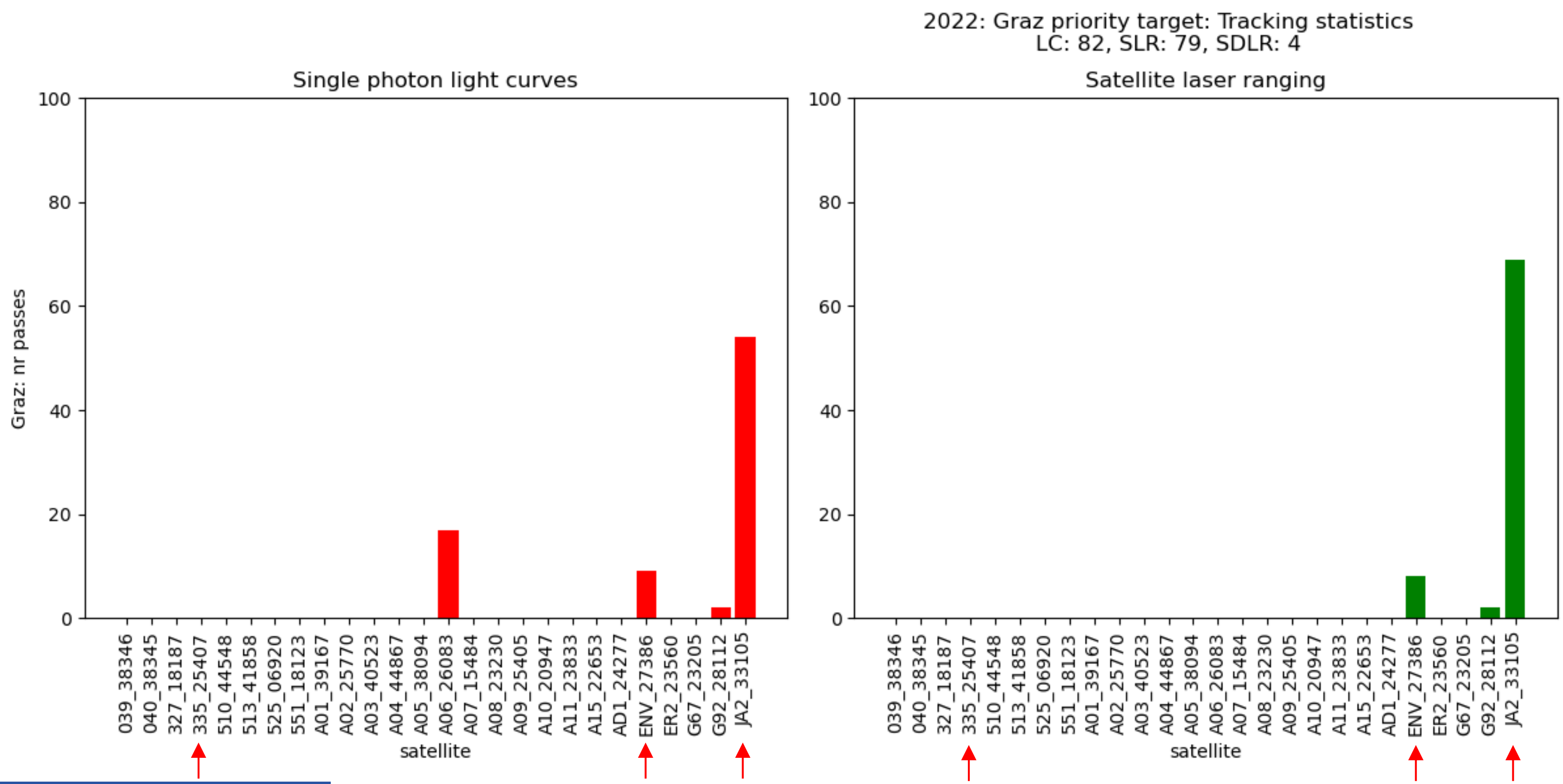

ÖAW IWF

# JOINT TRACKING CAMPAIGN

Selected targets:

- Jason-2
- Envisat
- SL-16 rocket body

Summary:

- Observation sessions including one TIRA pass, maximum 24 hours / session
- Each session: Graz, Zimmerwald collects data of all possible passes, TIRA collects one radar pass
- Simulaneous tracking not necessary but welcome
- Observation schedules were distributed to partners

ÖAW IWF

# JOINT TRACKING CAMPAIGN

## Preferred observation characteristics: sensor

| | TIRA | Graz | Zimmerwald |
|---|---|---|---|
| Available or most efficient operation time (in terms of SNR) | Daytime | After dusk | After dusk |
| Clear sky needed | No | Yes | Yes |
| Satellite visibility | Not required | Sunlit | Sunlit |
| Tracking topocentric elevation range (avoid tracking through keyhole) | 5° - 85° | 5° - 85° | 5° - 85° |
| Closest approach topocentric elevation angle | ≥ 50° | ≥ 30° | ≥ 30° |
| Minimum Moon distance (topocentric angle) to avoid optical noise | 0° | 5° at night | 5° at night |
| Sat. closest approach position fully sunlit? (to assure for longer visibility of the target) | No | Preferred | Preferred |
| | | | |
| **Data generated** | Imaging radar<br>RCS | Satellite laser ranging<br>Space debris laser ranging<br>Single photon light curve | Light curve<br>Satellite laser ranging |

# ! DANKE FÜR IHRE AUFMERKSAMKEIT !



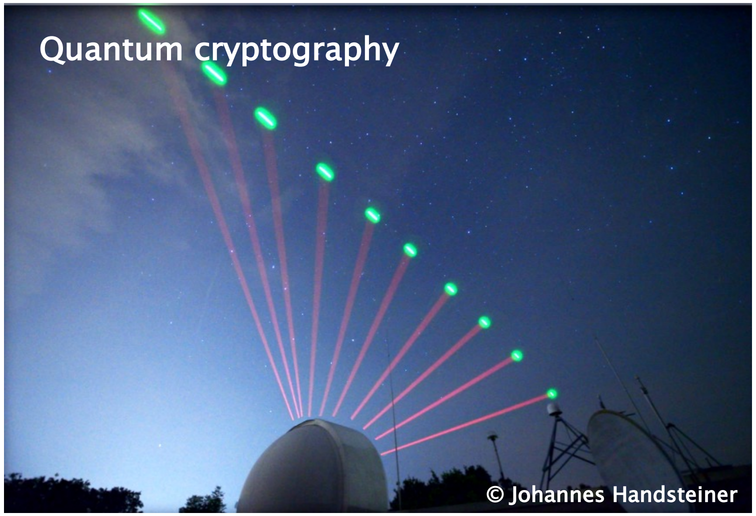


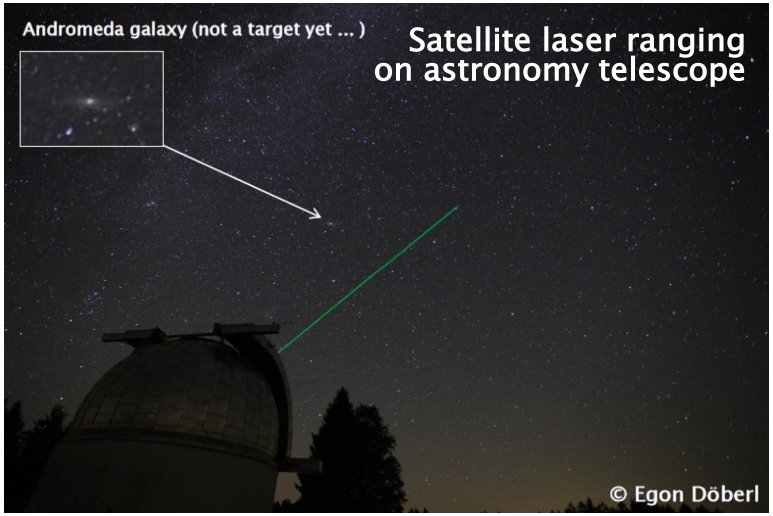


Fraunhofer
FHR
Fraunhofer Institute for
High Frequency Physics and
Radar Techniques FHR
D. Cerutti-Maori, C. Carloni, J. Rosebrock, I. Maouloud
Radar observations with the TIRA system

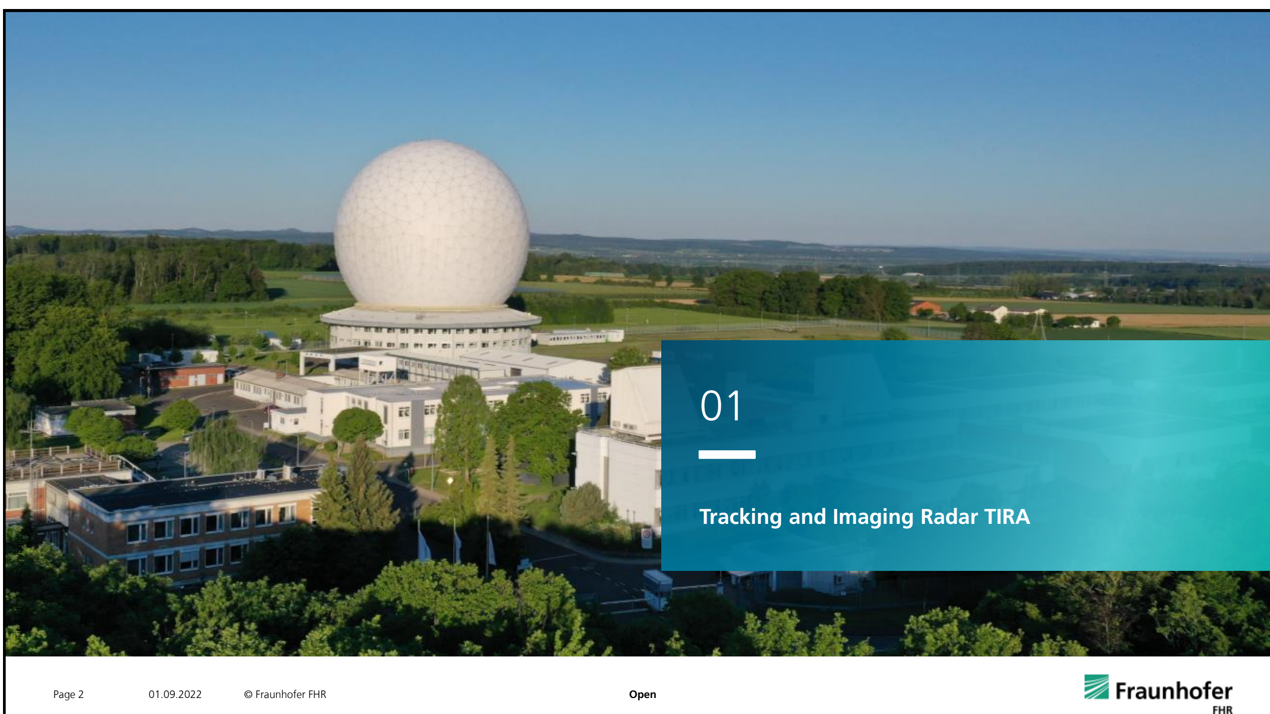
01
Tracking and Imaging Radar TIRA
Page 2
01.09.2022
© Fraunhofer FHR
Open
Fraunhofer
FHR

# Tracking and Imaging Radar (TIRA)

## Different kinds of measurements for attitude motion estimation

- **L-band tracking radar**
  - RCS curve

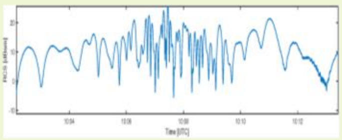

- **Ku-band imaging radar**
  - RTI plot

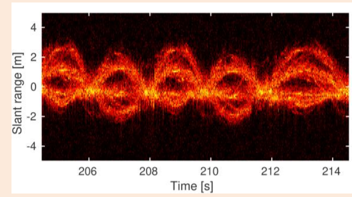


  - Series of ISAR images

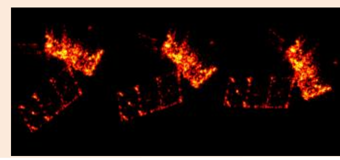



# Tracking and Imaging Radar (TIRA)

## Different kinds of measurements for attitude motion estimation

- **RCS curve (L-band tracking radar)**
  - Estimation of the apparent angular velocity through spectral analysis
  - **Applicability**
    - At least 2 periods have to be observed
    - Works well for (fast) tumbling objects with single rotation axis

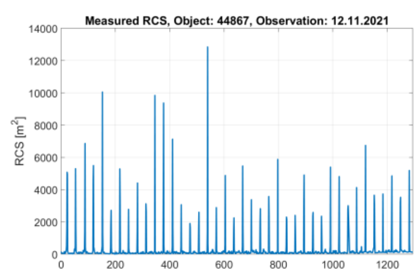


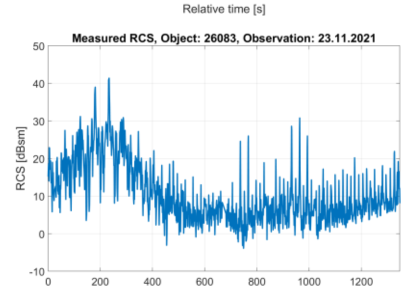

## Tracking and Imaging Radar (TIRA)

Different kinds of measurements for attitude motion estimation

- RCS curve (L-band tracking radar)
- **RTI plot (Ku-band imaging radar)**
  - Estimation of the apparent angular velocity through spectral analysis
  - **Applicability**
    - At least 1 period has to be observed
    - Works well for (fast) tumbling objects

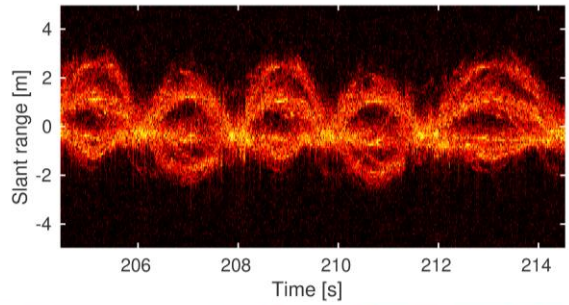


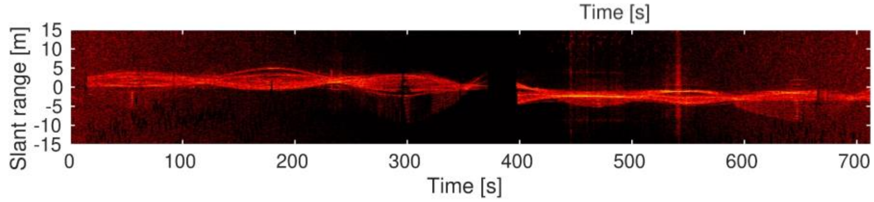




## Tracking and Imaging Radar (TIRA)

Different kinds of measurements for attitude motion estimation

- RCS curve (L-band tracking radar)
- RTI plot (Ku-band imaging radar)
- **Series of ISAR images (Ku-band imaging radar)**
  - Estimation of the velocity vector (angular velocity and spin axis) and of the initial state through a ML approach
  - **Applicability**
    - Slow tumbling objects (to avoid under-sampling issues in the ISAR images)
    - Assumes a constant rotational velocity vector during the observation time (or at least a part of it)

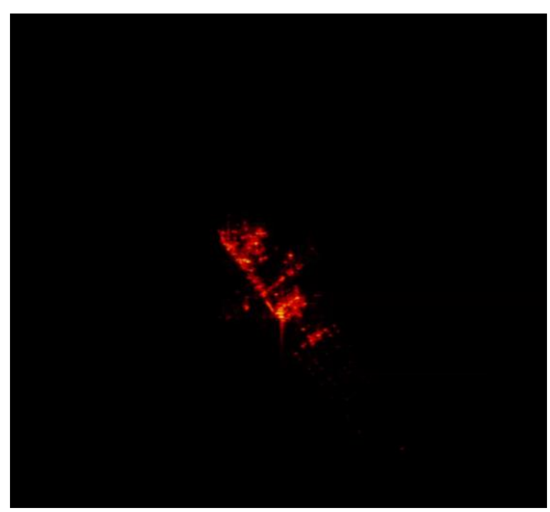

## Estimation of the attitude motion of space objects
### Ku-band imaging radar

1. Generate radar image series



## Conducted measurements

L-band tracking radar and Ku-band imaging radar

- TRKI (13.10): 02009a, 27386, Envisat
- TRKI (12.11): 02009a, 27386, Envisat
- TRKI (13.10): 08032a, 33105, Jason-2
- TRKI (29.10): 19063b, 44548, R/B CZ-2D
- TRK (12.11): 19090d, 44867, R/B CZ-3B (no imaging data)
- TRKI (23.11): 00008c, 26083, Globalstar M060

  Open Fraunhofer FHR

## Conducted measurements

TRKI (13.10 / 12.11): Envisat

- L-band signature
  - Complex tumbling object
  - No clear periodicity could be observed
  - The attitude motion of Envisat changed and does not follow the observed decreasing rotational velocity with stable spin axis observed in the past years (2013-2017)
- ISAR image
  - No external damage could be observed
  - The change in the attitude motion is not caused by a major collision

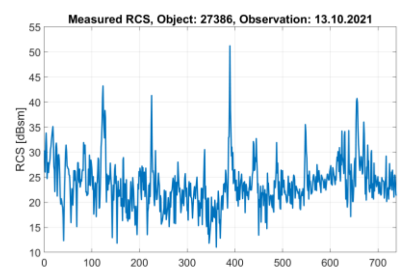


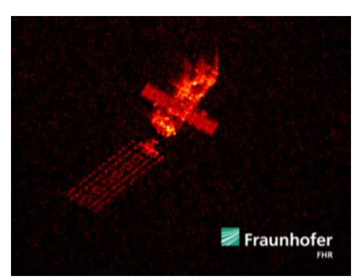


  Open Fraunhofer FHR

## Conducted measurements
TRKI (13.10 / 12.11): Envisat

- RTI plot
  - Time between two nodes is approximately 110 s
  - Object rotates around 180 deg during this time
  - Apparent angular velocity is around 1.6 deg/s

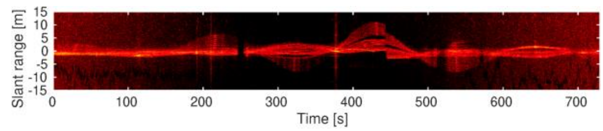


- ISAR image series and WGM
  - The best match is achieved with the rotational velocity vector [ 0.5; 1.07; 1.2 ] deg/s (ECI J2000); estimated angular velocity: 1.68 deg/s
  - Decreasing match with the projected WGM towards the end of the passage
  - Complex tumbling motion, assumption of constant rotational velocity vector is not fulfilled



## Conducted measurements
TRKI (13.10): Jason-2

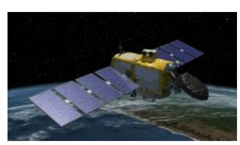

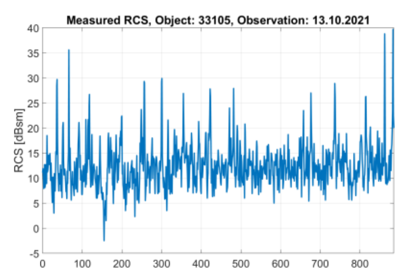


- L-band signature
  - Complex tumbling object, no clear periodicity could be observed
- ISAR image
  - No external damage could be observed
  - Solar panel planes appear to be orthogonal to each other
  - The image was produced assuming a rotational velocity of 9 deg/s about an axis orthogonal to the orbit plane. In the inertial system the assumed rotational velocity vector is [-5.5; 6.1; -3.7 ] deg/s (ECI J2000)
  - The cross-range scaling of the image confirms this assumption
- RTI plot
  - Apparent angular velocity is around 9 deg/s

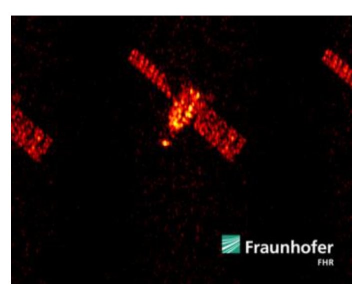

# Conducted measurements

## TRKI (29.10): R/B CZ-2D

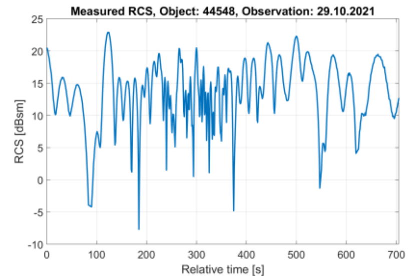


- L-band signature
  - Slow rotating object
  - No periodicity could be observed
- ISAR image
  - No external damage could be observed
  - The image was produced assuming the object to rest in the inertial system
- RTI plot
  - Apparently no rotation
  - Object assumed to rest in the inertial system

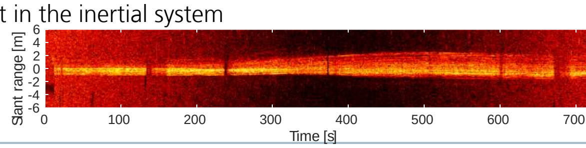


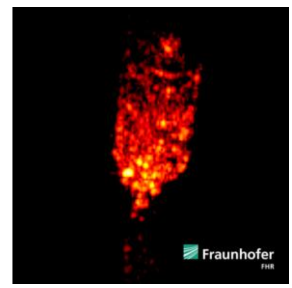




# Conducted measurements

## TRK (12.11): R/B CZ-3B

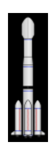

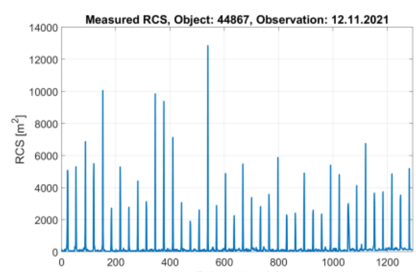


- L-band signature
  - Fast tumbling object
  - Probably single axis motion
  - Apparent spin frequency: 0.031 Hz / 2 due to the object symmetry
  - Apparent rotation period: 32.6 s * 2 due to the object symmetry

## Conducted measurements

TRKI (23.11): Globalstar M060

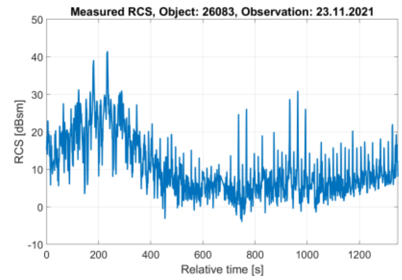


- L-band signature
  - Fast tumbling object with complex motion
  - Region 1, t<600s, apparent rotational velocity ~6.8 deg/s
  - Region 2, t>600s, apparent rotational velocity ~13 deg/s
- ISAR image
  - Undersampling in the cross-range direction causes aliasing
  - The image was produced at relative time 480 s assuming a rotational velocity of 6 deg/s with rotation axis orthogonal to the orbit plane ([ -4.7; -0.8; -3.7 ] deg/s, ECI J2000)
- RTI plot
  - Very faint maximal range spans at approx. 448 s and 508 s lead to an apparent rotational velocity of 6 deg/s confirming the order of magnitude of the L-band result

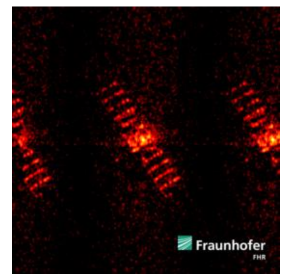




Fraunhofer FHR

Fraunhofer Institute for High Frequency Physics and Radar Techniques FHR

# Thank you for your attention! Questions?

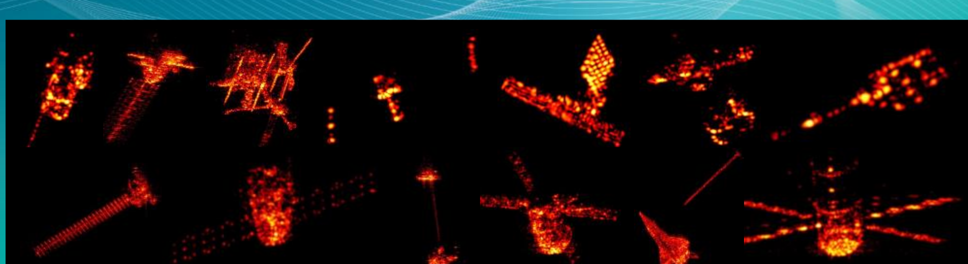


Fraunhofer
FHR
Fraunhofer Institute for
High Frequency Physics and
Radar Techniques FHR
Contact
Dr. Delphine Cerutti-Maori
Delphine.Cerutti-Maori@fhr.fraunhofer.de

# Tumbling Motion Assessment for Space Debris Objects

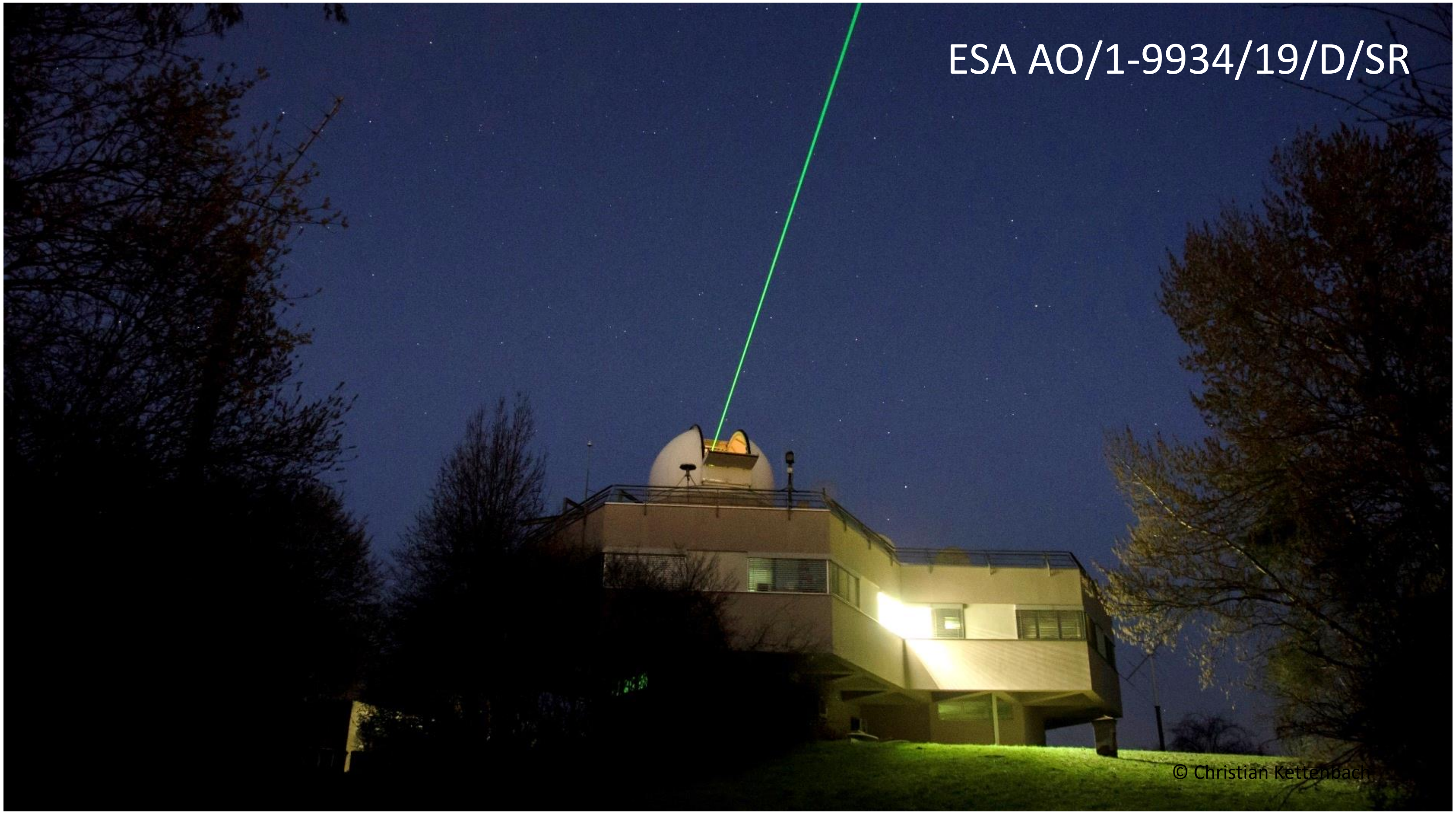


Daniel Kucharski, Michael Steindorfer, Franz Koidl, Georg Kirchner, Peiyuan Wang

Institut für Weltraumforschung, Österreichische Akademie der Wissenschaften

# Environmental characteristics

The selection process of objects-of-interest was based on environmental characteristics analysis.

Estimation of the environmental forces and torques is not exactly possible without knowing how an artificial object interacts with the external factors, but we can characterize environmental phenomena that lead to and affect the tumbling motion.

The environmental forces and torques can be divided into separate categories:

1. Monopolar
gravitational field, the force vector changes once per orbital revolution.

2. Bipolar
magnetic field, force vector changes twice per revolution.

3. Directional
solar irradiation flux, charged particle flux, residual atmospheric particles. The flux direction can change periodically.

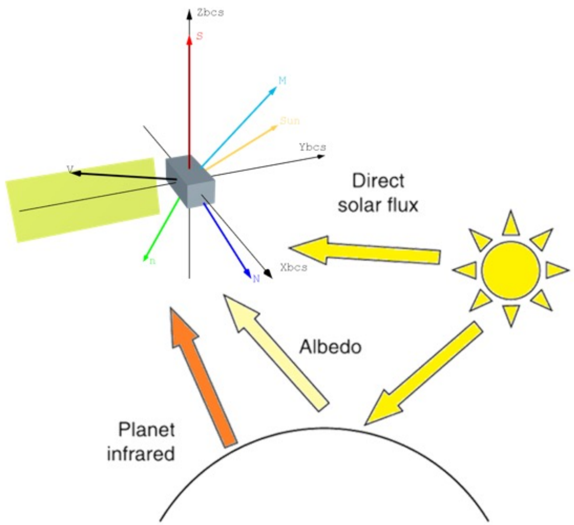


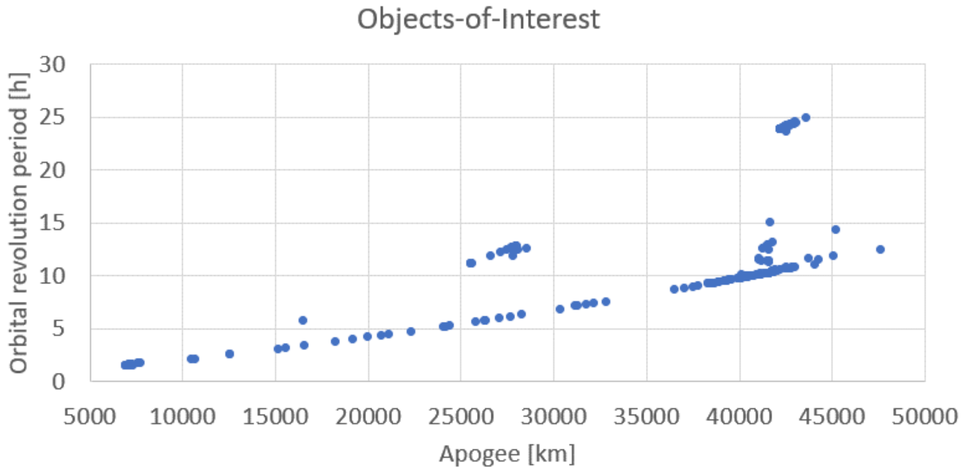


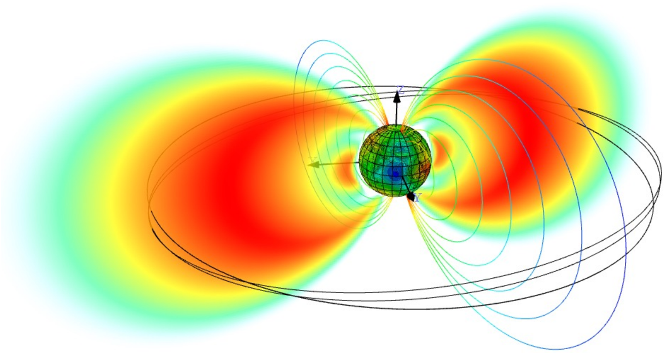

# Environmental characteristics

Periodical effects on spinning Jason-2

- Use TLE to simulate orbital configuration at constant time step (0.1 day)
- Apply FFT for identification of the periodical signals in the simulated time series
- The change of the orbital configuration wrt the Sun stimulates tumbling motion


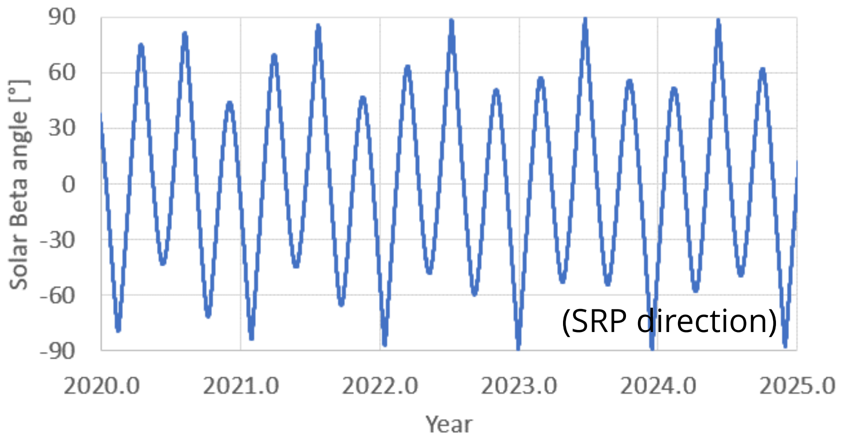


All ~300 objects-of-interest is processed and characterized in terms of expected periodicity in the tumbling motion due to the changes in the orbital configuration.

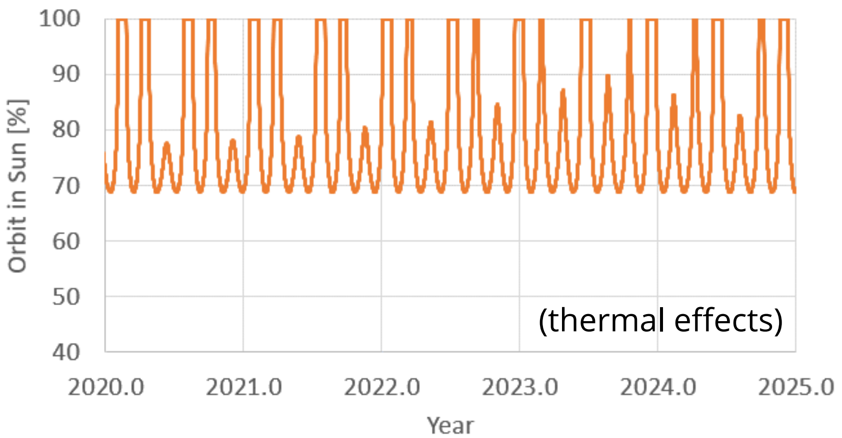


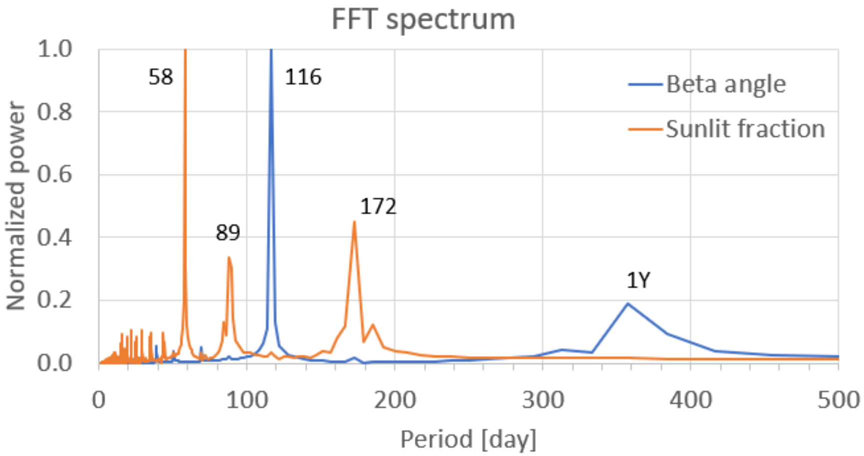

# Satellite attitude observation

High rate laser and optical tracking allows for accurate attitude measurement of the active and passive satellites.

Graz SLR station simultaneously performs laser ranging and light curve measurements (since 2015).

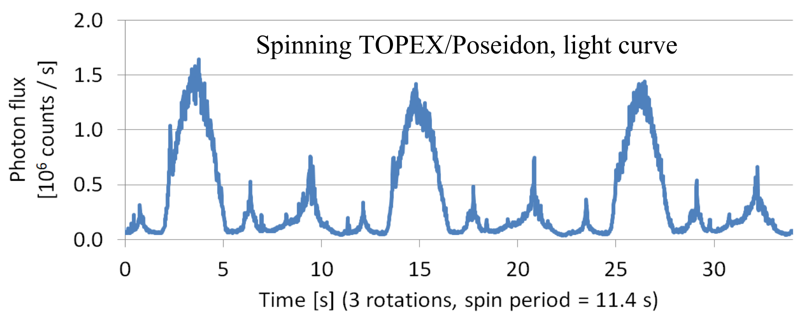


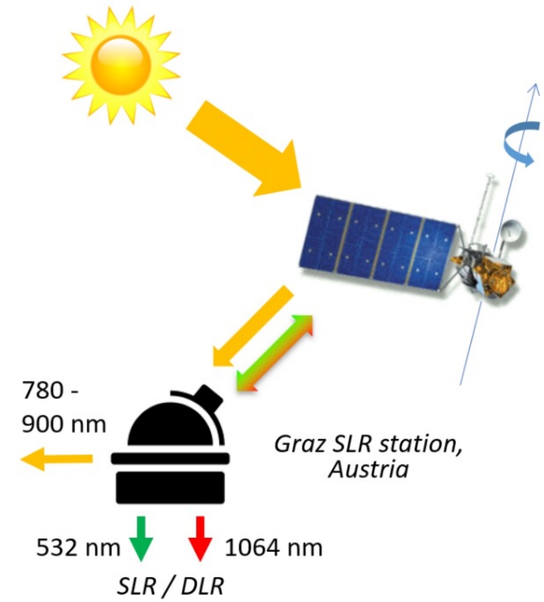


The hypertemporal light curves measured at the single photon resolution present a high level of details due to the fact that the photon counters do not integrate the incoming optical signal (as opposed to the CCD technology).

The high-rate SLR allows for the mm-accuracy absolute range measurements that reveal motion of the individual corner cube retroreflectors wrt the satellite CoM.

The pattern of the data distribution depends on:
- LC: the angular configuration Sun-Satellite-Observer
- SLR: the range between the Satellite and Observer optical reflection and reference points

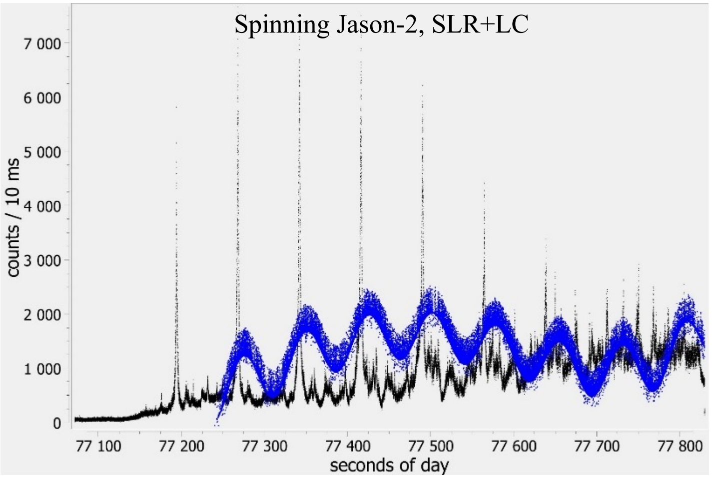


M. Steindorfer

## Tumbling Motion Observation - Data Analysis Sheet. Graz, 28 June 2015, 22:31:26

Object: COSMOS 2276 [GLONASS]
NORAD: 23043
Cospar: 1994-021a
Launch: 11 April, 1994
Apogee alt.: 19180 km
Perigee alt.: 19081 km
Inclination: 64.8°
Orb. period: 11.3 h
RCS: 4.1 m2
Object age: 21.2 y
Exp. spin status: -
Mag: -

Result summary

Frequency analysis
Period: 59.172 s

Spin phase folding
Period: 58.712 s

Topocentric

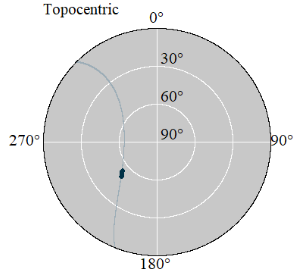


Single-photon light curve (1994-021a), Graz 28 June 2015, 22:31:26

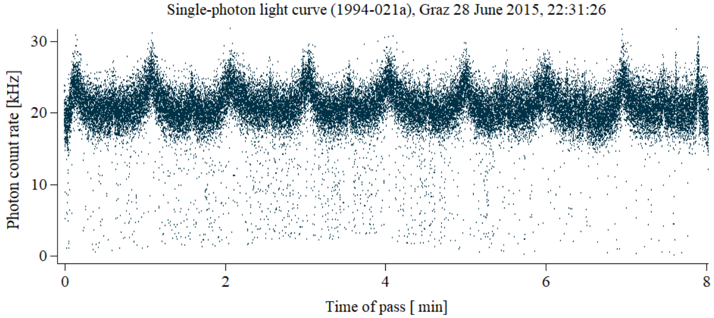


Pass information
Duration: 8m:02s
Data points: 47227
Data rate: 100.0 Hz

Closest approach
Topo el: 54.4°
Slant range: 20025 km
Phase angle: 55.5°
Sim. app. mag.: 11.8
Solar Beta angle: -3.5°

Frequency spectrum

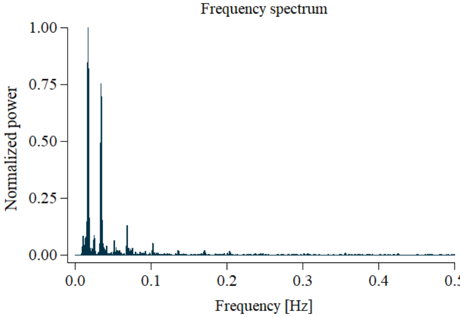


Max peak profile

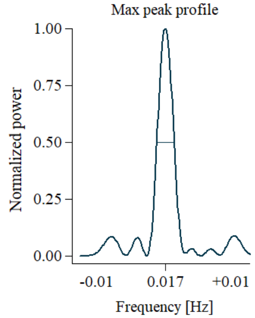


Frequency analysis
Frequency: 0.017 Hz
Period: 59.172 s
FWHM: 1.891 mHz
SNR: 21.0
CoVar: 4.751 %

Folded spin phase

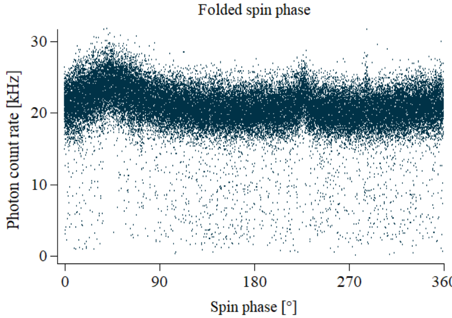


Parameter search

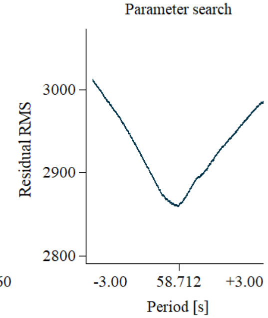


PDM
Period: 58.712 s

## Tumbling Motion Observation - Data Analysis Sheet. Zimmerwald, 17 March 2019, 0:29:02

Object: COSMOS 2276 [GLONASS]
NORAD: 23043
Cospar: 1994-021a
Launch: 11 April, 1994
Apogee alt.: 19180 km
Perigee alt.: 19081 km
Inclination: 64.8°
Orb. period: 11.3 h
RCS: 4.1 m2
Object age: 24.9 y
Exp. spin status: -
Mag: -

Result summary

Frequency analysis
Period: 49.261 s

Spin phase folding
Period: 48.950 s

Topocentric

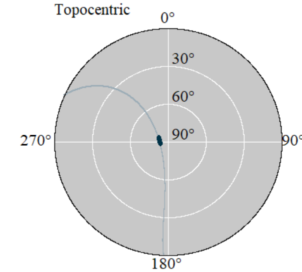


Light curve (1994-021a), Zimmerwald 17 March 2019, 0:29:02

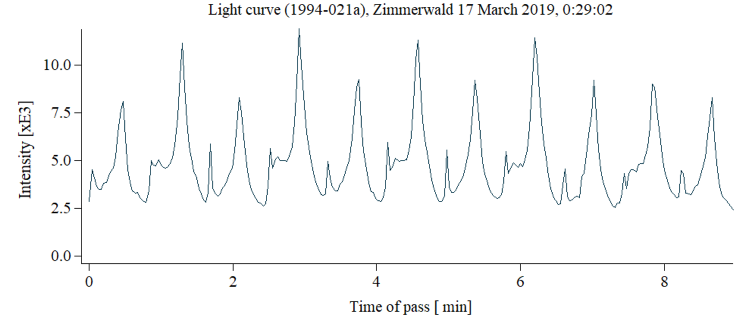


Pass information
Duration: 8m:58s
Data points: 269
Data rate: 0.5 Hz

Closest approach
Topo el: 83.8°
Slant range: 19144 km
Phase angle: 43.8°
Sim. app. mag.: 11.5
Solar Beta angle: 32.2°

Frequency spectrum

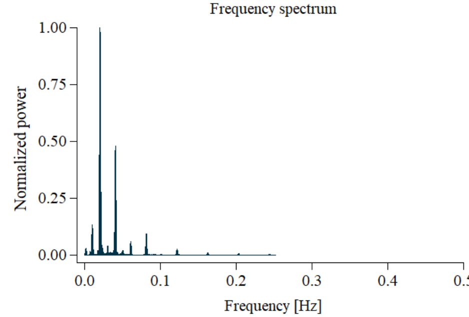


Max peak profile

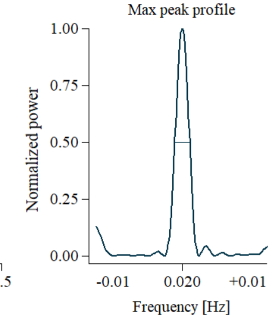


Frequency analysis
Frequency: 0.020 Hz
Period: 49.261 s
FWHM: 1.696 mHz
SNR: 28.2
CoVar: 3.548 %

Folded spin phase

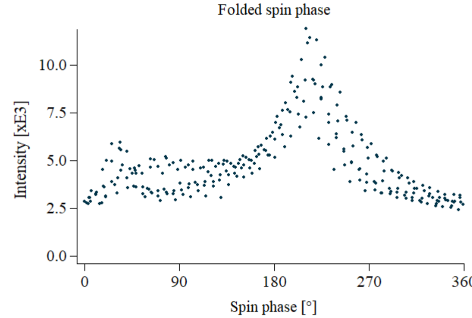


Parameter search

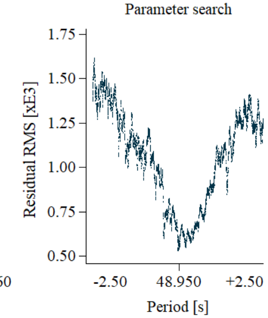


PDM
Period: 48.950 s

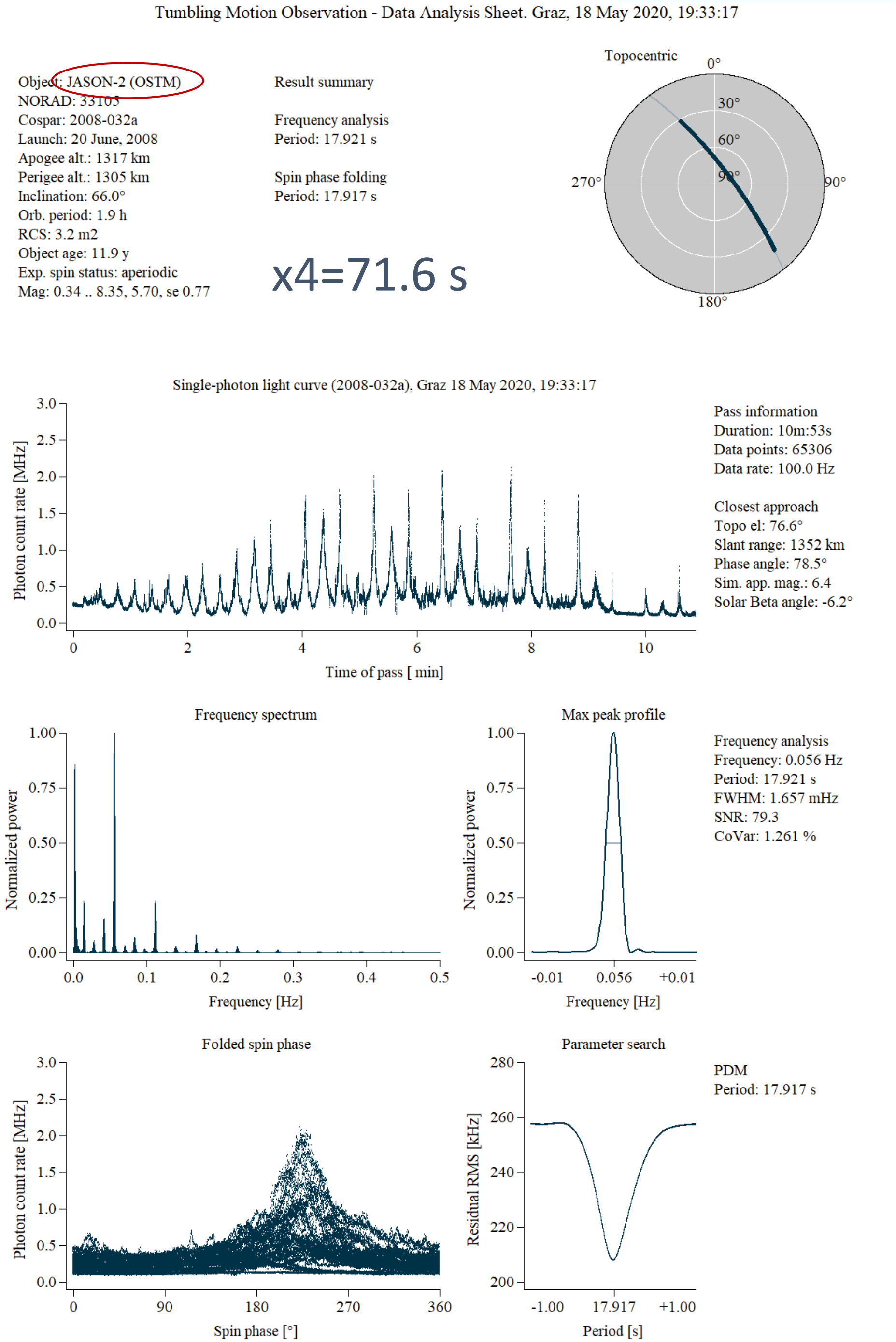
Tumbling Motion Observation - Data Analysis Sheet. Graz, 18 May 2020, 19:33:17
Object: JASON-2 (OSTM)
NORAD: 33105
Cospar: 2008-032a
Launch: 20 June, 2008
Apogee alt.: 1317 km
Perigee alt.: 1305 km
Inclination: 66.0°
Orb. period: 1.9 h
RCS: 3.2 m2
Object age: 11.9 y
Exp. spin status: aperiodic
Mag: 0.34 .. 8.35, 5.70, se 0.77
Result summary
Frequency analysis
Period: 17.921 s
Spin phase folding
Period: 17.917 s
x4=71.6 s
Topocentric
0°
30°
60°
90°
90°
180°
270°
Single-photon light curve (2008-032a), Graz 18 May 2020, 19:33:17
Photon count rate [MHz]
Time of pass [ min]
Pass information
Duration: 10m:53s
Data points: 65306
Data rate: 100.0 Hz
Closest approach
Topo el: 76.6°
Slant range: 1352 km
Phase angle: 78.5°
Sim. app. mag.: 6.4
Solar Beta angle: -6.2°
Frequency spectrum
Normalized power
Frequency [Hz]
Max peak profile
Normalized power
Frequency [Hz]
Frequency analysis
Frequency: 0.056 Hz
Period: 17.921 s
FWHM: 1.657 mHz
SNR: 79.3
CoVar: 1.261 %
Folded spin phase
Photon count rate [MHz]
Spin phase [°]
Parameter search
Residual RMS [kHz]
Period [s]
PDM
Period: 17.917 s

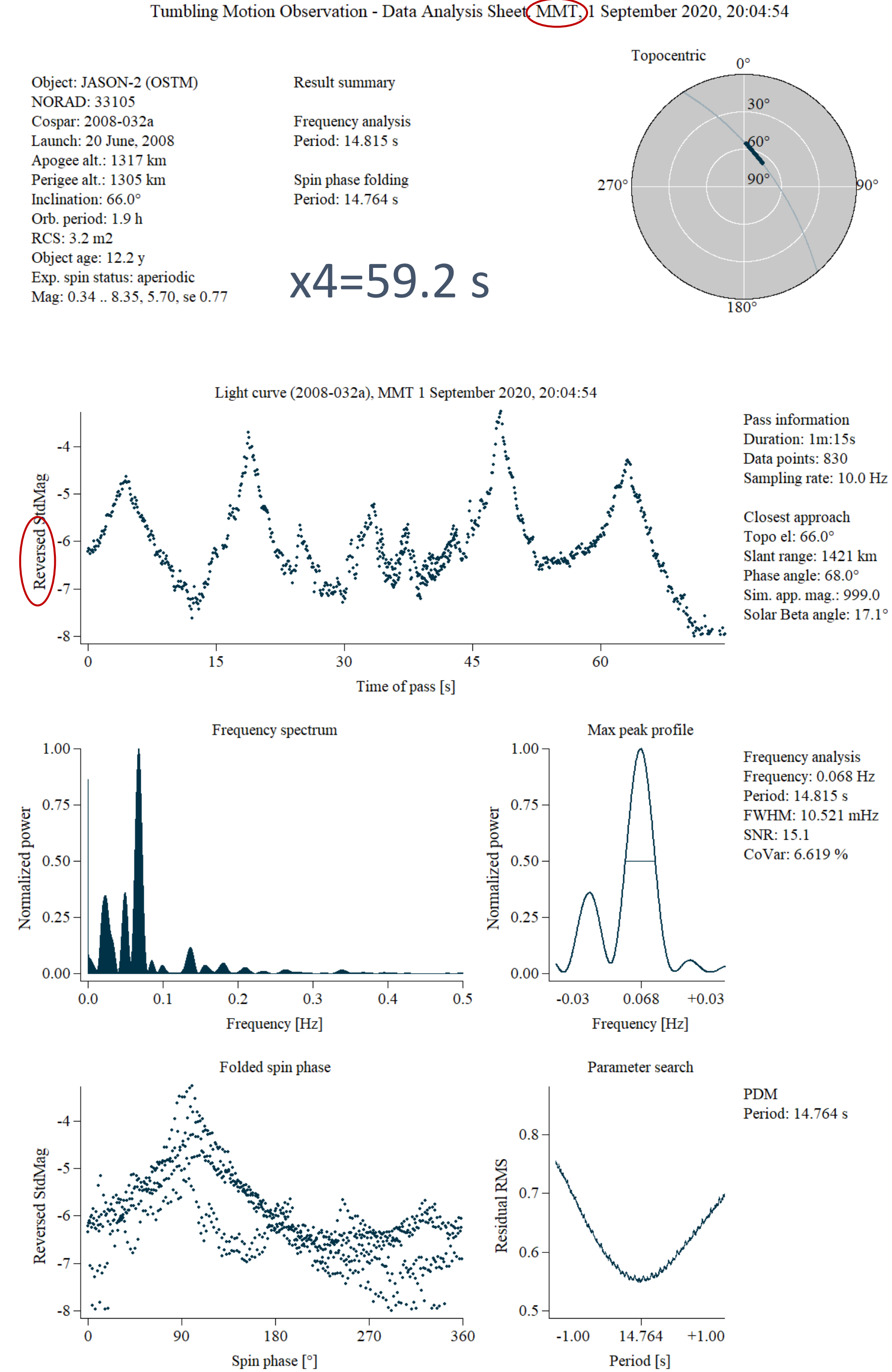
Tumbling Motion Observation - Data Analysis Sheet. MMT, 1 September 2020, 20:04:54
Object: JASON-2 (OSTM)
NORAD: 33105
Cospar: 2008-032a
Launch: 20 June, 2008
Apogee alt.: 1317 km
Perigee alt.: 1305 km
Inclination: 66.0°
Orb. period: 1.9 h
RCS: 3.2 m2
Object age: 12.2 y
Exp. spin status: aperiodic
Mag: 0.34 .. 8.35, 5.70, se 0.77
Result summary
Frequency analysis
Period: 14.815 s
Spin phase folding
Period: 14.764 s
x4=59.2 s
Topocentric
0°
30°
60°
90°
90°
180°
270°
Light curve (2008-032a), MMT 1 September 2020, 20:04:54
Reversed StdMag
Time of pass [s]
Pass information
Duration: 1m:15s
Data points: 830
Sampling rate: 10.0 Hz
Closest approach
Topo el: 66.0°
Slant range: 1421 km
Phase angle: 68.0°
Sim. app. mag.: 999.0
Solar Beta angle: 17.1°
Frequency spectrum
Normalized power
Frequency [Hz]
Max peak profile
Normalized power
Frequency [Hz]
Frequency analysis
Frequency: 0.068 Hz
Period: 14.815 s
FWHM: 10.521 mHz
SNR: 15.1
CoVar: 6.619 %
Folded spin phase
Reversed StdMag
Spin phase [°]
Parameter search
Residual RMS
Period [s]
PDM
Period: 14.764 s

## Tumbling Motion Observation - Data Analysis Sheet. MMT, 24 October 2019, 2:10:54

Object: NOAA 3
NORAD: 6920
Cospar: 1973-086a
Launch: 6 November, 1973
Apogee alt.: 1510 km
Perigee alt.: 1500 km
Inclination: 102.1°
Orb. period: 1.9 h
RCS: 2.5 m2
Object age: 46.0 y
Exp. spin status: periodic, 54.4 s
Mag: 4.79 .. 10.30, 7.97, se 0.56

Result summary

Frequency analysis
Period: 25.840 s

Spin phase folding
Period: 25.339 s

x2=51.6 s

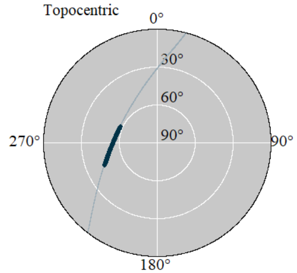


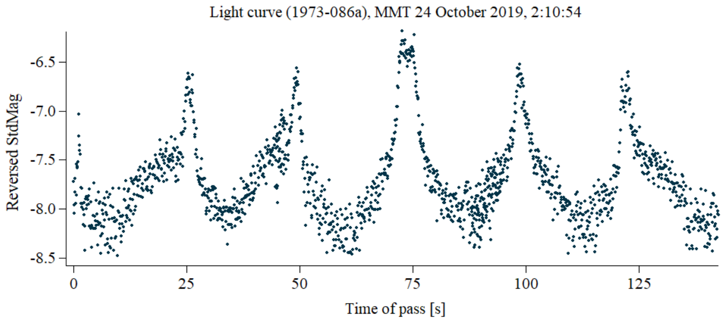


Pass information
Duration: 2m:23s
Data points: 1497
Sampling rate: 10.0 Hz

Closest approach
Topo el: 58.5°
Slant range: 1716 km
Phase angle: 45.3°
Sim. app. mag.: 6.3
Solar Beta angle: 57.5°

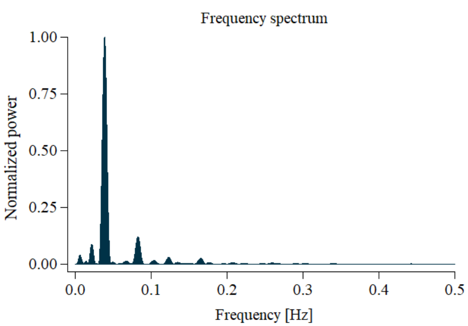


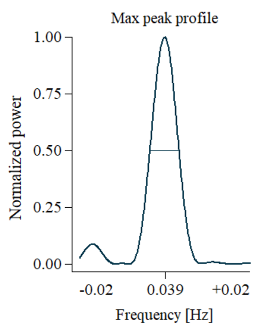


Frequency analysis
Frequency: 0.039 Hz
Period: 25.840 s
FWHM: 6.809 mHz
SNR: 13.4
CoVar: 7.472 %

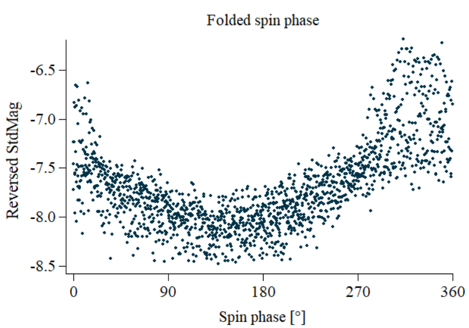


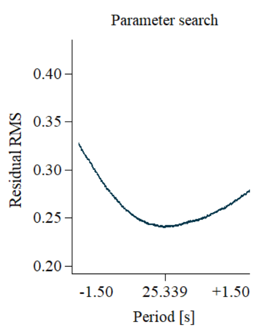


PDM
Period: 25.339 s

## Tumbling Motion Observation - Data Analysis Sheet. MMT, 9 November 2020, 1:54:17

Object: NOAA 3
NORAD: 6920
Cospar: 1973-086a
Launch: 6 November, 1973
Apogee alt.: 1510 km
Perigee alt.: 1500 km
Inclination: 102.1°
Orb. period: 1.9 h
RCS: 2.5 m2
Object age: 47.0 y
Exp. spin status: periodic, 54.4 s
Mag: 4.79 .. 10.30, 7.97, se 0.56

Result summary

Frequency analysis
Period: 26.385 s

Spin phase folding
Period: 25.959 s

x2=52.8 s

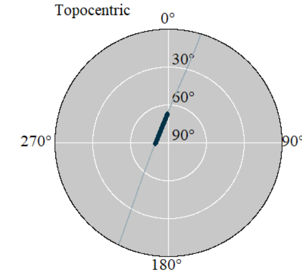


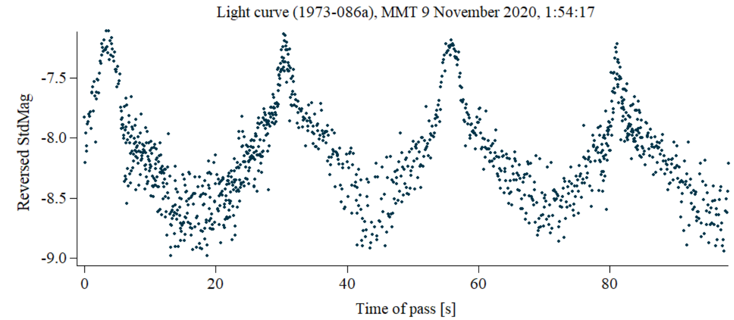


Pass information
Duration: 1m:38s
Data points: 1243
Sampling rate: 10.0 Hz

Closest approach
Topo el: 81.0°
Slant range: 1529 km
Phase angle: 58.7°
Sim. app. mag.: 6.3
Solar Beta angle: 60.7°

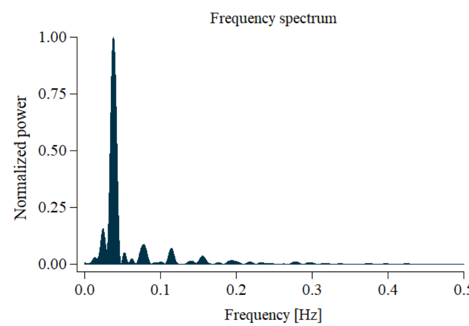


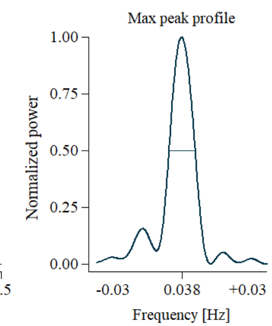


Frequency analysis
Frequency: 0.038 Hz
Period: 26.385 s
FWHM: 9.150 mHz
SNR: 9.8
CoVar: 10.253 %

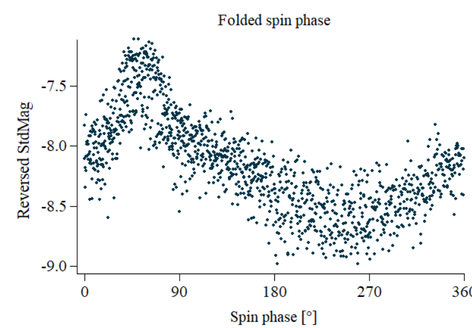


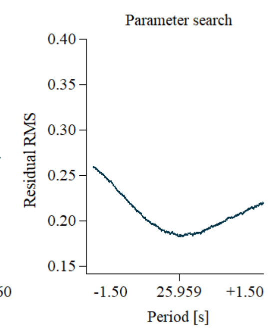


PDM
Period: 25.959 s

# Description of rotation
# Spin vector definition

Rotational motion of a rigid object about its center of mass can be characterized by the spin angular momentum vector $\boldsymbol{L}$ oriented in an external, right-handed Cartesian coordinate system $\mathbb{R}^3$ about which the body spins in a counter-clockwise direction at an angular rate equal to the magnitude of $\boldsymbol{L}$.

During an overhead pass of a satellite above a ground tracking system, it is possible to predict an inertial, satellite-centered unit direction vector $\widehat{\boldsymbol{T}}$ toward the telescope. Transformation of $\widehat{\boldsymbol{T}}$ from an external $\mathbb{R}^3$ ($\widehat{\boldsymbol{T}}_{\mathbb{R}^3}$) to a spacecraft body-centered and -fixed coordinate system (BCS) can be realized by $\widehat{\boldsymbol{T}}_{BCS} = \boldsymbol{A}\widehat{\boldsymbol{T}}_{\mathbb{R}^3}$, where the attitude tensor $\boldsymbol{A}$ between the external and the embedded reference frames is a rotation matrix computed by:

$$\boldsymbol{A} = \boldsymbol{R}_2(-x_P)\boldsymbol{R}_1(-y_P)\boldsymbol{R}_3(\gamma)\boldsymbol{R}_1\left(\frac{\pi}{2} - \delta\right)\boldsymbol{R}_3\left(\frac{\pi}{2} + \alpha\right)$$

where the $\boldsymbol{R}_1$, $\boldsymbol{R}_2$ and $\boldsymbol{R}_3$ are the standard rotation matrices about the x, y and z-axis respectively.

# Description of rotation
# Spin vector definition

The orientation of $\boldsymbol{L}$ in $\mathbb{R}^3$ ($\boldsymbol{L}_{\mathbb{R}^3}$) is defined by spherical angles $\alpha$, $\delta$ corresponding to right ascension and declination in the case of Earth Centered Inertial reference frame (ECI, J2000) being an external system.

Rotation angle $\gamma$ increases at the rate of $\omega = \|\boldsymbol{L}\|$, while the pole coordinates $x_P$ and $y_P$ describe the relative position of $\boldsymbol{L}$ with respect to the satellite body axis $+Z_{BCS}$. In this work we assume that the body's pole axis coincides with the axis of rotation, thus $x_P$ and $y_P$ are 0.

For a given spin vector $\boldsymbol{L}_{\mathbb{R}^3}$ it is possible to find the relative orientation of $\widehat{\boldsymbol{T}}_L$ (satellite-centered observer direction vector) by:

$$\widehat{\boldsymbol{T}}_L = \boldsymbol{R}_1\left(\frac{\pi}{2} - \delta\right)\boldsymbol{R}_3\left(\frac{\pi}{2} + \alpha\right)\widehat{\boldsymbol{T}}_{\mathbb{R}^3}$$

where the azimuthal motion of $\widehat{\boldsymbol{T}}_L$ about $\boldsymbol{L}$ during a satellite pass is known as an apparent rotation effect.

# Timeseries analysis – epoch methods

Several methods can support high level of automation of the tumbling motion determination processes:

- Savitzky-Golay filters – for timeseries approximation, detrending with time derivatives.
- Spectral analysis (Lomb) – for apparent rate determination.
- Phase Dispersion Minimization – for apparent and inertial periodicity determination.
- Autocorrelation – for apparent periodicity.
- Inertial PDM mapping – for spin vector orientation.

Apparent PDM

Typical, apparent periodicity as seen by the observer.
The phase coordinate of a data point is computed as a fraction of a fixed (tested) period.

Inertial PDM

Based on the attitude tensor transformation.
The phase coordinate of a data point is derived through the inertial-to-body transformation of a satellite-centered phase vector. The body-fixed azimuth of the transformed phase vector is the phase coordinate of the observed data point.
This method requires modelling a time-dependent, satellite attitude tensor that takes the satellite spin vector $\bar{L}$ as an input. Optimization of $\bar{L}$ (orientation and magnitude) minimizes dispersion of the folded pattern (measured by the variance ratio $\Theta$).

# Apparent and Inertial Phase Folding – **Lightcurve**

CNES

Object: JASON-2 (OSTM)
NORAD: 33105
Cospar: 2008-032A
Launch: 20 June, 2008
Apogee alt.: 1317 km
Perigee alt.: 1305 km
Inclination: 66.0°
Orb. period: 1.9 h
RCS: 3.2 m2
Object age: 12.6 y
Exp. spin status: aperiodic
Mag: -1.17 .. 8.38, 5.70, se 0.81
datafile: JA202017_CT

Result summary

Frequency analysis
Period: 17.194 s

Spin phase folding
Period: 0.000 s

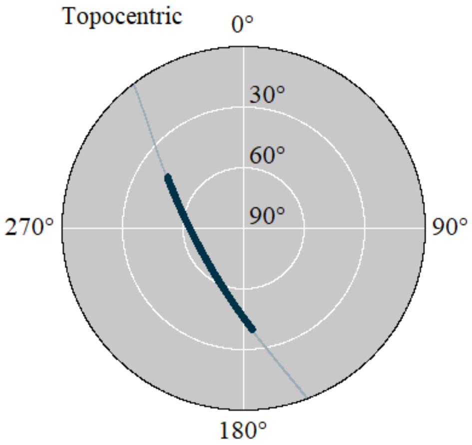


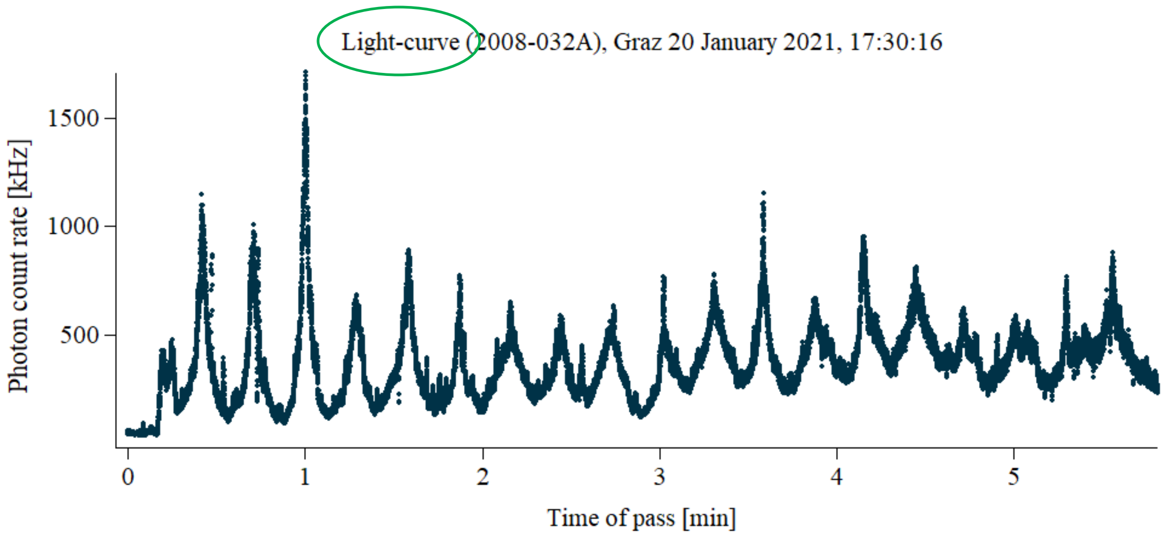


Pass information
Duration: 5m:49s
Data points: 34864
Data rate: 100.0 Hz

Closest approach
Topo el: 66.4°
Slant range: 1419 km
Phase angle: 94.0°
Sim. app. mag.: 7.0
Solar Beta angle: -64.7°

ÖAW IWF

# Apparent and Inertial Phase Folding – **SLR**

CNES

Object: TOPEX/POSEIDON
NORAD: 22076
Cospar: 1992-052A
Launch: 10 August, 1992
Apogee alt.: 1344 km
Perigee alt.: 1331 km
Inclination: 66.0°
Orb. period: 1.9 h
RCS: 7.8 m2
Object age: 21.9 y
Exp. spin status: periodic, 9.6 s
Mag: -2.75 .. 9.31, 5.01, se 1.16
datafile: top16923

Result summary

Frequency analysis
Period: 11.810 s

Spin phase folding
Period: 0.000 s

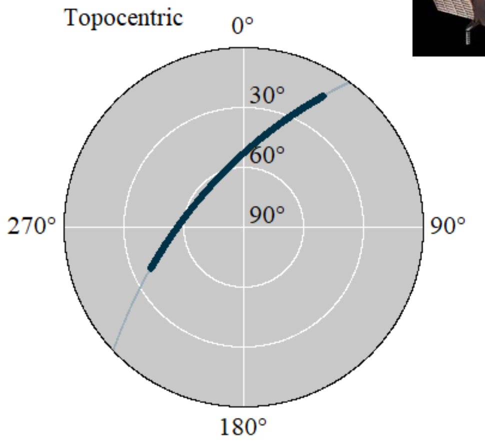


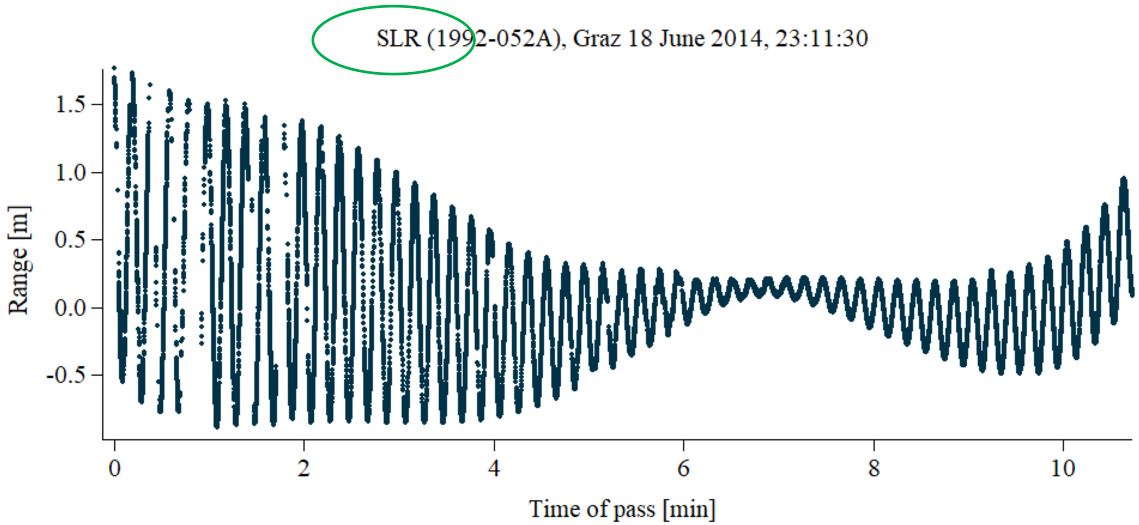


Pass information
Duration: 10m:44s
Data points: 476170
Data rate: 1705.2 Hz

Closest approach
Topo el: 64.3°
Slant range: 1468 km
Phase angle: 87.1°
Sim. app. mag.: 6.8
Solar Beta angle: 38.7°

# Timeseries analysis, Jason-2 **light curve**

A. Lomb | B. Apparent PDM | C. Inertial PDM

1. Averaged data

2. Approximated data

3. 1st derivative

# Timeseries analysis, Jason-2 **light curve**

CNES

Approximated data, with 3° moving polynomial fit (SGF).
Polynomial window 3 s, step 0.1s; Orthogonal polynomial fit (Gram method).

1a)

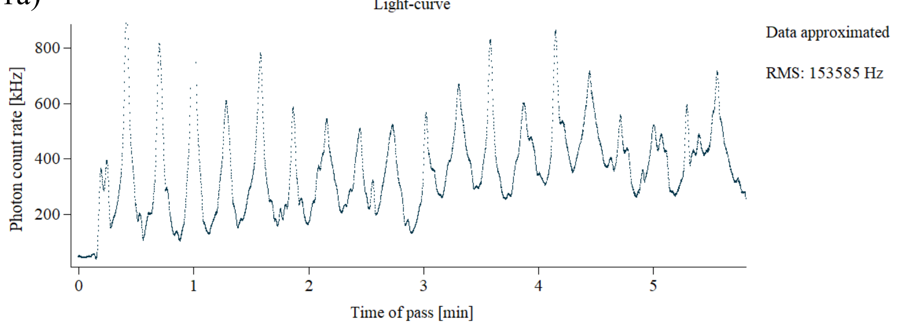


2a)

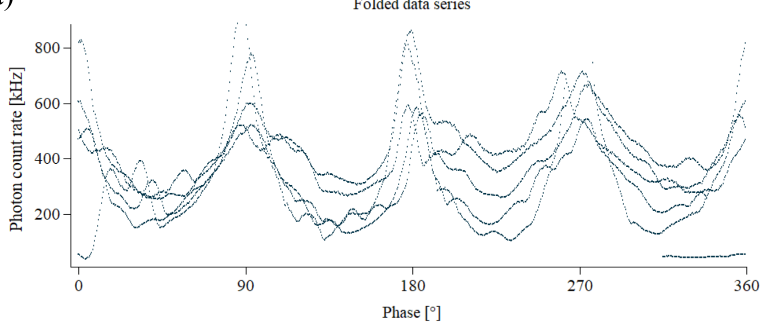


1b)

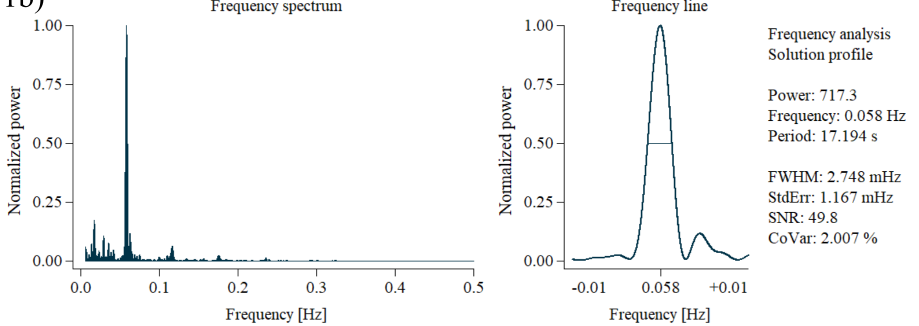


2b)

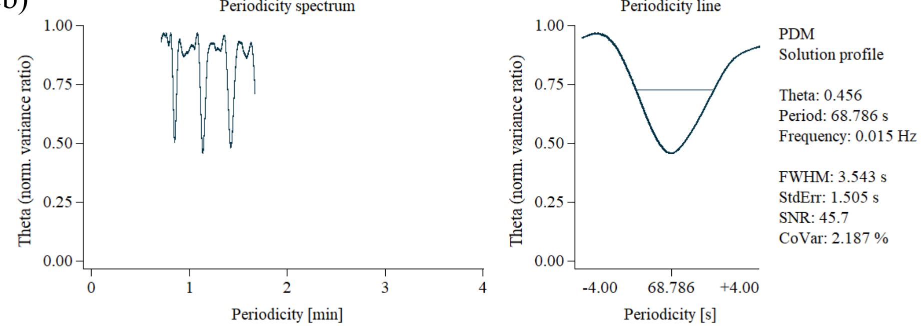


The profile of the solution line allows finding the statistical parameters of the dominant signal:

- Full Width at Half-Maximum (FWHM) of the solution line represents the errors and inaccuracies of the analysis related to the sampling noise or apparent rotation and frequency shift effects.
- Signal-to-Noise Ratio (SNR). Assuming Gaussian distribution of the solution ($f_{max}$) error it is possible to calculate its standard deviation as $\sigma = \frac{FWHM}{2\sqrt{\ln(4)}}$ and $SNR = \frac{f_{max}}{\sigma}$. Here, the standard deviation represents the noise and other negative interference to the measured signal.
- Coefficient of Variation (CoVar) measures relative variability and is defined as the standard deviation divided by the mean, multiplied by 100 %: $CoVar = \frac{\sigma}{f_{max}} \cdot 100\%$.

# Comparison of Lomb and PDM on approximated and derivative timeseries (Jason-2 lightcurve)

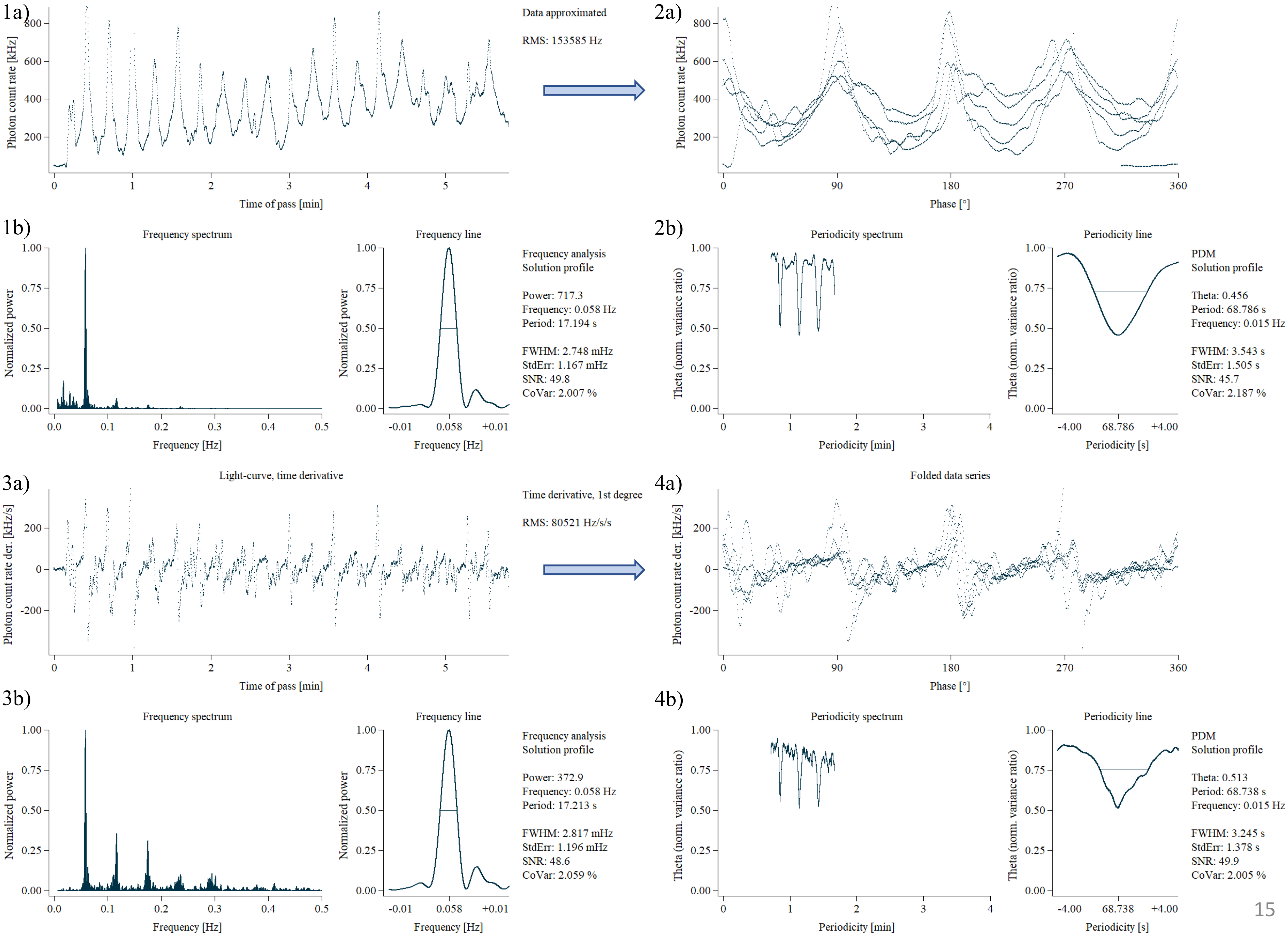

# Timeseries analysis, Jason-2 **light curve**


CNES

## Apparent vs. Inertial PDM

1a) Approximated data

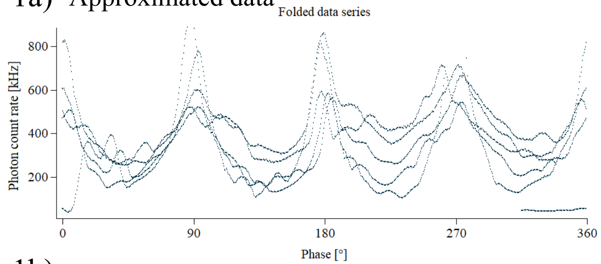


2a) Approximated data

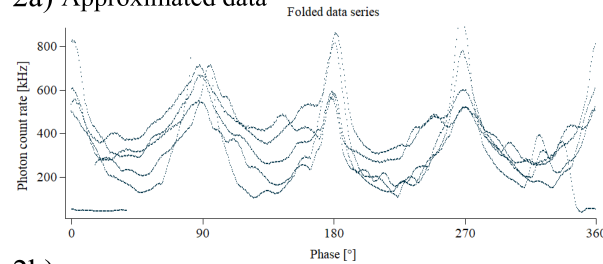


1b)

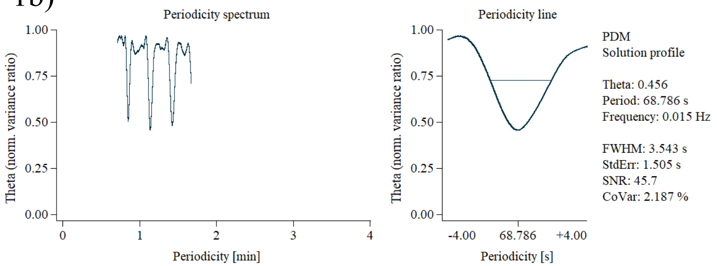


2b)

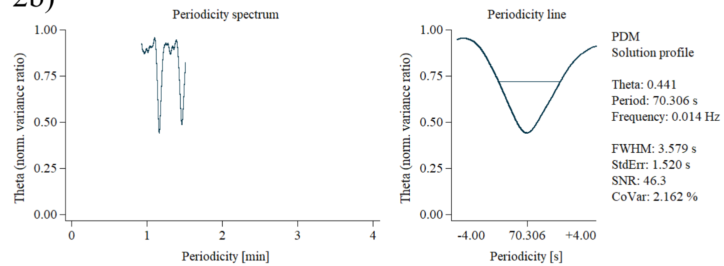


3a) 1st time derivative

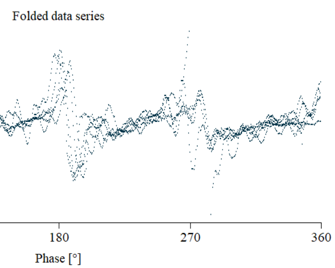


4a) 1st time derivative

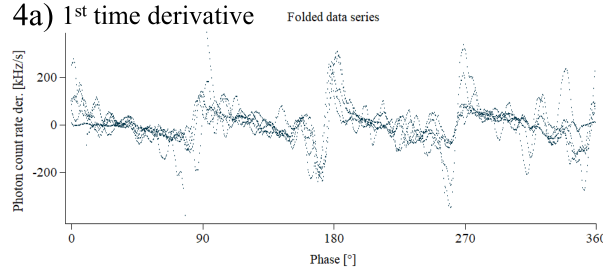


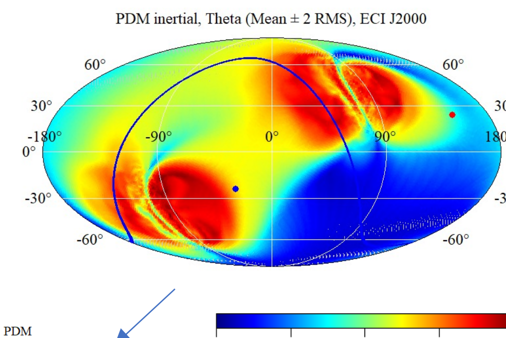


3b)

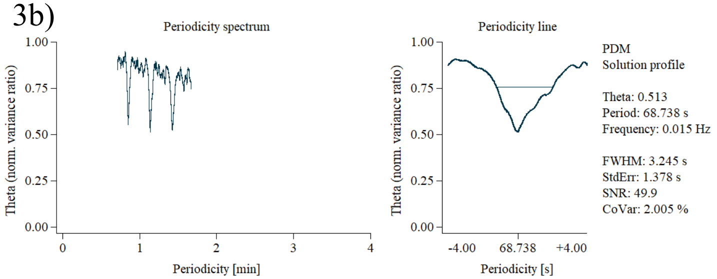


4b)

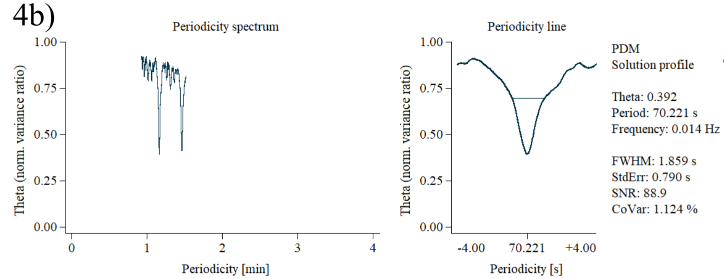


Theta: mean ± 2 RMS
(RMS of all Theta points
on the map)

# Timeseries analysis, TOPEX **SLR**

A. Lomb | B. Apparent PDM | C. Inertial PDM

1. Averaged data
2. Approximated data
3. 1st derivative

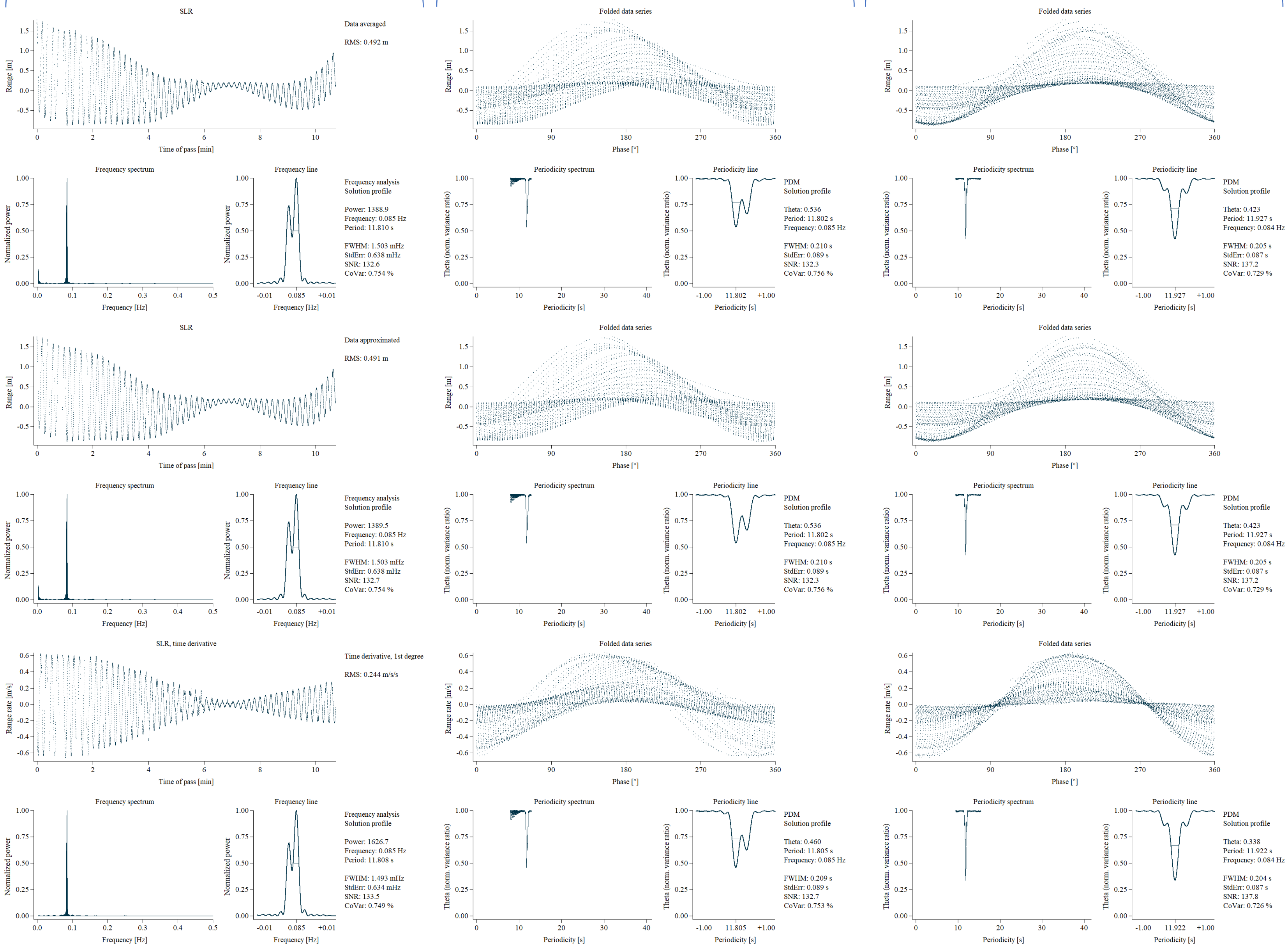

# Comparison of Lomb and PDM on approximated and derivative timeseries (Topex **SLR**)

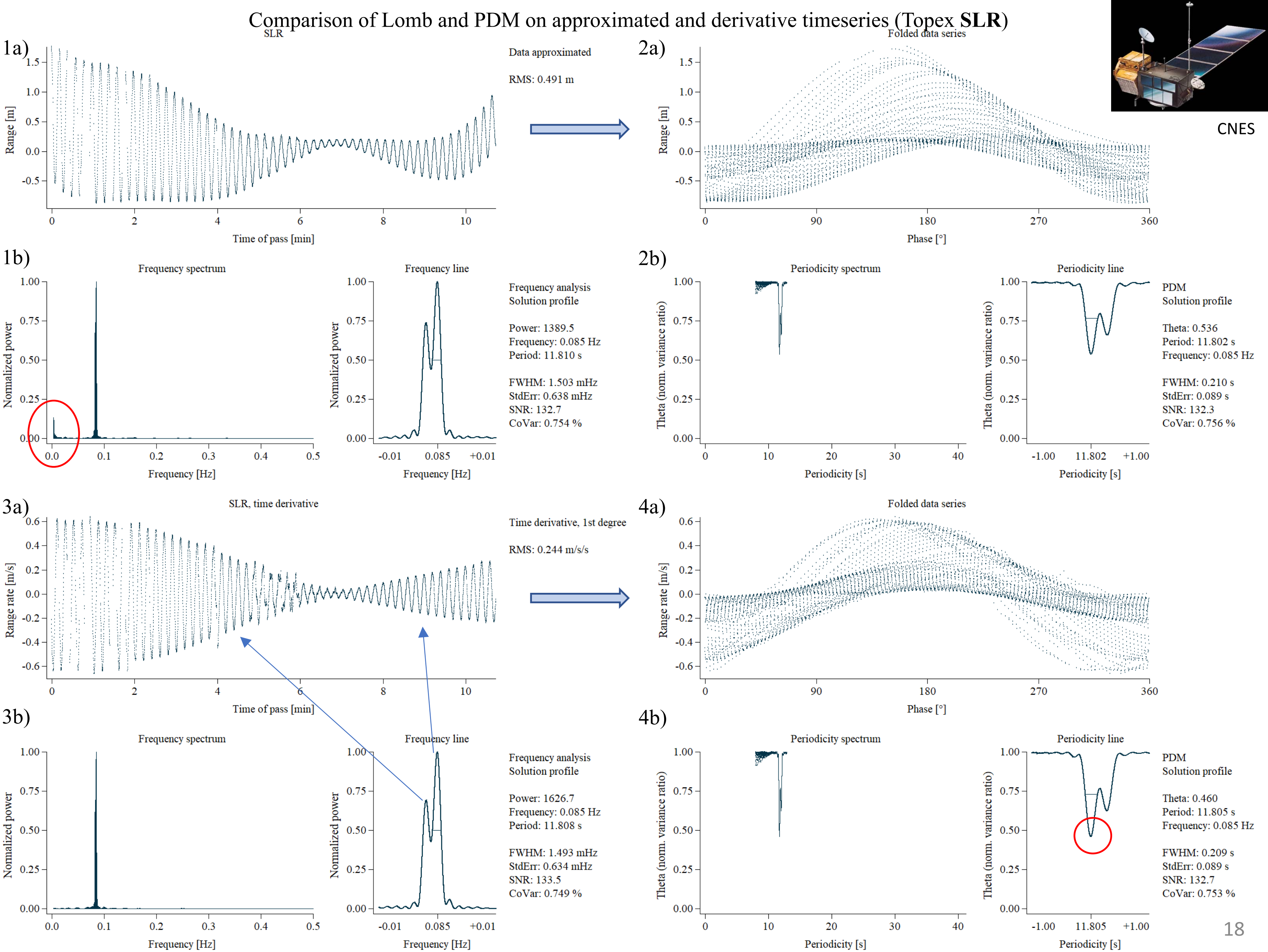

# Timeseries analysis, TOPEX **SLR**

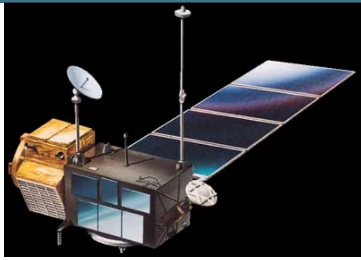


## Apparent vs. Inertial PDM

1a) Approximated data

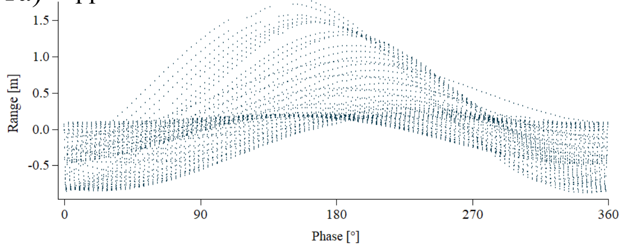


1b)

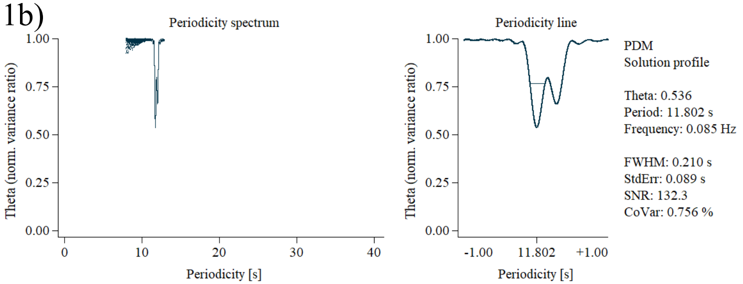


2a) Approximated data

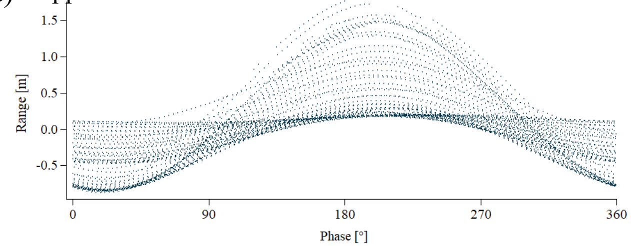


2b)

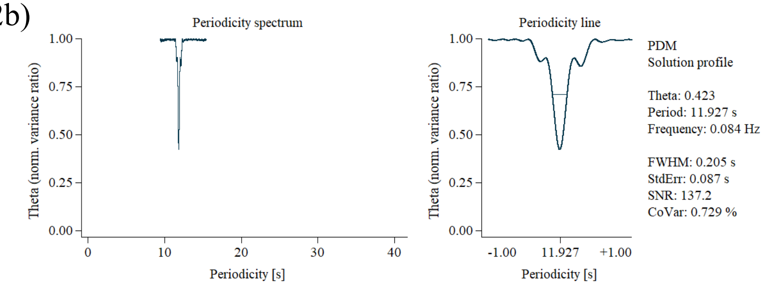


3a) 1st time derivative

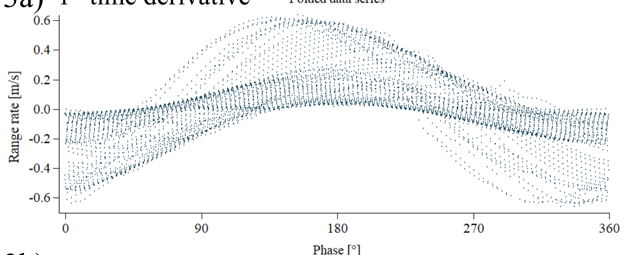


3b)

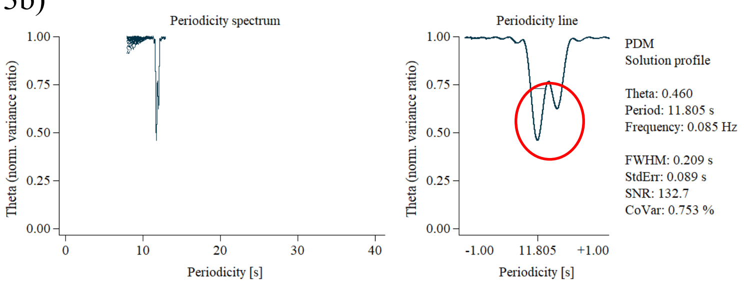


4a) 1st time derivative

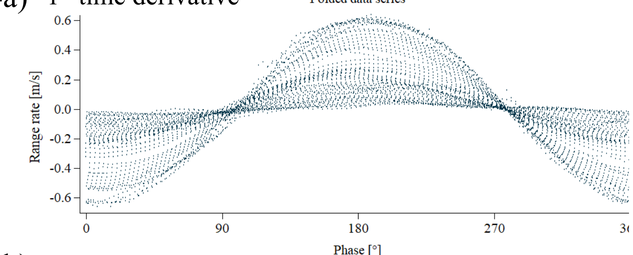


4b)

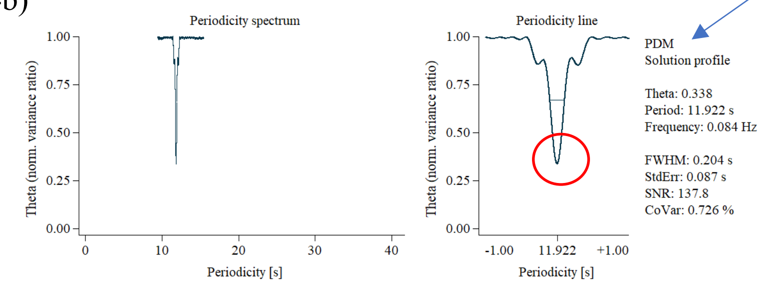


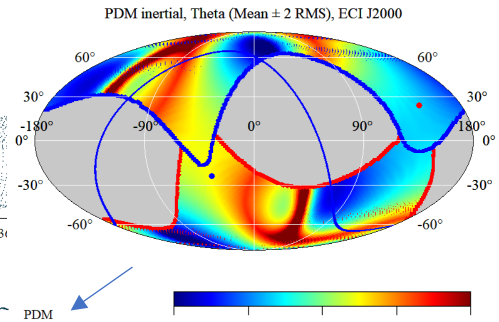


Theta: mean ± 2 RMS
(RMS of all Theta points
on the map)

# Results of the epoch methods

Object: DMSP 5D-2 F8 (USA 26)
NORAD: 18123
Cospar: 1987-053A
Launch: 20 June, 1987
Apogee alt.: 839 km
Perigee alt.: 820 km
Inclination: 98.7°
Orb. period: 1.7 h
RCS: 3.0 m2
Object age: 34.3 y
Exp. spin status: periodic, 10.9 s
Mag: -1.28 .. 9.92, 5.46, se 0.89
datafile: 55128218_ct

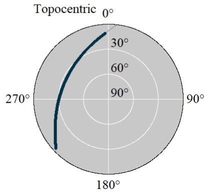


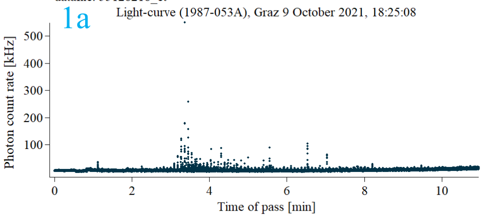


Pass information
Duration: 10m:57s
Data points: 65567
Data rate: 100.0 Hz

Closest approach
Topo el: 34.2°
Slant range: 1338 km
Phase angle: 122.5°
Sim. app. mag.: 8.0
Solar Beta angle: -74.3°

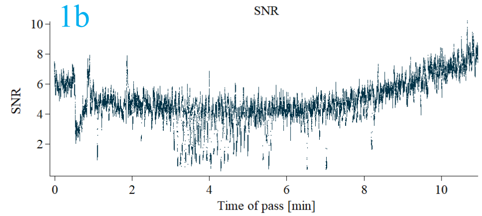



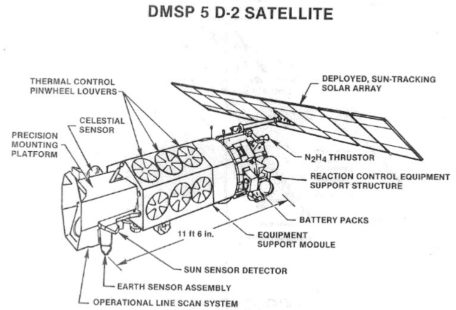


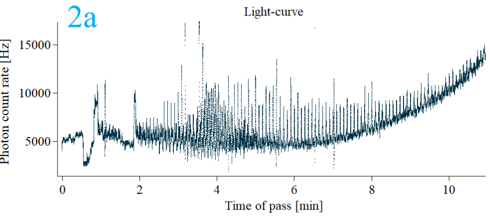


Data approximated

RMS: 2401 Hz

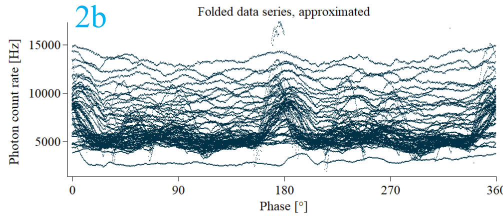


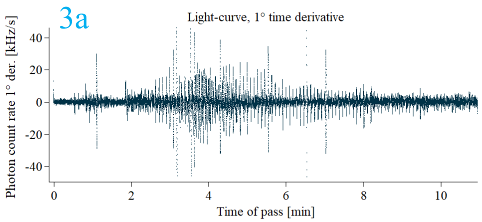


Time derivative, 1°

RMS: 4706 Hz/s


Approximated data: 2-a,b, 4-a,b,c
Time derivative: 3-a,b, 5-a,b,c

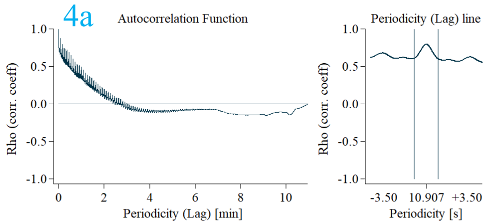


ACF
Solution profile

Rho: 0.792
Period: 10.907 s
Frequency: 0.092 Hz
FWHM: 1.736 s
StdDev: 0.737 s
SNR: 14.8
CoVar: 6.759 %

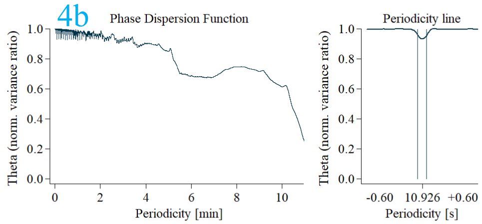


PDM
Solution profile

Theta: 0.932
Period: 10.926 s
Frequency: 0.092 Hz
FWHM: 0.115 s
StdDev: 0.049 s
SNR: 223.9
CoVar: 0.447 %

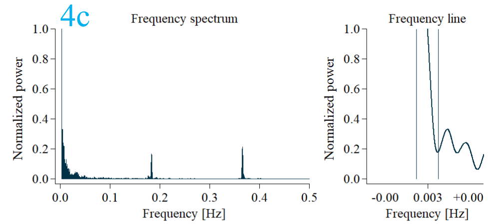


Frequency analysis
Solution profile

Power: 5567.6
Frequency: 0.003 Hz
Period: 328.501 s
FWHM: 1.826 mHz
StdDev: 0.776 mHz
SNR: 3.9
CoVar: 25.476 %

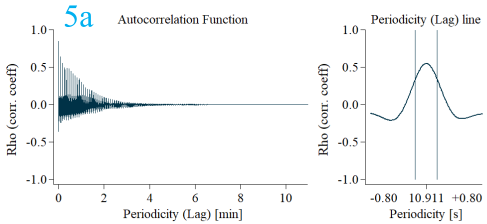


ACF
Solution profile

Rho: 0.555
Period: 10.911 s
Frequency: 0.092 Hz
FWHM: 0.364 s
StdDev: 0.155 s
SNR: 70.6
CoVar: 1.416 %

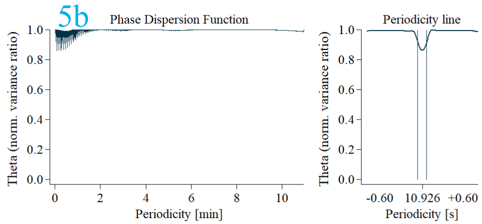


PDM
Solution profile

Theta: 0.861
Period: 10.926 s
Frequency: 0.092 Hz
FWHM: 0.110 s
StdDev: 0.047 s
SNR: 234.4
CoVar: 0.427 %

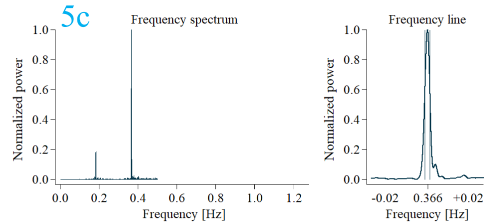


Frequency analysis
Solution profile

Power: 1551.3
Frequency: 0.366 Hz
Period: 2.733 s
FWHM: 2.070 mHz
StdDev: 0.879 mHz
SNR: 416.2
CoVar: 0.240 %

# Results of the epoch methods

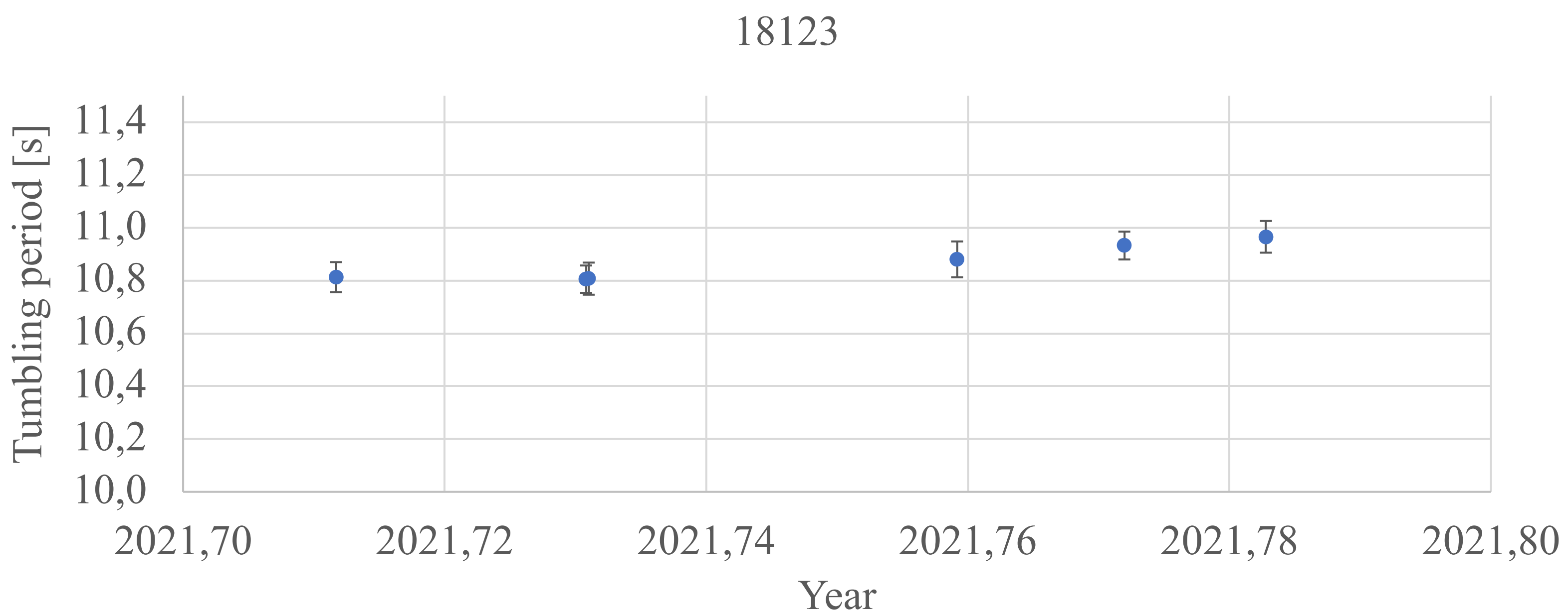


| SatCat | |
|---|---|
| Name | DMSP Block 5D-2 F8 |
| COSPAR | 1987-053A |
| NORAD | 18123 |
| Apogee_altitude_[km] | 839 |
| Perigee_altitude_[km] | 820 |
| Orbital_period_[h] | 1.692 |
| Inclination_[deg] | 98.7 |
| RCS_[m2] | 2.96 |
| Launch_date | 6/20/1987 |
| Age_[year] | 34.7 |
| Source_or_ownership | us |

| DISCOS | |
|---|---|
| Class | Payload |
| Shape | Cyl + 1 Pan |
| CS_min_[m2] | 1.767 |
| CS_max_[m2] | 10.5 |
| CS_ave_[m2] | 9.012 |
| Mass_[kg] | 815.7 |
| Span_[m] | 6.9 |
| Height_[m] | 6.9 |
| Diameter_[m] | 1.5 |
| Depth_[m] | 0 |
| Width_[m] | 0 |

| MMT | |
|---|---|
| Variability | periodic |
| Period_[s] | 10.9 |
| StdMag_Clear | 5.5 |
| | |
| | |
| | |
| | |
| | |
| | |
| | |
| | |

# Results of the epoch methods

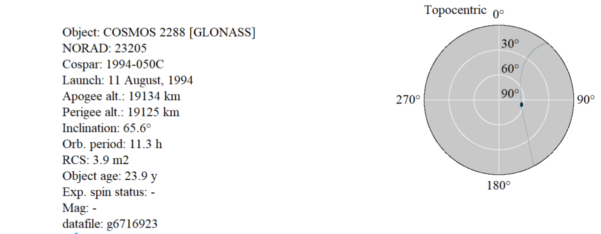


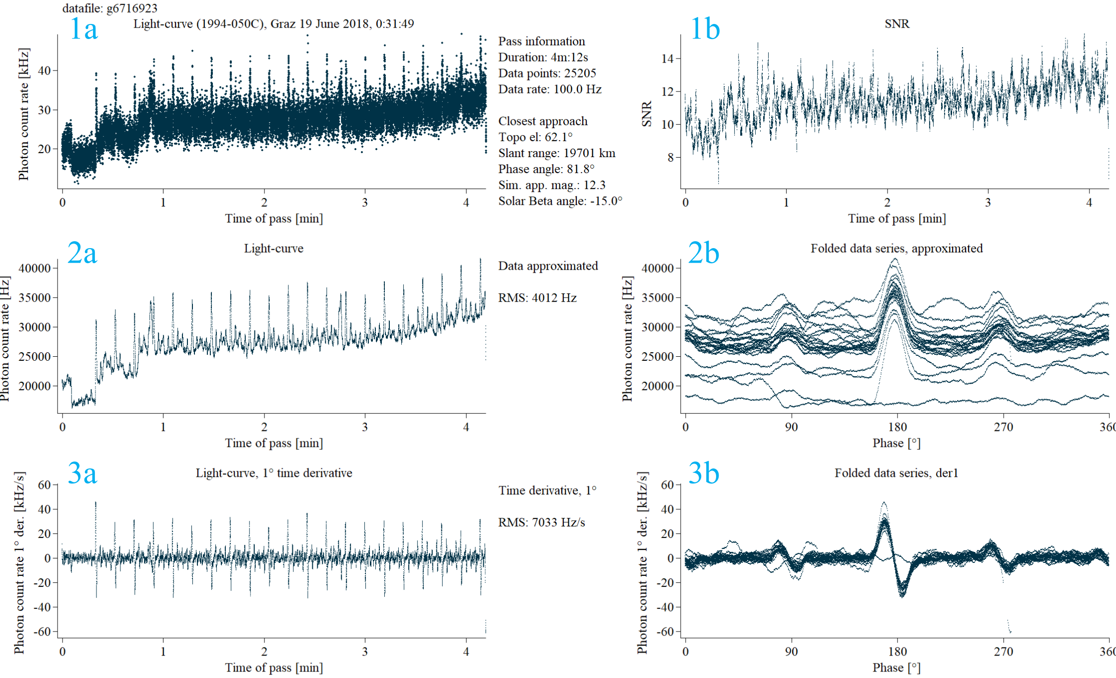


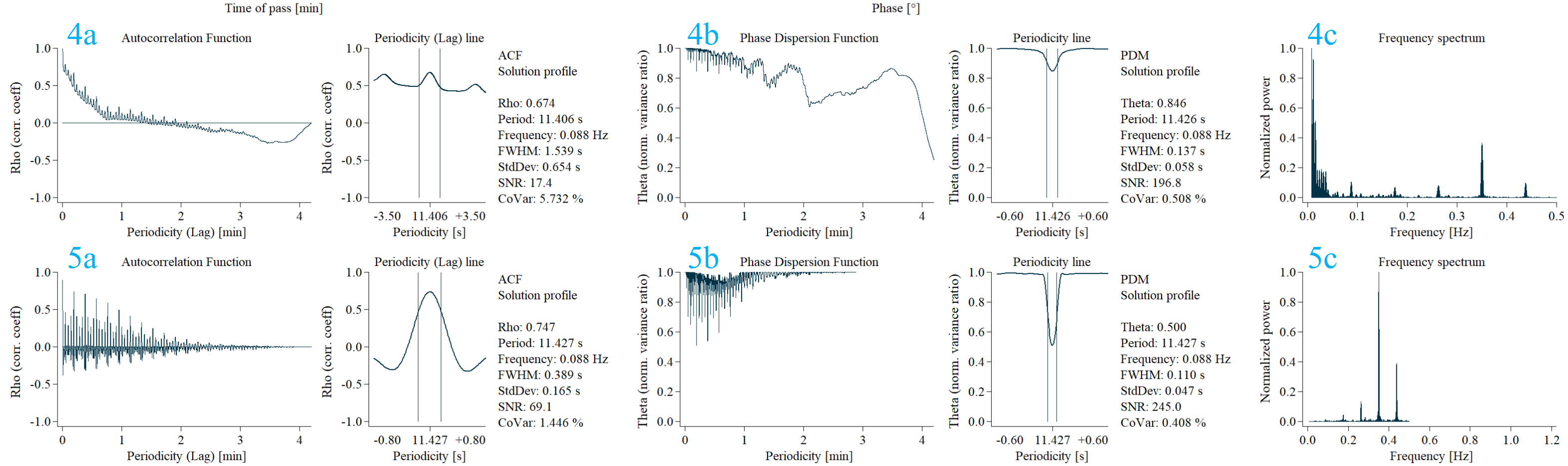


Approximated data: 2-a,b, 4-a,b,c
Time derivative: 3-a,b, 5-a,b,c

# Results of the epoch methods

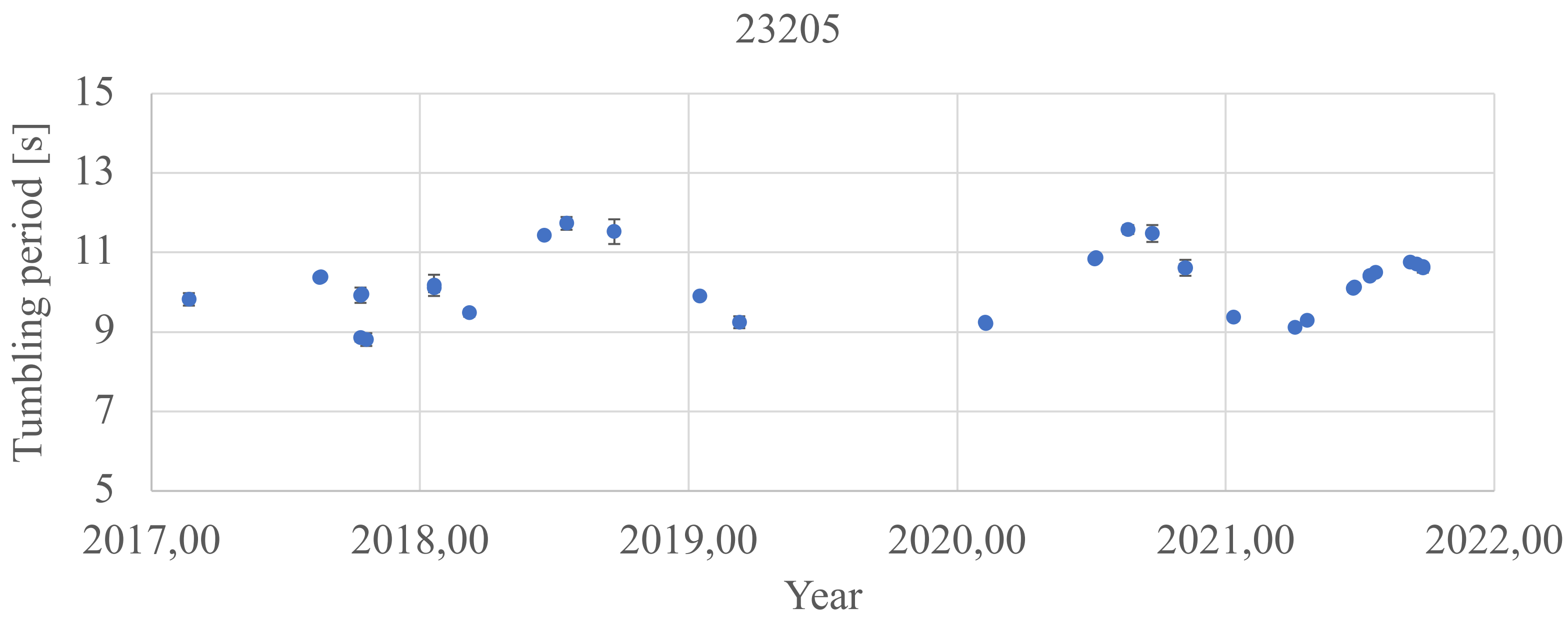


| SatCat | |
|---|---|
| Name | Cosmos-2289 |
| COSPAR | 1994-050C |
| NORAD | 23205 |
| Apogee_altitude_[km] | 19135 |
| Perigee_altitude_[km] | 19125 |
| Orbital_period_[h] | 11.262 |
| Inclination_[deg] | 65.6 |
| RCS_[m2] | 3.948 |
| Launch_date | 8/11/1994 |
| Age_[year] | 27.5 |
| Source_or_ownership | cis |

| DISCOS | |
|---|---|
| Class | Payload |
| Shape | Cyl + 2 Pan |
| CS_min_[m2] | 4.052 |
| CS_max_[m2] | 24.972 |
| CS_ave_[m2] | 14.748 |
| Mass_[kg] | 1288.4 |
| Span_[m] | 7.8 |
| Height_[m] | 4 |
| Diameter_[m] | 1.5 |
| Depth_[m] | 0 |
| Width_[m] | 0 |

| MMT | |
|---|---|
| Variability | N/A |
| Period_[s] | -1 |
| StdMag_Clear | 999 |
| | |
| | |
| | |
| | |
| | |
| | |
| | |
| | |

# Results of the epoch methods

Object: KIKU-6 (ETS-VI)
NORAD: 23230
Cospar: 1994-056A
Launch: 28 August, 1994
Apogee alt.: 38772 km
Perigee alt.: 8468 km
Inclination: 15.3°
Orb. period: 14.4 h
RCS: 38.6 m2
Object age: 26.6 y
Exp. spin status: periodic, 5.3 s
Mag: 0.61 .. 6.02, 4.47, se 0.63
datafile: a0809417_ct

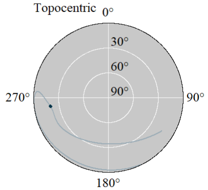


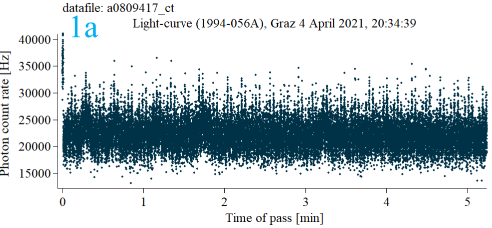


Pass information
Duration: 5m:15s
Data points: 31464
Data rate: 100.0 Hz

Closest approach
Topo el: 19.9°
Slant range: 41711 km
Phase angle: 107.2°
Sim. app. mag.: 14.8
Solar Beta angle: 8.7°

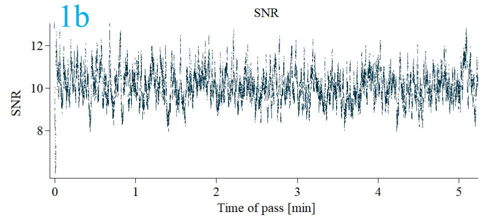



NASDA (JAXA)

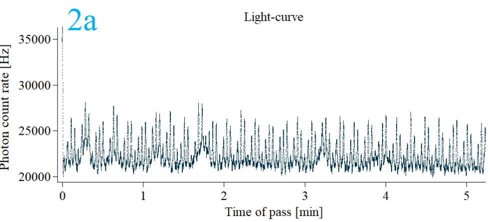


Data approximated

RMS: 1511 Hz

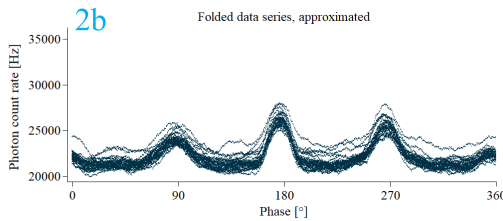


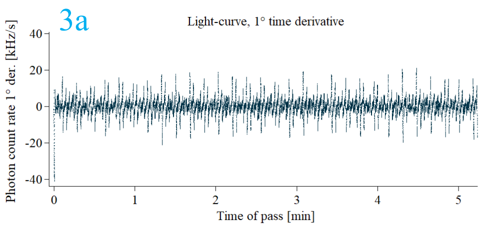


Time derivative, 1°

RMS: 4892 Hz/s

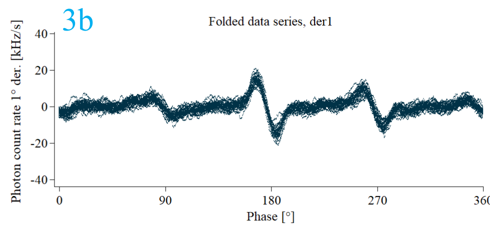


Approximated data: 2-a,b, 4-a,b,c
Time derivative: 3-a,b, 5-a,b,c

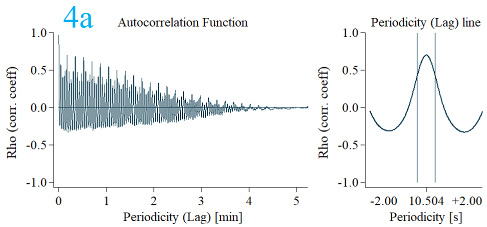


ACF
Solution profile

Rho: 0.703
Period: 10.504 s
Frequency: 0.095 Hz
FWHM: 0.750 s
StdDev: 0.319 s
SNR: 33.0
CoVar: 3.033 %

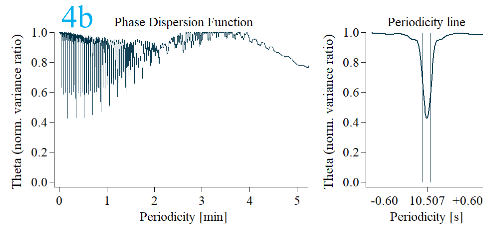


PDM
Solution profile

Theta: 0.423
Period: 10.507 s
Frequency: 0.095 Hz
FWHM: 0.106 s
StdDev: 0.045 s
SNR: 233.8
CoVar: 0.428 %

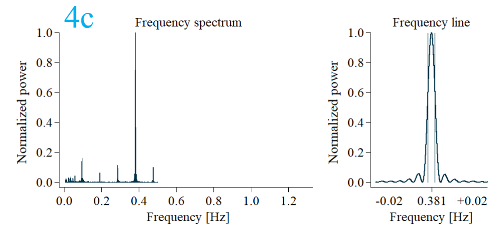


Frequency analysis
Solution profile

Power: 6371.3
Frequency: 0.381 Hz
Period: 2.627 s
FWHM: 2.896 mHz
StdDev: 1.230 mHz
SNR: 309.5
CoVar: 0.323 %

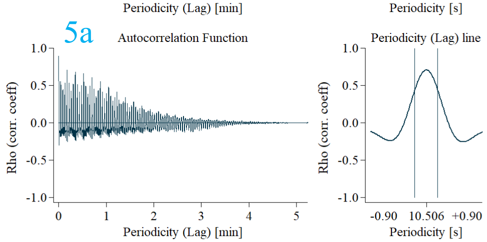


ACF
Solution profile

Rho: 0.716
Period: 10.506 s
Frequency: 0.095 Hz
FWHM: 0.433 s
StdDev: 0.184 s
SNR: 57.2
CoVar: 1.750 %

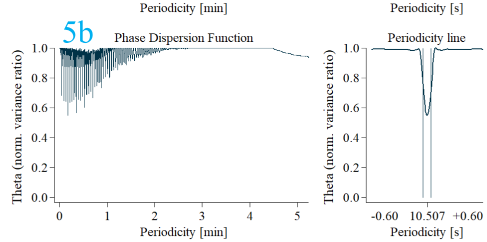


PDM
Solution profile

Theta: 0.540
Period: 10.507 s
Frequency: 0.095 Hz
FWHM: 0.094 s
StdDev: 0.040 s
SNR: 262.1
CoVar: 0.381 %

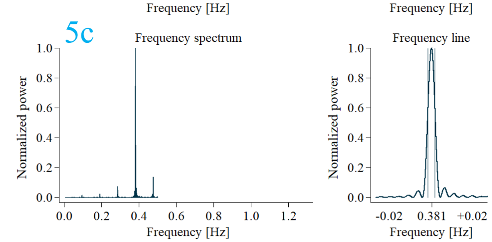


Frequency analysis
Solution profile

Power: 3548.1
Frequency: 0.381 Hz
Period: 2.626 s
FWHM: 2.870 mHz
StdDev: 1.219 mHz
SNR: 312.5
CoVar: 0.320 %

# Results of the epoch methods

Object: GLOBALSTAR M025
NORAD: 25770
Cospar: 1999-031A
Launch: 10 June, 1999
Apogee alt.: 2049 km
Perigee alt.: 2046 km
Inclination: 52.0°
Orb. period: 2.1 h
RCS: 2.3 m2
Object age: 22.1 y
Exp. spin status: periodic, 4.6 s
Mag: -3.58 .. 9.43, 6.18, se 1.00
datafile: a0219320_ct

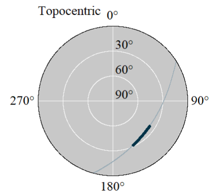


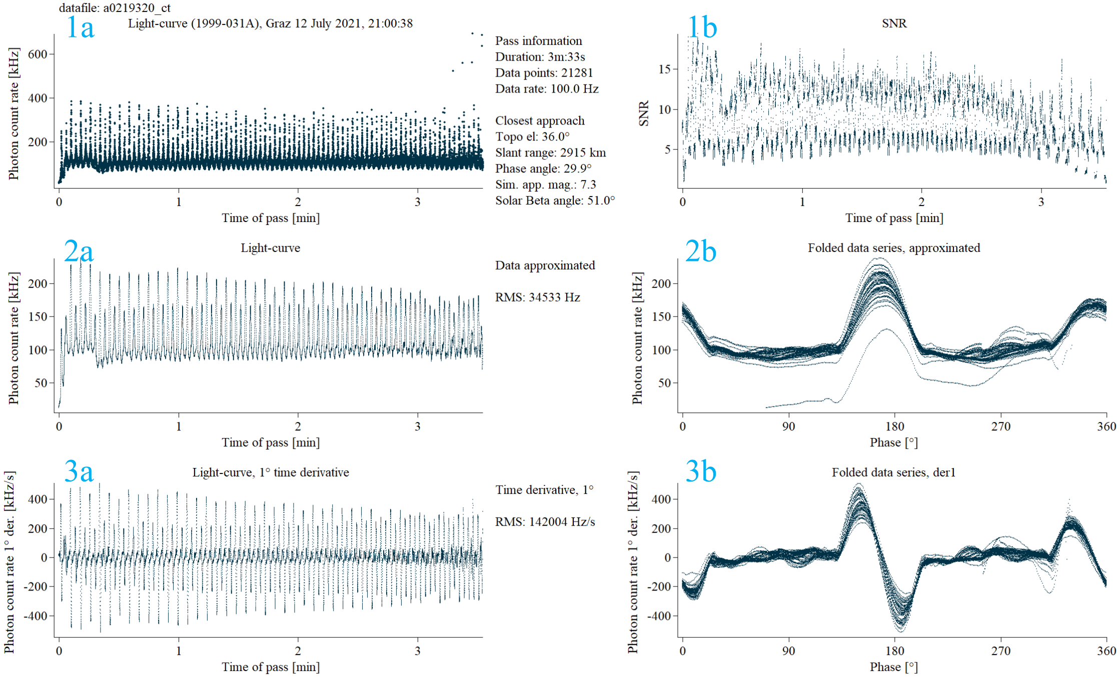


Approximated data: 2-a,b, 4-a,b,c
Time derivative: 3-a,b, 5-a,b,c

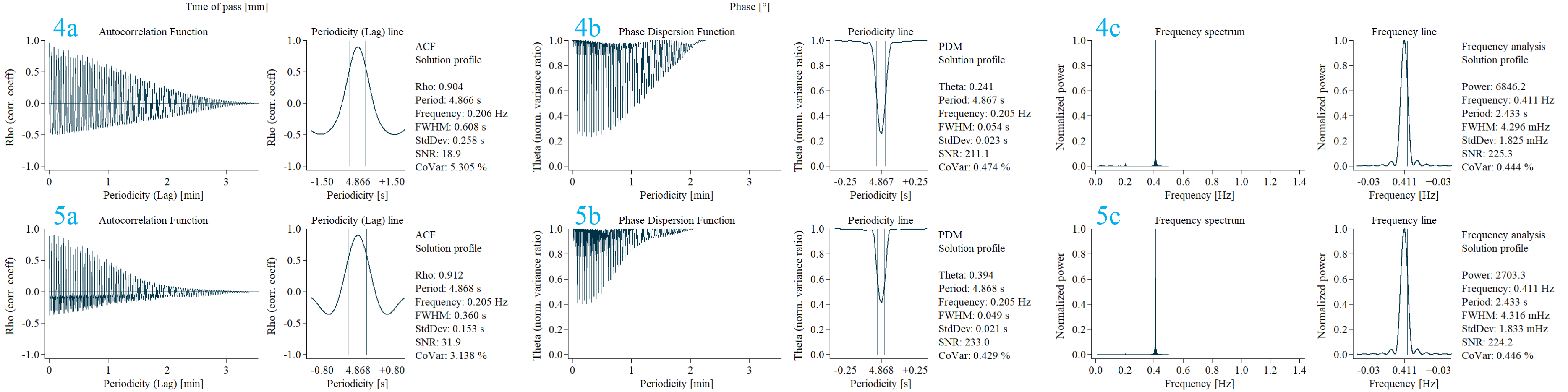

# Results of the epoch methods

Object: JASON-2 (OSTM)
NORAD: 33105
Cospar: 2008-032A
Launch: 20 June, 2008
Apogee alt.: 1317 km
Perigee alt.: 1305 km
Inclination: 66.0°
Orb. period: 1.9 h
RCS: 3.2 m2
Object age: 11.9 y
Exp. spin status: aperiodic
Mag: -1.17 .. 8.38, 5.70, se 0.81
datafile: ja213919_ct

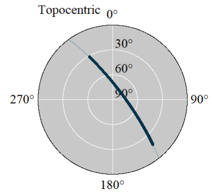


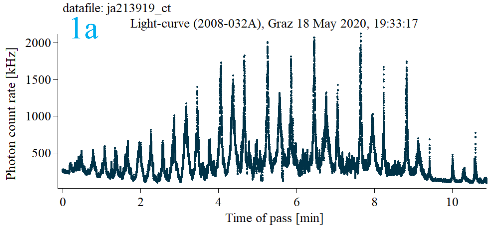


Pass information
Duration: 10m:53s
Data points: 65306
Data rate: 100.0 Hz

Closest approach
Topo el: 77.0°
Slant range: 1351 km
Phase angle: 78.4°
Sim. app. mag.: 6.4
Solar Beta angle: -6.4°

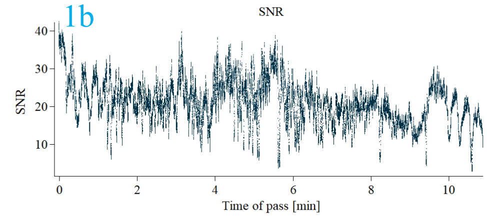


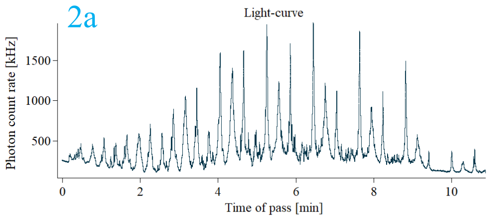


Data approximated

RMS: 256361 Hz

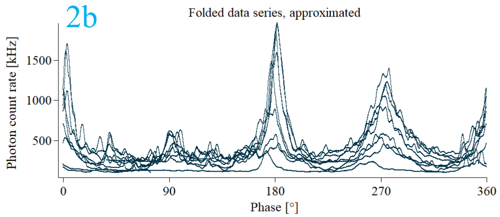


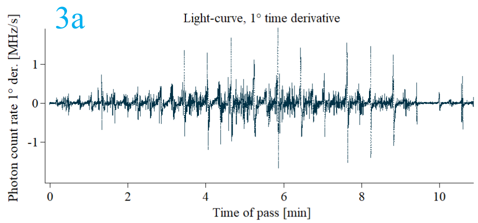


Time derivative, 1°

RMS: 203327 Hz/s

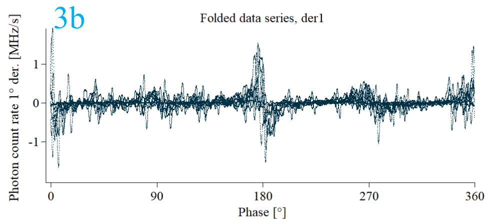


Approximated data: 2-a,b, 4-a,b,c
Time derivative: 3-a,b, 5-a,b,c

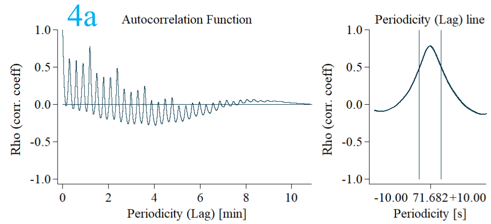


ACF
Solution profile

Rho: 0.775
Period: 71.682 s
Frequency: 0.014 Hz
FWHM: 4.574 s
StdDev: 1.943 s
SNR: 36.9
CoVar: 2.710 %

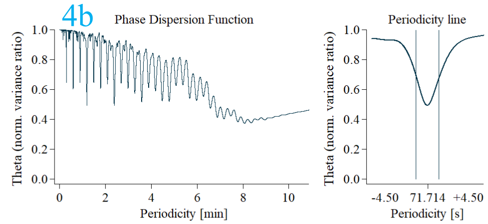


PDM
Solution profile

Theta: 0.497
Period: 71.714 s
Frequency: 0.014 Hz
FWHM: 2.127 s
StdDev: 0.903 s
SNR: 79.4
CoVar: 1.259 %

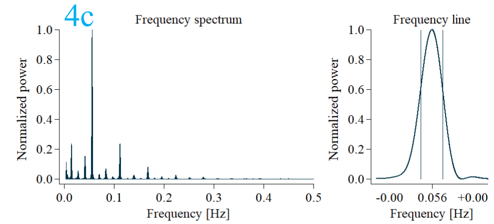


Frequency analysis
Solution profile

Power: 8471.4
Frequency: 0.056 Hz
Period: 17.935 s
FWHM: 1.823 mHz
StdDev: 0.774 mHz
SNR: 72.0
CoVar: 1.388 %

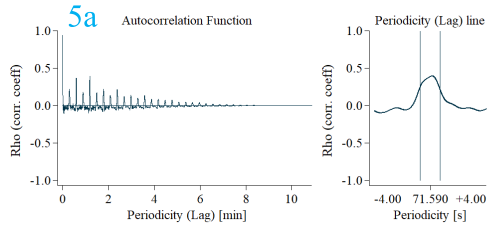


ACF
Solution profile

Rho: 0.395
Period: 71.590 s
Frequency: 0.014 Hz
FWHM: 1.707 s
StdDev: 0.725 s
SNR: 98.8
CoVar: 1.012 %

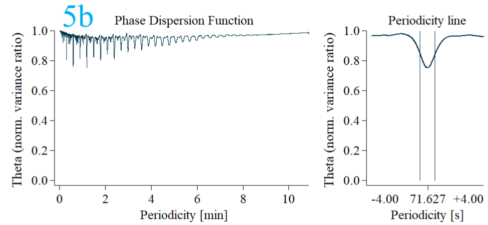


PDM
Solution profile

Theta: 0.753
Period: 71.627 s
Frequency: 0.014 Hz
FWHM: 1.271 s
StdDev: 0.540 s
SNR: 132.7
CoVar: 0.754 %

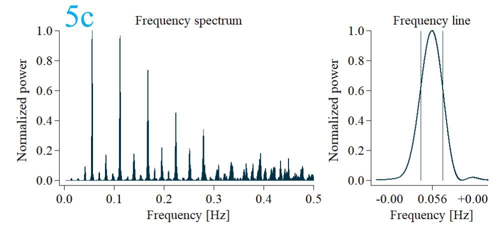


Frequency analysis
Solution profile

Power: 1608.6
Frequency: 0.056 Hz
Period: 17.931 s
FWHM: 1.871 mHz
StdDev: 0.794 mHz
SNR: 70.2
CoVar: 1.424 %

# Results of the epoch methods

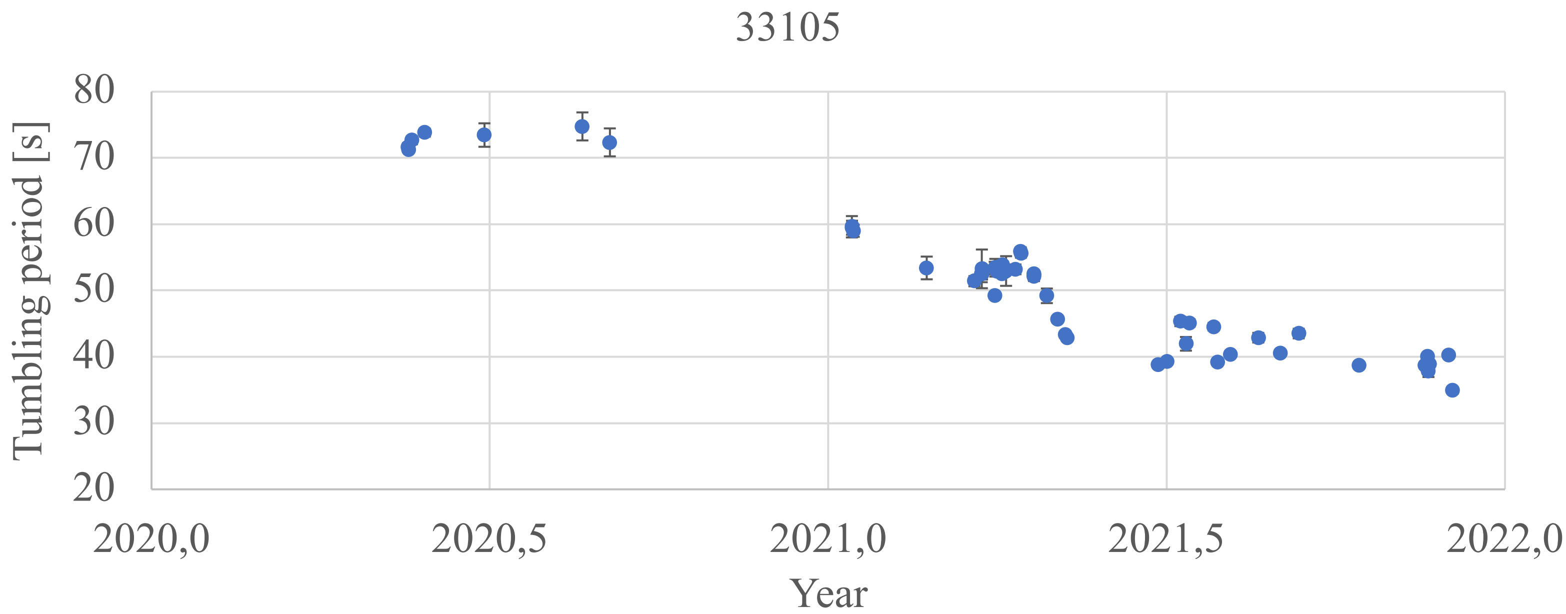


| SatCat | |
|---|---|
| Name | Jason-2 |
| COSPAR | 2008-032A |
| NORAD | 33105 |
| Apogee_altitude_[km] | 1317 |
| Perigee_altitude_[km] | 1305 |
| Orbital_period_[h] | 1.863 |
| Inclination_[deg] | 66 |
| RCS_[m2] | 3.162 |
| Launch_date | 6/20/2008 |
| Age_[year] | 13.7 |
| Source_or_ownership | fr |

| DISCOS | |
|---|---|
| Class | Payload |
| Shape | Box + 2 Pan |
| CS_min_[m2] | 3.61 |
| CS_max_[m2] | 22.433 |
| CS_ave_[m2] | 12.823 |
| Mass_[kg] | 506 |
| Span_[m] | 9.7 |
| Height_[m] | 3.7 |
| Diameter_[m] | 0 |
| Depth_[m] | 1.9 |
| Width_[m] | 0 |

| MMT | |
|---|---|
| Variability | aperiodic |
| Period_[s] | 0 |
| StdMag_Clear | 5.7 |
| | |
| | |
| | |
| | |
| | |
| | |
| | |
| | |

# Results of the epoch methods

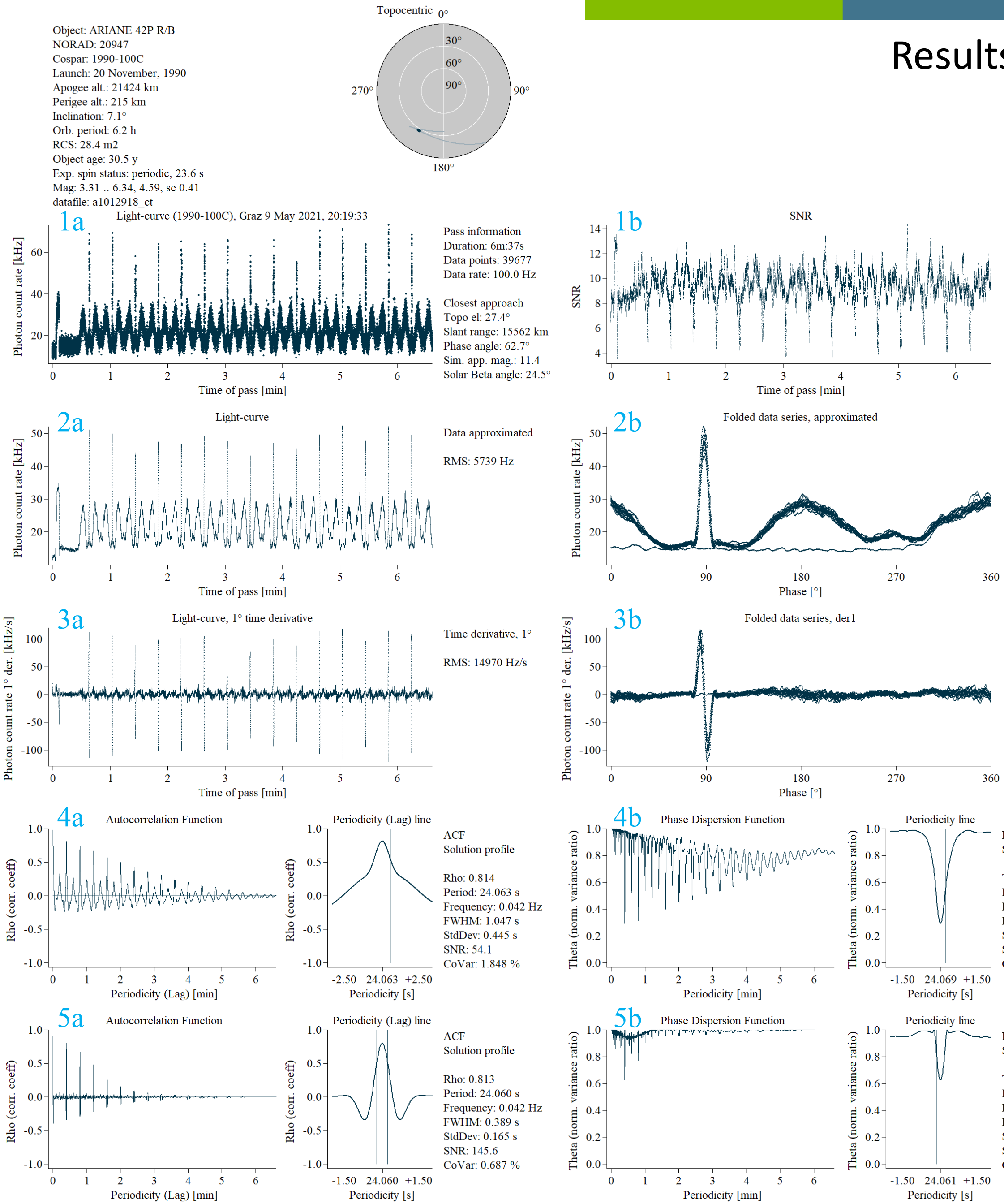


Approximated data: 2-a,b, 4-a,b,c
Time derivative: 3-a,b, 5-a,b,c

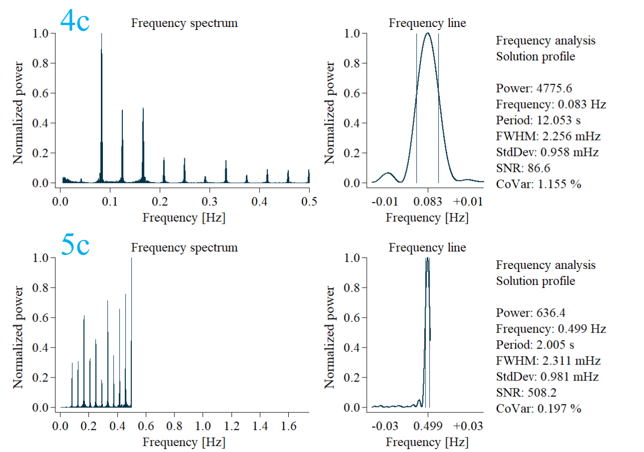

# Results of the epoch methods

Object: SL-16 R/B
NORAD: 25407
Cospar: 1998-045B
Launch: 28 July, 1998
Apogee alt.: 844 km
Perigee alt.: 835 km
Inclination: 71.0°
Orb. period: 1.7 h
RCS: 11.3 m2
Object age: 22.2 y
Exp. spin status: -
Mag: -
datafile: 33526802_ct

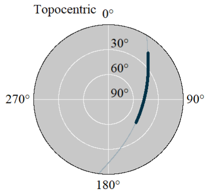


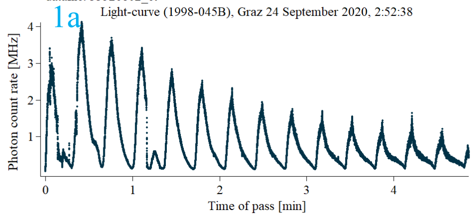


Pass information
Duration: 4m:52s
Data points: 29180
Data rate: 100.0 Hz

Closest approach
Topo el: 48.4°
Slant range: 1088 km
Phase angle: 102.8°
Sim. app. mag.: 6.7
Solar Beta angle: -45.5°

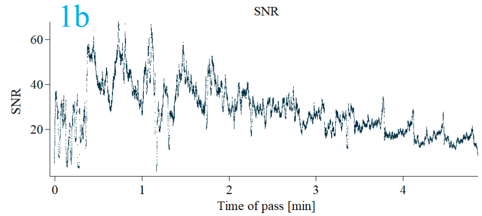


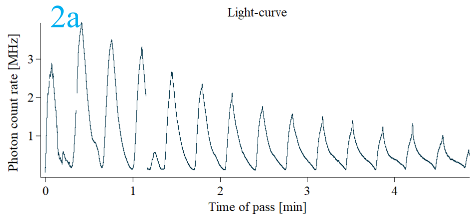


Data approximated

RMS: 792149 Hz

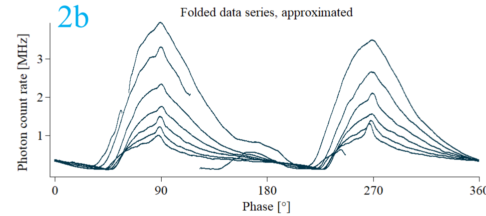


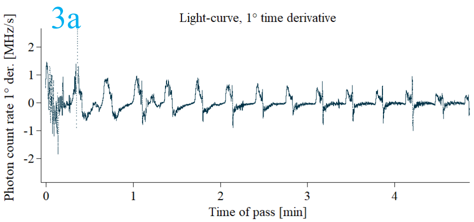


Time derivative, 1°

RMS: 304280 Hz/s


Approximated data: 2-a,b, 4-a,b,c
Time derivative: 3-a,b, 5-a,b,c

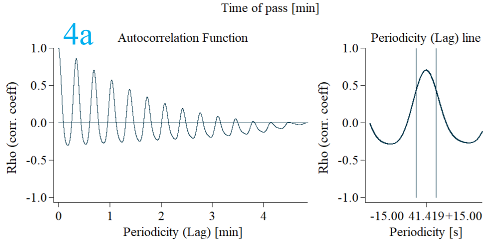


ACF
Solution profile

Rho: 0.708
Period: 41.419 s
Frequency: 0.024 Hz
FWHM: 6.304 s
StdDev: 2.677 s
SNR: 15.5
CoVar: 6.463 %

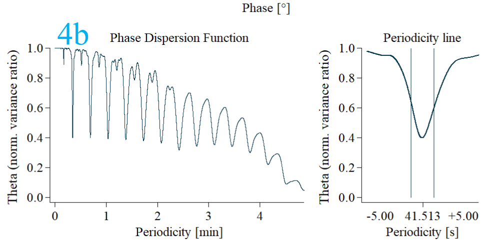


PDM
Solution profile

Theta: 0.401
Period: 41.513 s
Frequency: 0.024 Hz
FWHM: 2.432 s
StdDev: 1.033 s
SNR: 40.2
CoVar: 2.487 %

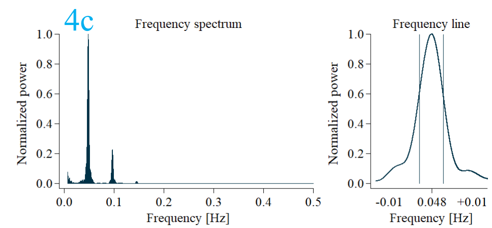


Frequency analysis
Solution profile

Power: 7037.0
Frequency: 0.048 Hz
Period: 20.784 s
FWHM: 3.474 mHz
StdDev: 1.475 mHz
SNR: 32.6
CoVar: 3.067 %

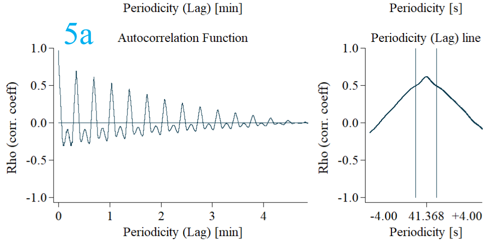


ACF
Solution profile

Rho: 0.613
Period: 41.368 s
Frequency: 0.024 Hz
FWHM: 1.775 s
StdDev: 0.754 s
SNR: 54.9
CoVar: 1.822 %

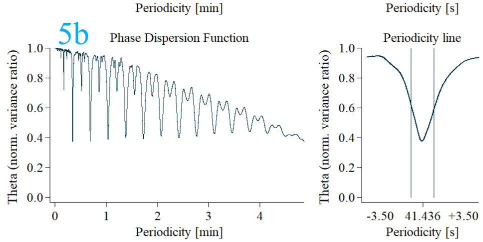


PDM
Solution profile

Theta: 0.390
Period: 41.436 s
Frequency: 0.024 Hz
FWHM: 1.721 s
StdDev: 0.731 s
SNR: 56.7
CoVar: 1.764 %

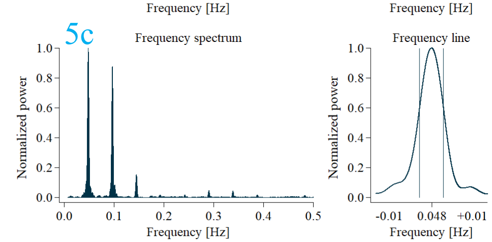


Frequency analysis
Solution profile

Power: 4072.6
Frequency: 0.048 Hz
Period: 20.767 s
FWHM: 3.459 mHz
StdDev: 1.469 mHz
SNR: 32.8
CoVar: 3.051 %

# Results of the epoch methods

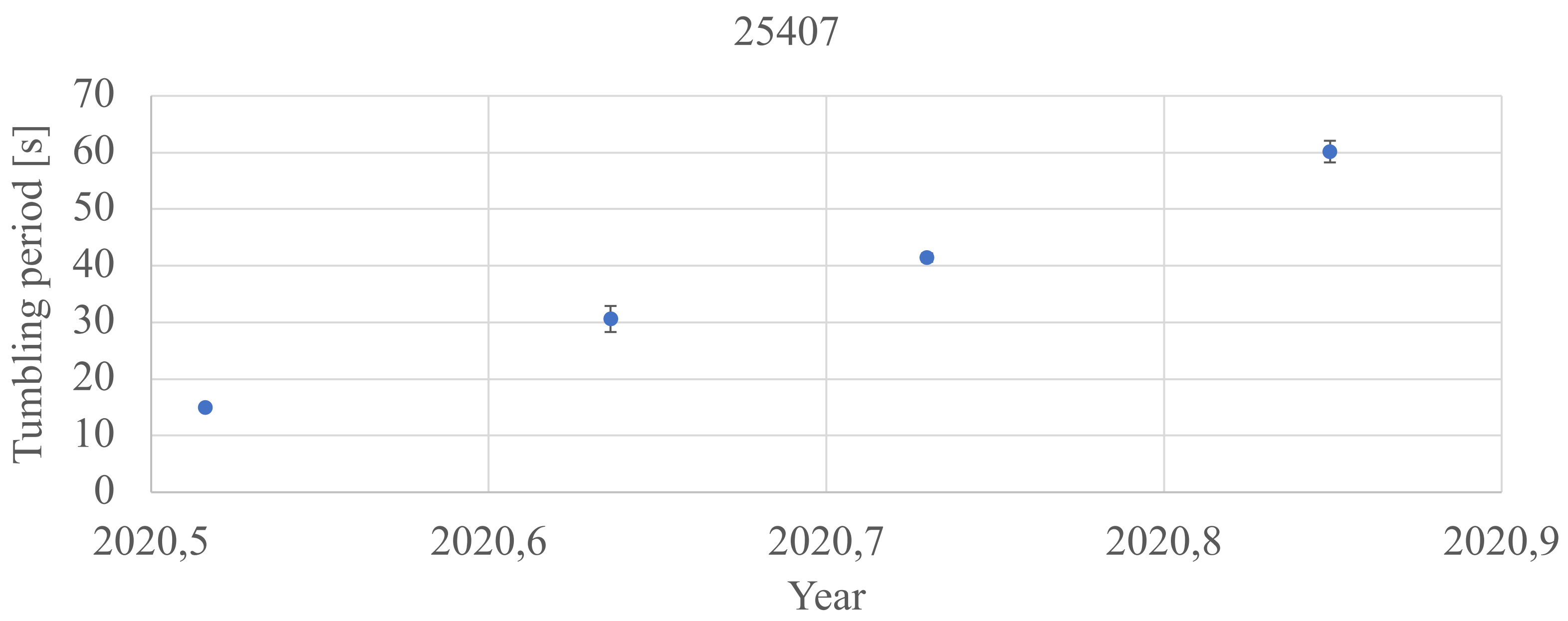


| SatCat | |
|---|---|
| Name | Zenit-2 second stage |
| COSPAR | 1998-045B |
| NORAD | 25407 |
| Apogee_altitude_[km] | 844 |
| Perigee_altitude_[km] | 835 |
| Orbital_period_[h] | 1.695 |
| Inclination_[deg] | 71 |
| RCS_[m2] | 11.342 |
| Launch_date | 7/28/1998 |
| Age_[year] | 23.6 |
| Source_or_ownership | cis |

| DISCOS | |
|---|---|
| Class | Rocket Body |
| Shape | Cyl |
| CS_min_[m2] | 11.946 |
| CS_max_[m2] | 44.908 |
| CS_ave_[m2] | 39.973 |
| Mass_[kg] | 8226 |
| Span_[m] | 11.1 |
| Height_[m] | 11.1 |
| Diameter_[m] | 3.9 |
| Depth_[m] | 0 |
| Width_[m] | 0 |

| MMT | |
|---|---|
| Variability | N/A |
| Period_[s] | -1 |
| StdMag_Clear | 999 |
| | |
| | |
| | |
| | |
| | |
| | |
| | |
| | |

# Results of the epoch methods

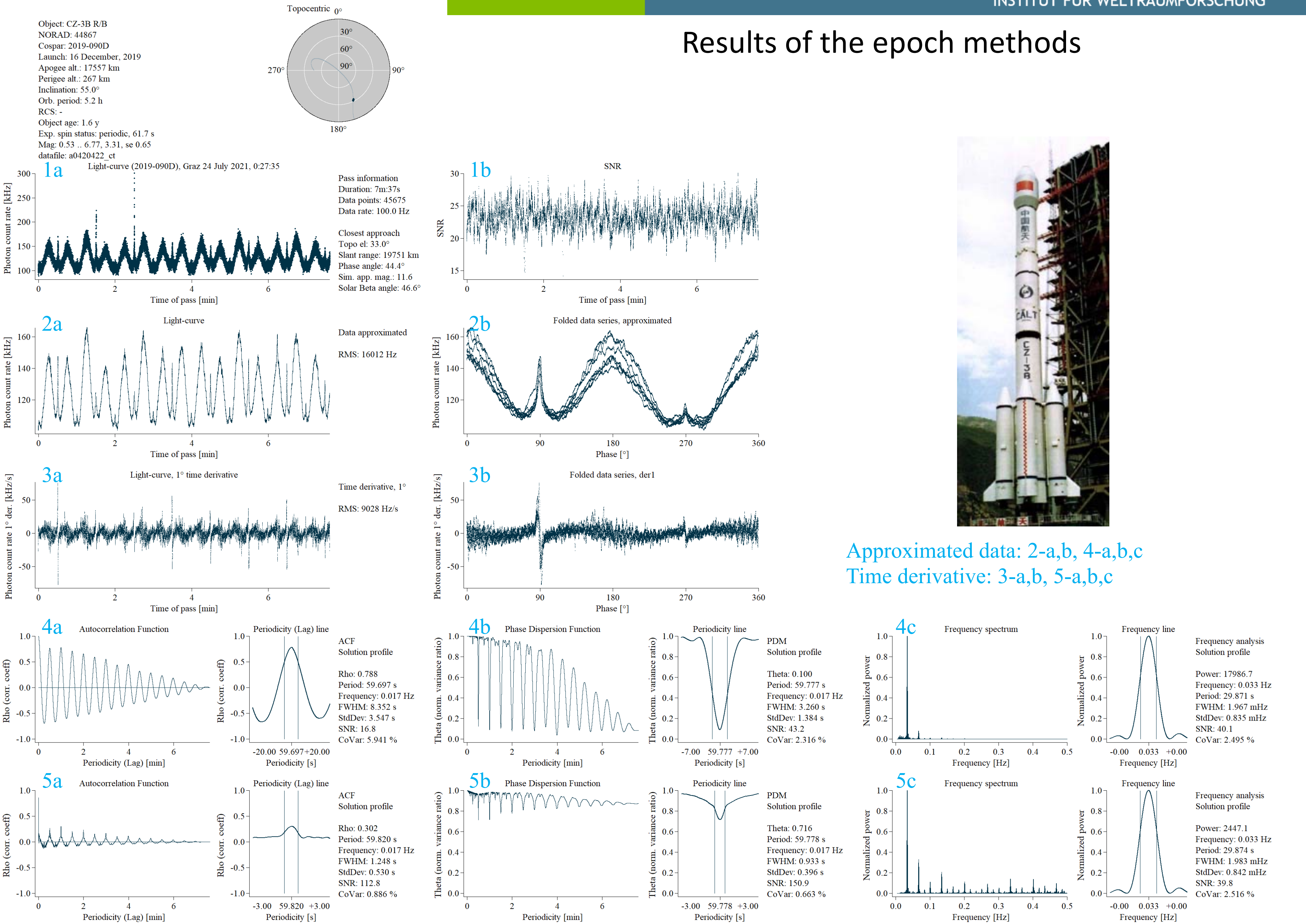


Approximated data: 2-a,b, 4-a,b,c
Time derivative: 3-a,b, 5-a,b,c

# Results of the epoch methods

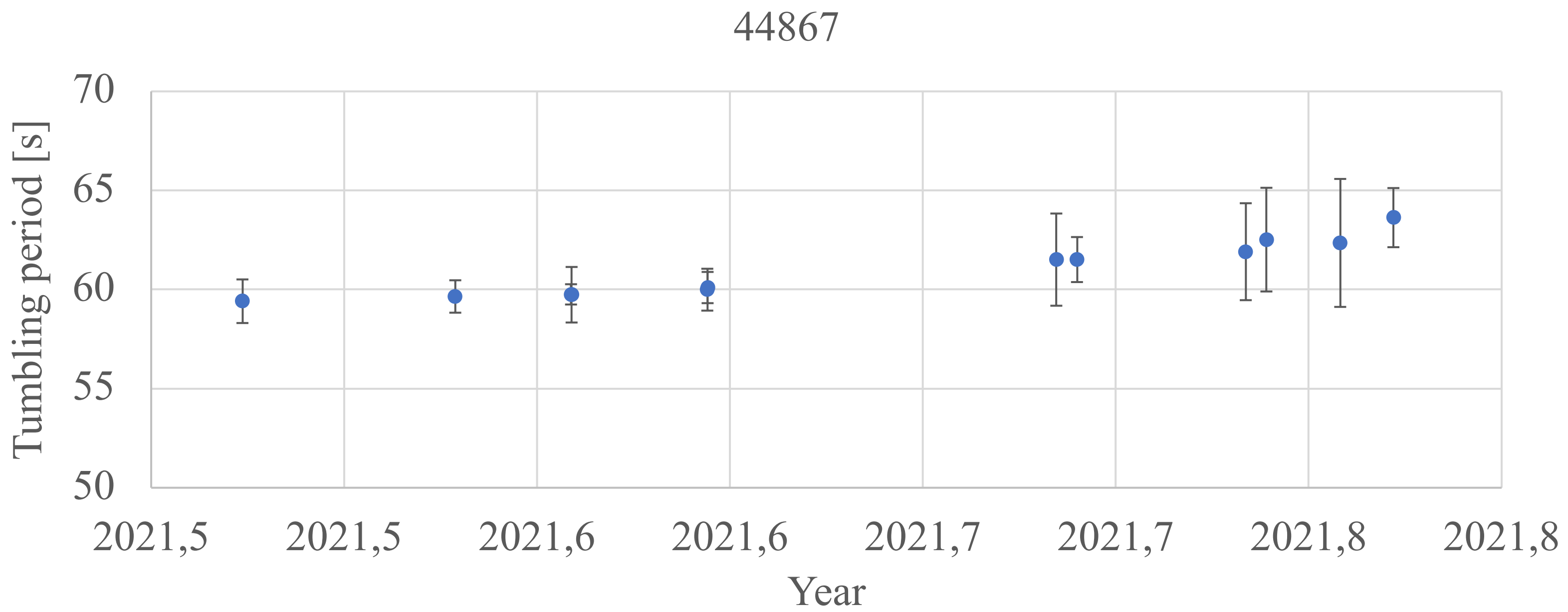


| SatCat | |
|---|---|
| Name | CZ-3B |
| COSPAR | 2019-090D |
| NORAD | 44867 |
| Apogee_altitude_[km] | 17561 |
| Perigee_altitude_[km] | 268 |
| Orbital_period_[h] | 5.228 |
| Inclination_[deg] | 55 |
| RCS_[m2] | -1 |
| Launch_date | 12/16/2019 |
| Age_[year] | 2.2 |
| Source_or_ownership | prc |

| DISCOS | |
|---|---|
| Class | Rocket Body |
| Shape | Cyl + 1 Nozzle |
| CS_min_[m2] | 7.069 |
| CS_max_[m2] | 39.134 |
| CS_ave_[m2] | 33.764 |
| Mass_[kg] | 2800 |
| Span_[m] | 3 |
| Height_[m] | 0 |
| Diameter_[m] | 0 |
| Depth_[m] | 0 |
| Width_[m] | 0 |

| MMT | |
|---|---|
| Variability | periodic |
| Period_[s] | 61.7 |
| StdMag_Clear | 3.3 |
| | |
| | |
| | |
| | |
| | |
| | |
| | |
| | |

# Data fusion

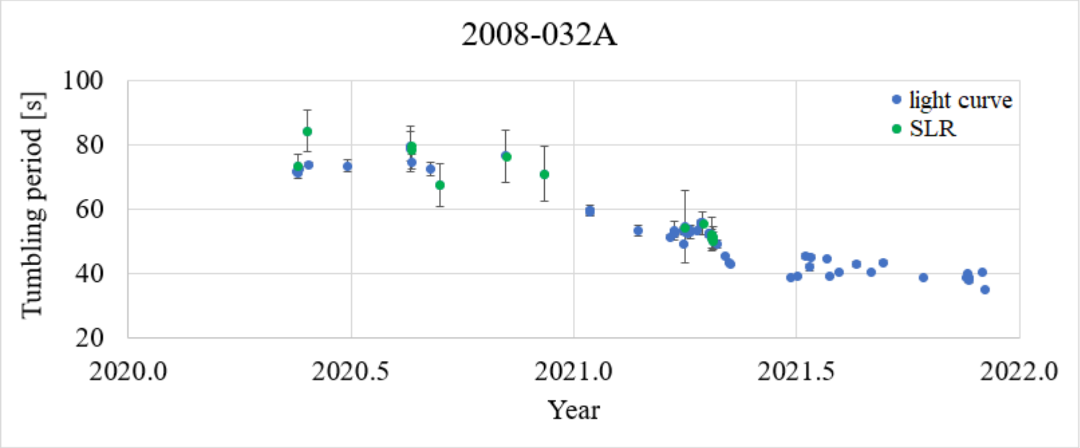


CNES

Observed spin period of Jason-2 determined with epoch analysis of Graz single-photon light curves (blue dot) and SLR data (green dot). Appendix C presents example analysis.

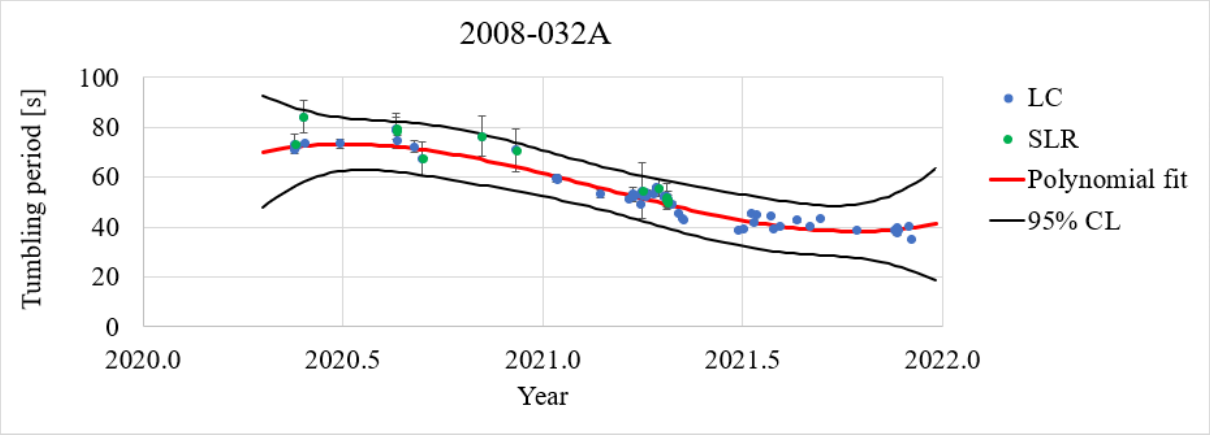


Fusion polynomial fit to light curve and SLR data with 95% confidence limits. A 3-degree weighted polynomial fit is constructed with fused spin period data from light curves and SLR observations of Jason-2.

# Data fusion

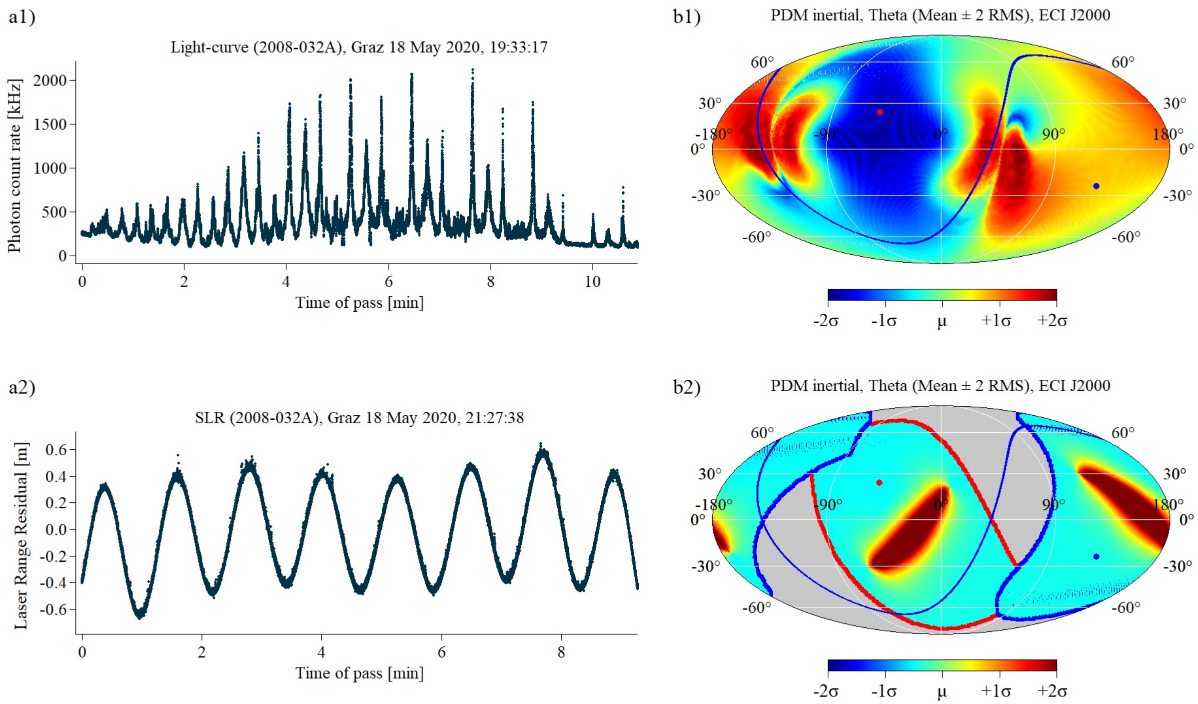


CNES

Jason-2 light curve (a1) and SLR (a2) data measured by Graz on 18 May, 2020.

Plots b1, b2 - present results of the inertial phase-folding applied to the respective time series.

Red and blue dots represent location of the positive and negative orbit normal vectors; a blue curve is a satellite orbital plane on the inertial sphere).

# Conclusions

- The tumbling motion determination processes can be efficiently performed with a set of epoch methods that extract frequency and periodicity spectra from the observational data,

- this, however, requires an initial data treatment with Savitzky-Golay Filters (SGF) that have powerful denoising and detrending properties, but come at high computational cost.

- The spin vector orientation determination with the epoch methods can deliver only approximate results – a range of possible solutions in a given coordinate system.

- During this project we have identified several areas where more research could lead to a higher level of automation of the tumbling motion determination (multi-pass analysis, variable degree of SGF).

# Danke für Ihre Aufmerksamkeit !